SCIENCE OF LIGHT

VOLUME 4 NUMBER 2

November

1955

Published by the

Institute for Optical Research

Tokyo University of Education

in collaboration with the

Spectroscopical Society of Japan

SCIENCE OF LIGHT

Science of Light contains reports of the Institute for Optical Research and contributions from other science bodies about similar subject.

All communications should be addressed to the director or to the librarian of the Institute.

The Institute for Optical Research

Tokyo University of Education

400, 4-chome, Hyakunin-machi, Sinjuku-ku, Tokyo, Japan

Printed by
Kokusai Bunken Insatsusha
Chiyoda-ku, Tokyo.

SCIENCE OF LIGHT VOLUME 4. NUMBER 2, 1955

Automatic Recording Double Beam Infrared Spectrophotometer

Keiei KUDO

Institute for Optical Research, Tokyo University of Education

(Received September 13, 1955)

An automatic recording double beam infrared spectrophotometer has been built guided by the papers of Baird, White and etc. Prism is of 60° Littrow mounted rock salt 8×6 cm faces. A comb with eight teeth is used as attenuator. Scannig speed varies from 15 minutes to 8 hours, response time is from 7 sec. to 21 sec. for full scale. Percentage of transmission is recorded with an accuracy of ±1% in error, and wave length with that of ±0.01 μ.

Linearity, scanning speed, gain and filter, slit width and resolution are described in detail.

1. Introduction

The double beam infrared spectrophotometer is known to be very convenient for direct measurement of the percentage of transmission, and has been studied by many workers[1)-14)].

At the institute, a spectrophotometer of this type using a thermocouple has been constructed and its resolution examined.

2. Selection of Chopping Frequency

Chopping frequency should be chosen with due consideration to the characteristics of the thermocouple used. With the equilibrium temperature θ_∞ of hot junction of the thermocouple, if the infrared radiation is suddenly intercepted,

1) J. D. Hardy and A. I. Ryer: Phys. Rev. **55** (1939) 1112.
2) W. M. Avery: J. Opt. Soc. Amer., **31** (1941) 633.
3) F. Lehrer: Zeits. f. Tech. Phy. **23** (1942) 169.
4) E. B. Baker and C. D. Robb: Rev. Sci. Instr. **14** (1943) 362.
5) G. B. B. M. Sutherland and H. W. Thompson: Trans. Faraday Soc. **41** (1945) 171.
6) R. F. Wild: Rev. Sci. Instr. **18** (1947) 436.
7) N. Wright and L. W. Herscher: J. Opt. Soc. Amer. **37** (1947) 211.
8) W. S. Baird, H. M. O'Bryan, G. Ogden, and D. Lee: J. Opt. Soc. Amer. **37** (1947) 754.
9) A. Savitsky and R. S. Halford. Rev. Sci. Intsr., **19** (1948) 155.
10) J. D. White and M. D. Liston: J. Opt. Soc. Amer. **40** (1950) 29.
11) D. F. Horning, G. E. Hyde and W. A. Adock: J. Opt. Soc. Amer. **40** (1950) 497.
12) F. M. Rugg, W. L. Calvert and J. J. Smoth: J. Opt. Soc. Amer. **41** (1950) 32.
13) R. A. Oetjen and L. C. Roess: J. Opt. Soc. Amer, **41** (1951) 203.
14) Catalogue of Hilger & Watts Ltd. May 1954.

the temperature $\theta(t)$ after the lapse of t sec. can be expressed by

$$\theta(t)=\theta_\infty e^{-t/\tau}\,, \tag{1}$$

decreasing exponentially from θ_∞ where τ is the time constant of the thermocouple, Then, if the junction at $\theta(t_1)=\theta_1$ is suddenly irradiated, the temperature goes up exponentially, approaching θ_∞ as given by the following equation.

$$\theta(t)=\theta_\infty-(\theta_\infty-\theta_1)e^{-(t-t_1)/\tau} \qquad (t\geqq t_1) \tag{2}$$

Substituting the temperature $\theta(t)$ by the corresponding thermoelectric force $E(t)$, we have for the equations (1) and (2)

$$E(t)=E_\infty e^{-t/\tau} \tag{1'}$$

$$=E_\infty-(E_\infty-E_1)e^{-(t-t_1)/\tau} \qquad (t\geqq t_1) \tag{2'}$$

Now, if the radiation is chopped by the sector into f c.p.s., and light signals of square wave are given to the thermocouple, the thermoelectromotive force of the thermocouple $E(t)$ increases exponentially according to (2') during $1/2f$ sec. while the beam is on, and decreases exponentially according to (1') during $1/2f$ sec. while the beam is off, and produces saw-toothed waves with the period of $1/2f$ sec. Illustration of the chopped light and the train of electromotive forces from the start of the sector is shown in Fig. 1. In a stationary state, if one of the minima is taken as the origin of time as shown in the figure, the thermoelectromotive force function becomes by calculation as follows:

$$E(t)=E_\infty\{e^{-1/2f\tau}/(1+e^{-1/2f\tau})\}e^{-t/\tau} \qquad (-1/2f\leqq t\leqq 0) \tag{3}$$

$$=E_\infty[1-\{1/(1+e^{-1/2f\tau})\}e^{-t/\tau}] \qquad (0\leqq t\leqq 1/2f) \tag{4}$$

Using these two equations, we have for the effective a.c. output $E_{\text{a.c.}}$ concerning the fundamental wave

$$E_{\text{a.c.}}=0.45E_\infty/(1+4\pi^2f^2\tau^2)^{1/2} \tag{5}$$

The relation between $E_{\text{a.c.}}/0.45E_\infty$ and $f\tau$ is shown in Fig. 2. Perceiving from the figure, when $f\tau$ is smaller than 0.16, the effective output becomes large and appreciable variation of the output is caused by the fluctuation of $f\tau$.

For the reason as will be mentioned later, an infrared spectrometer with such an a.c. thermocouple needs for its pre-amplifier a special transformer which is economical in that it can be made smaller in size in inverse proportion to the chopping frequency. And as for the other amplifiers, the higher the f.c.p.s. is, the easier they will be made. Hence, viewed from the electric system only, it is desirable to have f.c.p.s. as high as possible. But amplification of the amplifier is restricted by the Johnson noise level of resistance of the thermocouple

and its lead wire. Accordingly, it is not advisable to increase amplification in order to make up for the fallng off of output of the thermocouple due to large $f\tau$. On the other hand, if f.c.p.s. is made too low, the output from the thermocouple will be large, but at the same time, a large transformer will be

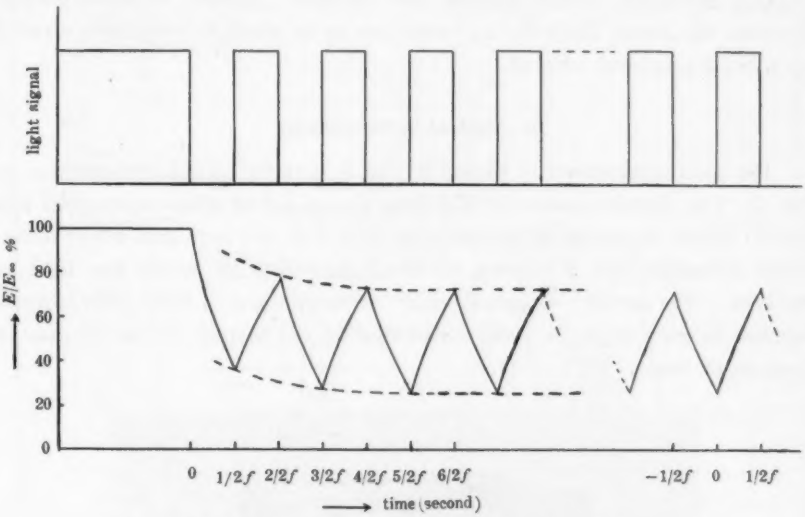

Fig. 1. Schematic diagram showing the response of thermocouple.

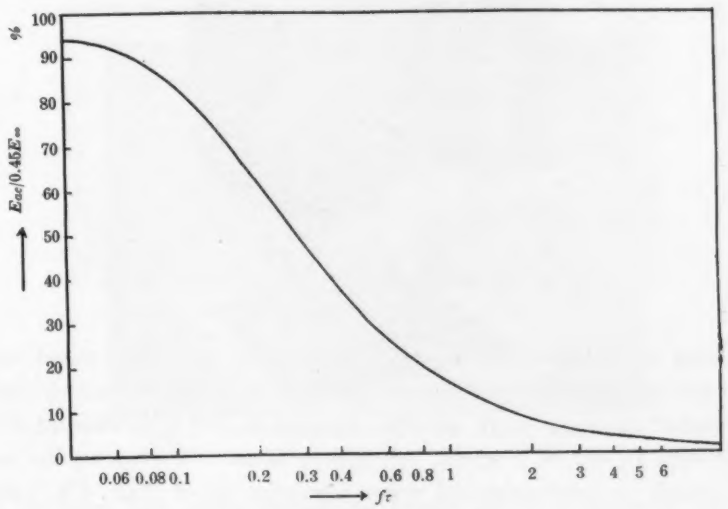

Fig. 2. $E_{ac}/0.54E_{\infty}$ vs. $f\tau$.

required and the amplifying will become troublesome. Therefore the chopping frequency f c.p.s. should be chosen by taking all three of the time constant, amplifier and output collectively into consideration.

Since the time constant of the assigned thermocouple was about 0.03 sec., the chopping frequency, which satisfies the condition $ft \leqq 0.16$, is below 5 c.p.s. However, the lowest figure for a.c. amplifiers to be made to function is about 5 c.p.s. So, 5 c.p.s. was adopted.

3. Optical Arrangement

The spectrophotometer is shown is Fig. 3, and its optical arrangement in Fig. 4. The infrared source S is carbon silicate rod of 4 mm in diameter and 5 cm in length, heated at about 1200°C by 40 V 8 A. and kept in a tubler water-cooled enclosure with a window of 10×30 mm, through which the light is observed. The source was made easily replaceble and a relay with bi-metal attached to the wall of the water cooler cuts off the heating current in case of stoppage of water.

Fig. 3. Complete spectrophotometer.

Facing the optical source, a pair of plane mirrors M_1, M_2 are placed, which reflect the light into two directions onto two spherical mirrors M_3 and M_4 forming two image of the source at W_1 and W_2. Between M_3 and W_1 a standard cell C_1 and between M_4 and W_2 a sample cell C_2 are placed. The spaces are made large enough to accommodate the largest absorption cell of 17 cm. Fig. 5 shows the part of the optical source and the position of the cells with cover removed.

W_1 is a comb-shaped attenuator, consisting of eight teeth. Each tooth is 3 mm in width at its base, 106 mm in length, and 0.5 mm in thickness. Its cross section is of trapezoid. W_2 is a subsidiary attenuator.

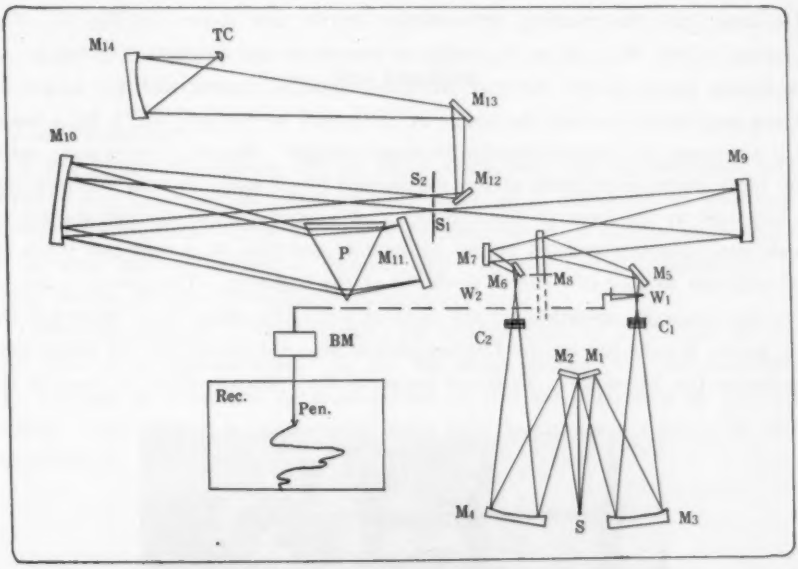

Fig. 4. Optical arrangement.

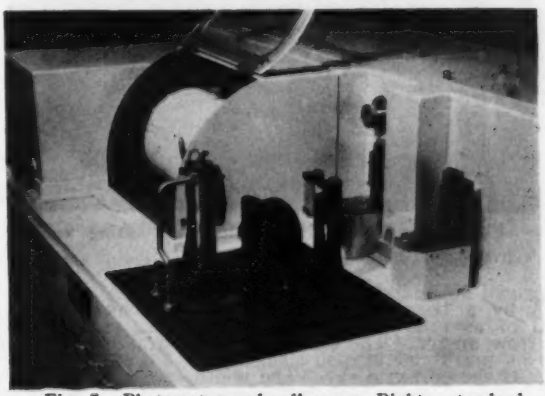

Fig. 5. Photometer and cell space. Right: standard cell, Left: absorption cell.

The beam that passes through the sample cell C_2 is made to fall on a spherical mirror M_9 by reflections of two mirrors M_6 and M_7. The other beam

through the standard cell C_1 is also made to fall on the same spherical mirror first by a mirror M_5 then by a semi-circular mirror M_8 which comes intermittently by rotation of 5 c.p.s. on its plane into the path of the first beam to intercept it so that the two beams fall alternately on the spherical mirror at 5 c.p.s. The attenuator and the rotating semi-circular mirror are shown in Fig. 6. The spherical mirror M_9 is 45 cm in radius of curvature and projects the image of the optical source on the entrance slit S_1 of bilateral opening with the height of 24 mm and curved so that the image of S_1 formed on the exit slit S_2 by a beam of 2 μ through the monochromator becomes straight. M_{10} is a collimator, with the focal distance of 50 cm and is parobolized 7° off axis. As the entrance slit S_1 is placed at the focus of this collimator, the beam coming through the slit is made approximately parallel by the collimator, and falls on a rock salt prism of 60° with the surface of 8×6 cm produced at the Institute. This prism is set to give the minimum deviation for the light of 9 μ. The beam once dispersed by the prism is reflected by the Littrow mirror M_{11}, redispersed by the prism and returns to the collimator. Thus the image of the entrance slit S_1 is formed on

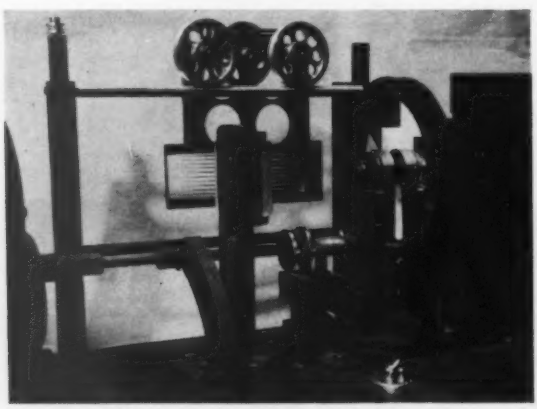

Fig. 6. Comb shaped attenuator and rotating semi-circular plane mirror.

the exit slit S_2 by a beam of certain wave length which can be varied by the turn of the Littrow mirror. The exit slit is of a straight edge, and housed on the same table as the entrance slit. The width of the former is made equal to that of the latter by bilateral adjustment by means of a screw.

The alternating beams after passing through the exit slit and reflected by two mirrors M_{12} and M_{13} impinge on M_{14} which is an elliptic mirror of about 3° off axis with the reduction ratio of 1/9, and projects the beam on the thermocouple

TC. As to the thermocouple, its receiving surface is 0.4×2.2 mm, d.c. sensitivity $4\,\mu V/\mu W$, time constant about 0.03 sec. and resistance about 2Ω. It is sealed in vacuum with a KBr window.

4. The Amplifier

a) *The preamplifier*

If the alternating beams are of equal intensities, the thermocouple will produce a d.c. electromotive force. But, if there is a difference in intensity, generated electromotive force will be saw-toothed, and it, is what is required for the present spectrophotometric measurement, and a special transformer is needed to pick up this alternating electromotive force.

Detectable intensity of light signals thus produced can be as feeble as the noise level of a thermocouple. As for the noise caused by a thermocouple, there are Johnson noise and the noise caused by thermal fluctuation at the hot junction. The former is predominant with the electromotive force e as expressed[15][16] by

$$\langle e^2 \rangle_{av} = (1.28 \cdot 10^{-10})^2 \, R\Delta f \quad (\text{volt})^2 \quad (\text{at } 300^\circ\text{K})$$

where, R is the resistance of the thermocouple including the lead wire, and Δf the frequency band width which passes through the amplifier. Now, if, $R = 2.5\Omega$, and $\Delta f = 2$. c.p.s, e will become $2.9 \cdot 10^{-10}$ volt. In this case, unless the signals are strong enough to produce more than 2.9×10^{-10} volt, they can not be discriminated from the noise. The electromotive force which is produced on the secondary side of the transformer is to be given to a tube to be amplified, but there is a noise of the tube which may be so strong as to damp the signals rendering the transformer useless. Of the tube noises, what is most troublesome for low frequency of about 5 c.p.s. is the Fricker noise which corresponds to several $M\Omega$ of the Johnson noise resistance. This noise level is about 1.000 times as large as that of the thermocouple of 2.5Ω. Accordingly, the signal voltage of Johnson noise level should be stepped up more than 1.000 times before it is given to the first tube of the preamplifier to make the light signals detectable. From the reasons given above, the secondary of the input transformer was made to have about $10\,M\Omega$ of impedance.

15) H. Nyguist: Phys. Rev. **32** (1928) 110.
16) L. C. Roess: Rev. Sci. Instr. **16** (1945) 172.

Besides the Flicker noise, the tube has the noise which is caused by sudden emission of groups of electron from the filament, and is often larger than the Flicker noise. This noise, however, can be eliminated by choosing a tube and eventually a tube 1620 was used as the first tube.

The input transformer was very sensitive to the electro-magnetic disturbance from outside. Therefore, it was shielded to about 120 db. and the first tube was placed adjacent to it. These were suspended with springs to damp mechanical disturbances. The distance between the thermocouple and the preamplifier was made as short as possible, about 15 cm, paying special attention to the effect of electro-magnetic induction.

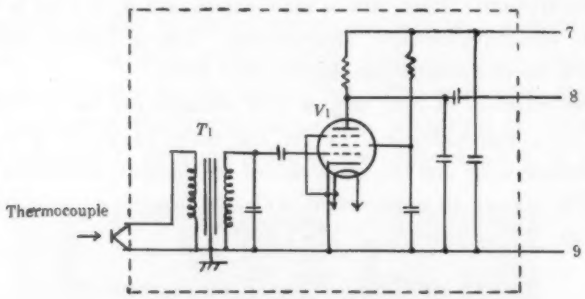

Fig. 7. Pre-amplifier.

The grid of the first tube was floated by a condenser as shown in Fig. 7, for the use of a battery for the bias not only causes noise as mentioned by White and Liston[10] but also requires frequent replacement.

b) *The Main Amplifier, Synchronous Rectilifier, Filter, Servo Amplifier and Power Source.*

As shown in Fig. 8, the main amplifier is a four stage amplifier with current

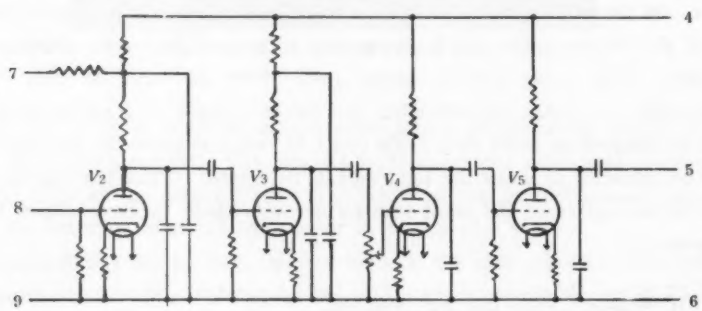

Fig. 8. Main amplifier.

negative feedback in each stage, and the values of the coupling and bias condensers between each stage were determined to make the frequency band width about 2 c.p.s. Q value of this amplifier was about 1.7. The frequency band width was decided to be 2 to make the best of the power supply of considerable fluctuation in frequency. A band narrower than 2 c.p.s. would have necessitated a special frequency stabilizer.

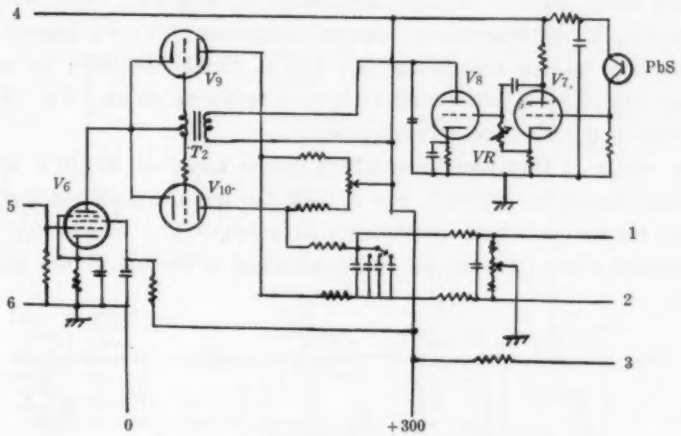

Fig. 9. Synchronous rectifier and filter.

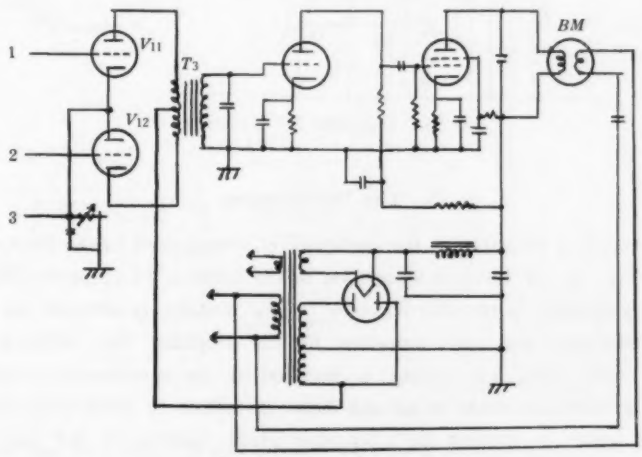

Fig. 10. Servo-amplifier.

As for the sychronous rectifier, a light from a midget lamp, chopped at 5 c.p.s., is projected on a PbS cell to send synchronized signals which are

amplified by the tube V_8 (Fig. 9). The phase of the amplified signals can be varied by choosing the value of VR. Hence, by giving the synchronized signals to two tubes V_9 and V_{10}, which serve as a pair of switches, and adjusting the phase to that of the input signal from V_4, the output signals are synchronously rectified. This circuit is similar to Schuster's[17].

The output of light signals thus rectified becomes a direct current by means of a filter and is given to 50 c.p.s. modulators V_{11} and V_{12}. Here, a.c. output corresponding to the difference of internal resistances of V_{11} V_{12} appears on the secondary side of the transformer T_3, and is further amplified by a servo amplifier, and supplied to the control coil of a balancing motor. Fig. 10 shows the circuits of the filter and serve-amplifier.

The voltage of B-source was stabilized in the range of 80–110 V with the arragement shown in Fig. 11. For filament heating, the stabilized source was used only for the first tube oscillating[10] at about 80 kc. Satisfactory results were obtained without paying any special attention to the rest of the tubes for heating.

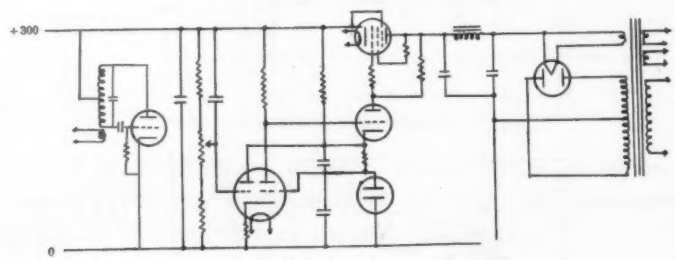

Fig. 11. Stabilizer for B voltage.

5. The Performance

The recording principle of the spectrometer is explained by the block diagram shown in Fig. 12. If there is absorption in the sample, 5 c.p.s. saw-toothed a.c. voltage is generated in the thermocouple. This voltage is stepped up by the input transformer, and then amplified by the amplifier into sinusoidal wave of a few volt. This a.c. voltage is rectified by the synchronous rectifier and given to the servo amplifier to set the motor in motion to balance the intensities of the two beams by moving the attenuator which coupled to the axis of the motor through a set of gears. The movement of the attenuator is transmitted to the recording pen. And if the motor operates, the attenuator always moves

17) N. A. Schuster: Rev. Sci. Instr. **22** (1951) 254.

towards the direction which will compensate the intensity difference of both beams.

The image of the edge of the attenuator is first adjusted, without the cells, just to screen the entrance slit to indicate 100%. When the cells are set, the subsidiary attenuator is used to compensate for the difference in absorption of

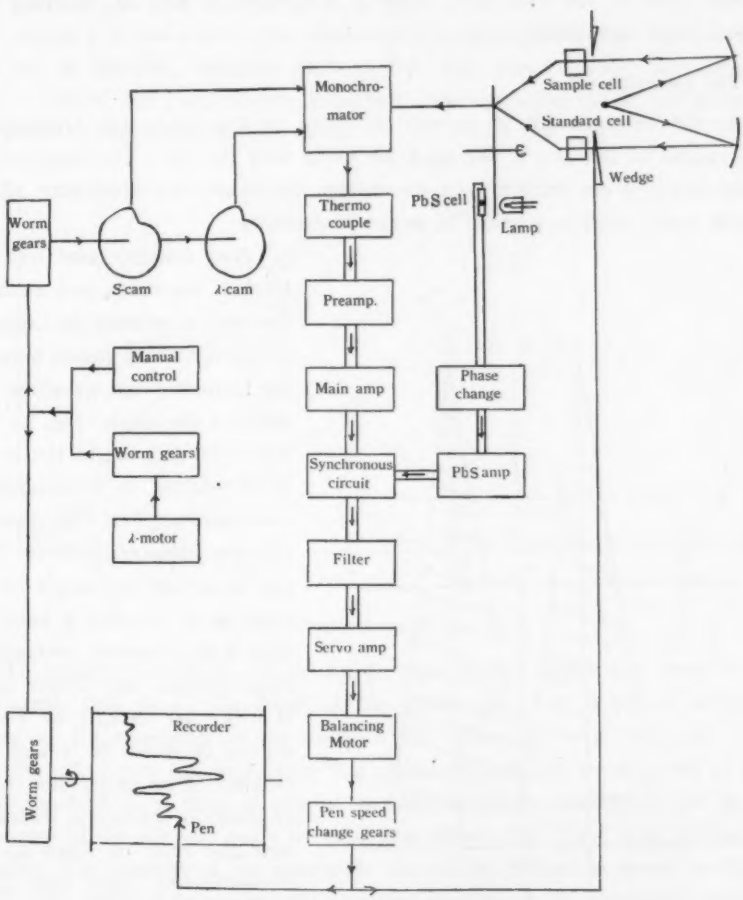

Fig. 12. Block diagram.

windows of the two cells. If the attenuating rate is proportional to the travelling distance of attenuator, the pen will record the transmission percentage of the sample.

Through a set of reducing gears, a wave length scanning motor turns the

recordinge drum, the wave length cam and the slit cam. The slit cam changes the widths of the slits, and the wave length cam turns the Littrow mirror changing the wave length for the pen to draw the curve of transmission percentage of the sample. If the attenuator is placed at the focus of the spherical mirror M_3 (Fig. 4), its image should be formed clearly both on the entrance and on the exit slits. This is a convenient way of checking the correctness of the optical system.

a) *The linearity.*

As the entrance slit is curved, the edge of the comb was arranged so that images of the tips of the teeth are along with the slit. The emissivity of optical source is not uniform over its surface, therefore, the attenuator should have as many teeth as possible to secure its linearity.

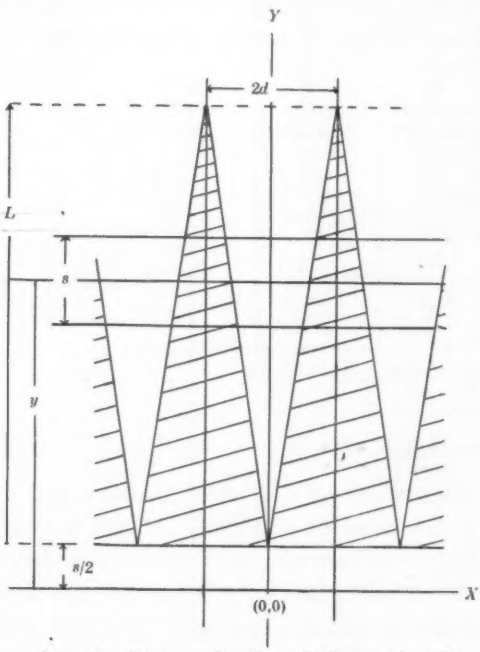

Fig. 13. Diagram for the calculation of comb linearity.

Now consider two adjacent teeth of the comb, and examine the relation between the intensity of the light that passes between the teeth and the travelling distance of the comb. Fig. 13 is a schematic diagram of the attenuator referred to a rectangular coordinates. Let the distance between adjacent teeth at their tips be 2d and the length of one tooth be L. Consider a beam of light with a narrow rectangular cross section, two longer sides of which are parallel to x-axis, and let its width be s and the ordinate of its center line be y as shown in the figure. Consider next the ratio of I and I_0, the intensities of light that goes through with and without the attenuator respectively. Assuming that the intensity distribution is uniform, following relations are obtained from simple calculations:

$$I/I_0=(1/2L)y^2 \quad (s\geqq y\geqq 0)\,, \qquad \text{for the beam at the bottom;}$$

$=(1/L)y-s/2L \quad (L\geqq s\geqq s)$;

$=1-(1/2sL)(L+s-y)^2 \quad (L+s\geqq y\geqq L)$, for the beam at the edge;

or if we put $s/\mu=\alpha$, $y/L=\eta$,

$I/I_0=(1/2\alpha)\eta^2 \quad (\alpha\geqq\eta\geqq 0)$,

$=\eta-(1/2)\alpha \quad (1\geqq\eta\geqq\alpha)$,

$=1-(1/2\alpha)(1+\alpha-\eta)^2 \quad (1+\alpha\geqq y\geqq 1)$.

Now taking α as parameter, the relation of I/I_0 vs. η is shown in Fig. 14. If α can not be ignored, linearity between 0% and $100\alpha/2$%, and that between $100\{1-(\alpha/2)\}$% and 100% become imperfect. And the larger the α, the narrower the range in which the linearity holds.

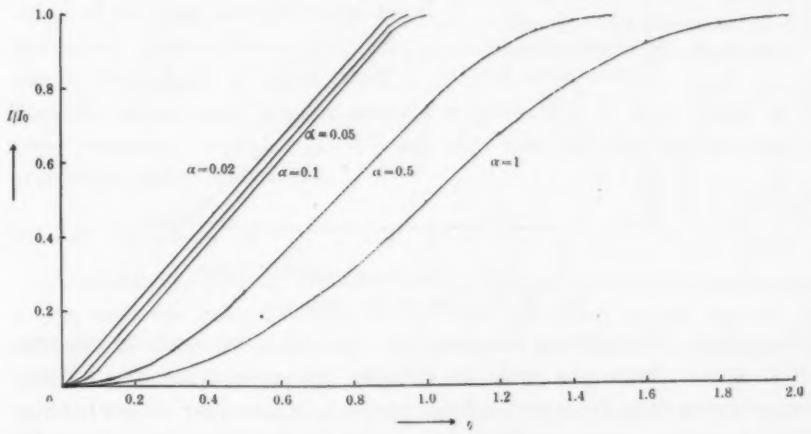

Fig. 14. Graph showing I/I_0 vs. η.

To make α negligible, the attenuator was placed where the beam is the narrowest, that is, at the focus of the mirror M_3 (Fig. 4) which forms the image of the attenuator on the entrance slit. Thus the beam with the width s in Fig. 13 is now the very beam that passes through the entrance slit of s in width, and if L is long α can be entirely ignored. Correction due to the curvature of the slit was made by assigning 106 mm for L and 8 for the number of teeth. The linearity of the attenuator was almost perfect as shown in Fig. 15 which was obtained by reading the travelled distance of the attenuator and the output of the amplifier, the linearity of which being examined beforehand.

b) *The scanning speed.*

The factors which determine the scanning speed are the sensitivity of detector, intensity of radiation and slit width, filter, response time, and width

of absorption band, among which the latter three are of importance. The response time should not be too short, otherwise, the attenuator might overshoot then move back and forth, and besides, it might oscillate irregularly responding

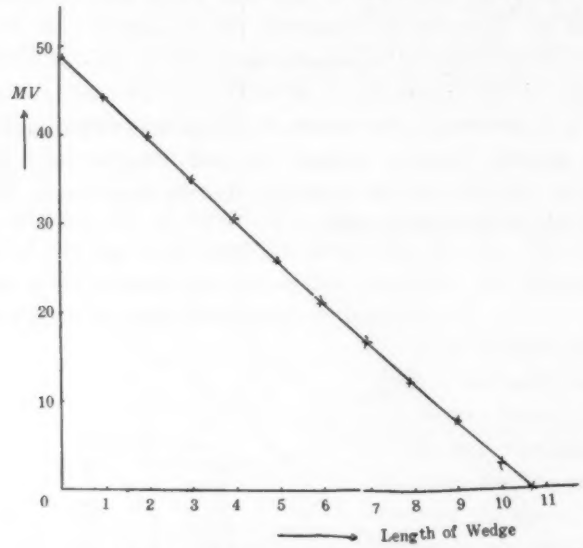

Fig. 15. Linearity of the attenuator.

to the noises. The response time used was 7,14 and 21 sec., and its alteration within narrow range was made by changing the value of the filter. With a given response time, the scanning speed should be adjusted for the pen to record a true absorption curve over the whole range of the confronted band. The more complex the spectra, the slower the speed should be.

If the response time is made considerably large, the pen will not respond to noises, Accordingly, even if the slit is made narrow, and the gain of the amplifier increased, the noises will not become conspicuous in the transmission curve. Signals received never fail to work the pen, so by slowing down the scanning speed to meet the response time, the pen follows the true transmission percentage. Therefore, in examining weak absorption bands, speed of both pen and scanning should be made slow, and if the slit is made narrow, resolution will be heightened. The Littrow mirror was made to scan from 1 to 15 μ in 15 minutes to 8 hours automatically. It can be also operated by hand.

c) *The gain and the filter.*

For recording, zero method was used. The gain and the filter should have appropriate values for satisfactory recording. If the gain of the amplifier is

increased and the filter is made large, turning of the balancing motor becomes faster, and the time lag caused by the filter would make the pen overshoot the mark. On the other hand, with a small filter, although the pen would respond accurately, noise becomes troublesome and the reproducibility becomes poor, and if the gain is reduced too much, the output would become deficient for the pen to respond, independently of the size of the filter.

When the scanning speed, the response time and the width of the slit are given, the most appropriate values of the gain and filter can be determined in the following way. The pen is first placed to point 100%. Then the sample beam is intercepted for a while. Fig. 16 is a record of the above operation, in which (*a*) is when both gain and filter are too large, (*b*) appropriate and (*c*) insufficient.

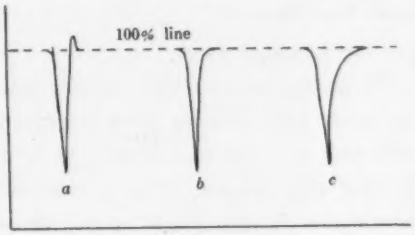

Fig. 16. Gain adjustment
a) too much gain b) proper gain
c) not enough gain.

d) ***The slit width.***

Theoretically speaking, resolving power of a spectrophotometer is determined by the dispersion and base length of the prism, the width of the slit and the focal length of the collimator. But in practice, it is influenced by the detecting method of the radiation energy. High resolution for a given slit width can be obtained only by well thought-out combination of characteristics of the thermocouple, gain of the amplifier, response time, scanning speed, etc. However, the main factor of influence is afterall the width of the slit. Although the narrower the slit, the higher the resolution, the detecting system may accompany troublesome noise. The width of the slit should therefore be determined by taking the detection system into consideration.

Arragement of detecting system can be varied to a great extent. The arrangement, excepting the scanning speed, adopted for recording spectrum over the whole region dispersed by the prism is as follows: The light beam on the sample cell side is screened and the pen is brought to record 0%. The gain and the filter are then adjusted to give a slight noise. Next, changing the system into single beam recording type, the width of the slit is set to give a uniform output over the range of 1~15 μ. Changing the system back to double beam recording, spectra of polystyrene and NH_3 were recorded to settle other conditions.

The arrangement will be wholly different if a different slit width is wanted. Limiting the number of arrangements to three, a slit lever is provided to give three regular slit widths. If the resolving power is not essential, a wider slit, lower gain, smaller filter and faster speeds for the pen and scanning are for quick recording.

e) *The resolving power.*

In oder to examine the resolving power, adequate samples should be used. As solids and solutions have comparatively wide absorption bands, gases are preferred, and analytical data[18)19)20)] by a grating spectrometer can be referred to. For this purpose, NH_3 is most suited with its 10.5 μ absorption band for examination in the region given by a rock salt prism. Fig. 17 shows a spectrum in the region of 1–15 μ of NH_3 which was recorded at a scanning speed of 50 minutes. As mentioned before, resolution depends on the coordination of detecting conditions. Fig. 18 shows four spectra of the 10.5 μ NH_3 band (ν_2 band) recorded under different conditions. The separations of the closest resolved

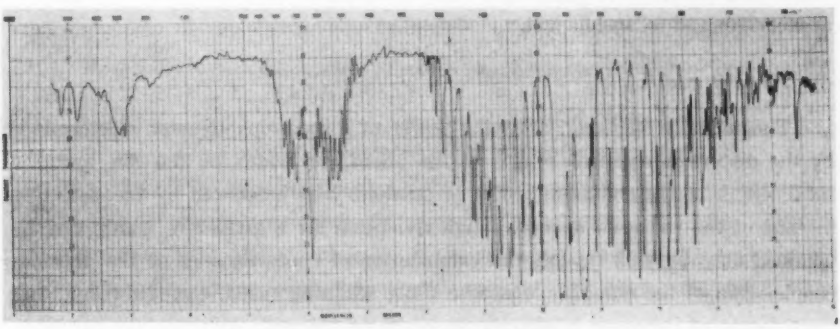

Fig. 17. Ammonia spectrum.
Scanning speed, 50 minutes. Cell length, 10 cm.

pairs of lines are indicated on each curve. On the fourth curve resolving power increases than on the third. In the region between 10.4 and 10.8 microns many lines, which are distinctly separated in a grating spectrometer and quadruple monochromator[21)], are merely separated. From the separation of these lines resolution at 10.5 μ is considered to be about 1.5 cm^{-1}. In the P-branches of $\nu_2(1^+-0^-)$, it is found that lines which are above J=2 are distinctly separated

18) H. Y. Sheng, E. E. Barker and D. M. Dennison: Phys. Rev. **60** (1941) 786.
19) Oetjen, Kao and Randall: Rev. Sci. Instr. **13** (1942) 515.
20) A. R. Downe, M. C. Magoon, Thomasine Purcell and Bryce: J. Opt Soc. Amer. **43** (1953) 941.
21) A. Walsh: J. Opt. Soc. Amer. **42** (1952) 496.

by the values of K. Resolutions at 12.5 μ is less than 1 cm^{-1}. These resolutions approached the Rayleigh limit.

Fig. 19 shows the spectrum of 1. 2. 4. trichlorobenzene in liquid state which

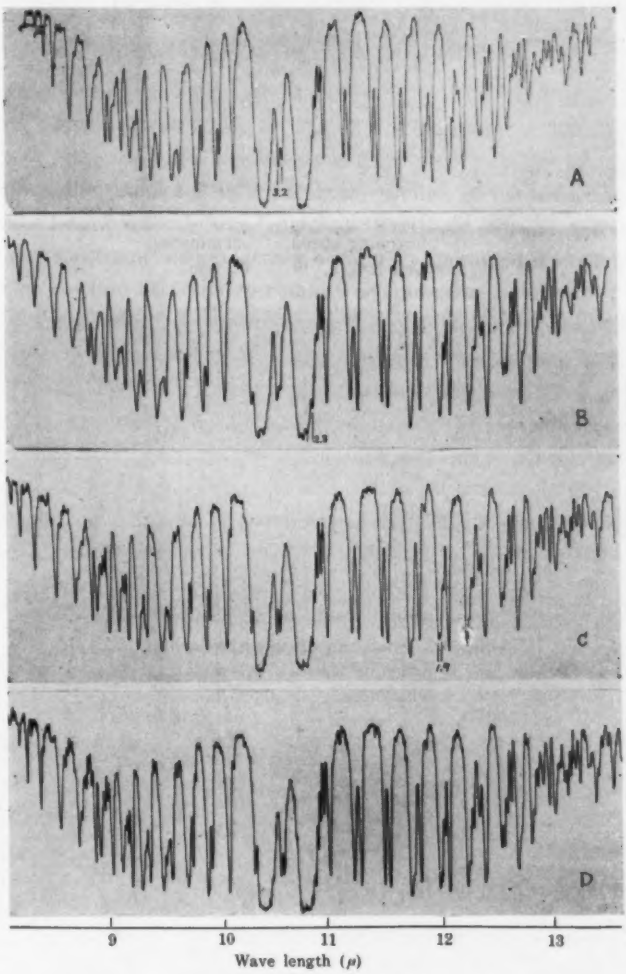

Fig. 18. Ammonia 10.5 μ band under various conditions.

	Scanning speed	Response	Gain
A	3.8 min/μ	7	4
B	8	14	5
C	15	21	8
D	30	21	9

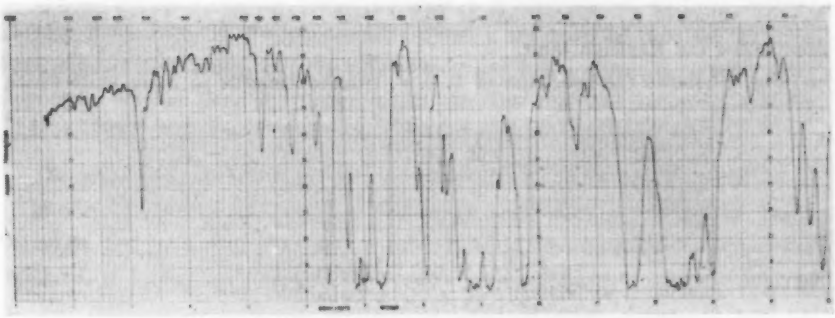

Fig. 19. Spectrum of 1. 2. 4 trichlorobenzene.
Scanning speed, 40 minutes.
Cell length, 0.1 mm.

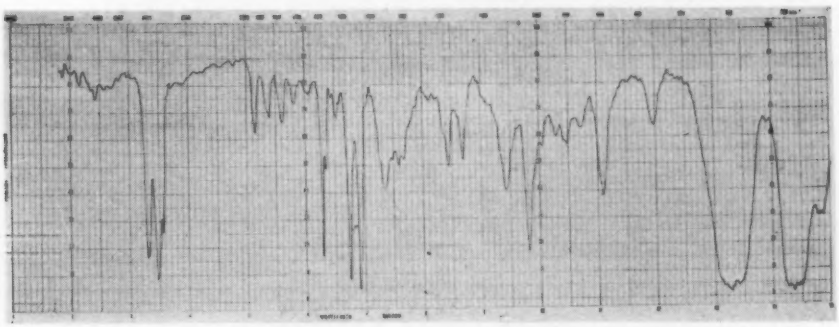

Fig. 20. Spectrum of polystyrene film.
Scanning speed, 30 minutes.
Thickness 0.085 mm.

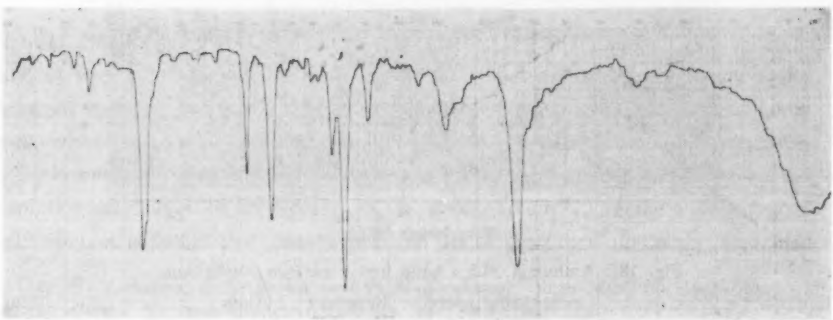

Fig. 21. Spectrum of benzene liquid.
Scanning speed 30 minutes.
Cell thickness 0.01 mm.

has many narrow absorption bands. Resolution is satsfactory.

The resolution in short wave length region can be examined with 6 μ NH_3 band and spectra of polystyrene film and benzene. As shown in Figs. 20 and 21, they are almost the same as those of Baird[8], White[10] and Hilger Ltd.[14].

f) *The scattered light and others.*

The transmission percentage agreed perfectly with the scale of the recording paper up to 14 μ, but above 14.5 μ, it was off the scale by 2% and 5% at 14.5 μ and 15 μ respectively owing to the scattered light caused chiefly by the blur on the surface of the prism and to some extent by that of the reflecting mirrors. Error in wave length reading was ± 0.01 μ. The blur impairs resolution and purity of the spectrum, makes strong absorption appear weak. Cleanliness of surfaces is an absolute necessity to obtain true transmission curve. Filter was not used, but the effect of the scattered light was kept down to minimum by encasing the spectrometer in an air-tight chamber with dehumidifying agents P_2O_5 and NaOH. Fig. 22 (1) shows the transmission curve of glass for the examination of the scattered light. Reproducibility is especially important in quantitative analysis. Fig. 22 (2) shows reproducibility of the transmission curve by the mylor film. Error is within 1%. Cells were the only parts exposed to outer air. Effects of water vapour and CO_2 in air were not observed as seen in Fig. 22 (3).

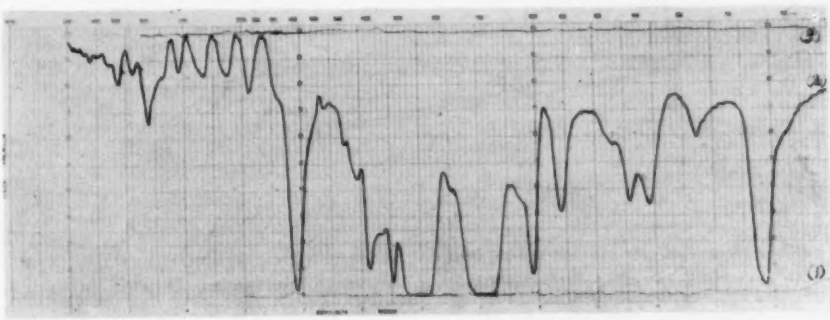

Fig. 22. (1) Transmission curve of glass plate.
(2) Two runs of mylor film (25 minutes).
(3) 100 percent transmission curve.

Acknowledgement

The author wishes to express his sincere thanks to Prof. Yoshio Fujioka, Director of the Institute, for his valuable advice and encouragement, to Dr.

Ryumyo Onaka for the design of the input transformer, to Mr. Masatoshi Nakamura for the construction of the thermocouple, and to Mr. Tadashi Miyazaki, in particular, for the construction of the amplifiers.

This research was carried out with financial support of the Ministry of Education.

On the Aberration of Optical System Used in Infrared Spectrometer

Keiei KUDO

Institute for Optical Research, Tokyo University of Education

(Received September 13, 1955)

Aberration of optical system in infrared spectrometer is discussed by using Seidel's aberration formula.

Result shows that, when a collimating mirror is used off-axially, a paraboloidal mirror is better than a spherical mirror, and when a spherical mirror is used, optical arrangement should be carefully planned and set.

1. Introduction

For infrared spectrometers, the aberration of optical system is a problem to be solved. Fig. 1 shows a schematic arrangement of a monochromator of an infrared spectrometer. S_1 and S_2 are the entrance and exit slits respectively, C

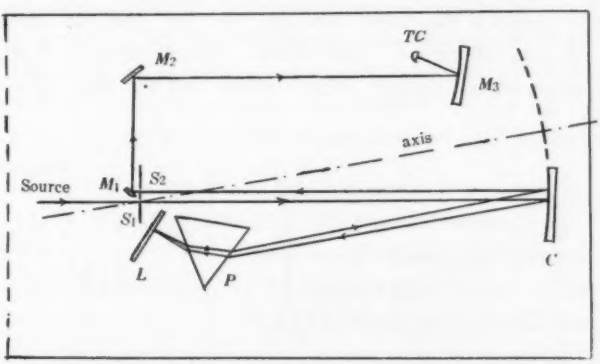

Fig. 1. Optical arrangement of infrared spectrometer. S_1, S_2, entrance and exit slits; C. collimator; P, Prism; L, Littrow mirror; M_1, M_2, plane mirrors; M_3, thermocouple mirror; TC, thermocouple.

the reflecting mirror called a collimator, P the prism, and L the plane mirror called the Littrow mirror. The collimator is used to make the light from the entrance slit placed in its focal plane into parallel rays and to project it onto the prism. The light which is dispersed by the prism is reflected by the Littrow mirror and dispersed again by the prism. Receiving this redispersed light, the

collimator forms spectrum on its focal plane. The exit slit is used to take out of the spectrum only the light of a certain wave length.

If monochromatic rays of light coming through the entrance slit are made parallel by the collimator, those dispersed will be also parallel provided that the prism is sound. In this case, the image of the entrance slit on the focal plane of the collimator will be very distinct. In other words, if the collimator is free from aberration, the light emitted from the entrance slit is focused on the exit slit. This is true only for paraxial rays. However, following special conditions in infrared spectrometer should be considered. Namely, "infrared energy is weak, and sensitivity of the detector is generally low." Therefore, in order to increase the available energy as much as possible, a collimator with small relative aperture, large prism and long slit should be used. Moreover, the collimator should be used off-axially. But this would redouble both spherical and axial aberrations. Since a spherical or a paraboloidal mirror is generally used as a collimator, question arises which one will give better results. Further, as the position of the stop, that is the prism, affects the aberrations, consideration should be given to the position of the prism.

For correct solution of these problems, a trigonometrical ray tracing should be performed. Seidel's aberration formula does not give an exact answer, nevertheless, it puts us on the right track. Optical system of an infrared spectrometer seems exceed slightly Seidel's region and the fifth order aberration

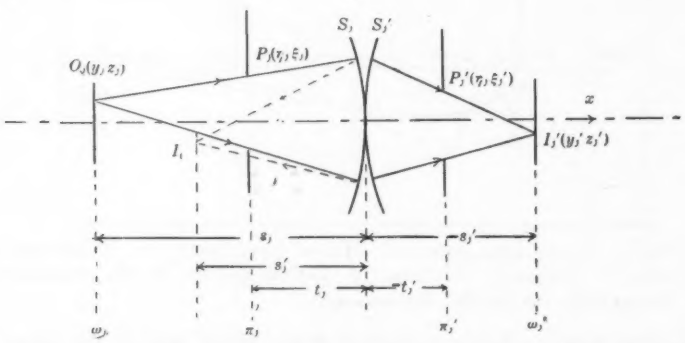

Fig. 2. Diagram showing the reflecting surface and reflcted rays inverted by the osculating plane at the apex of the mirror.

might be required to be taken into consideration. However, in this paper, the problem is limited to Seidel's region going into no further than the third order terms.

2. Expression for the Aberration of Collimator

According to Schwarzchild[1] and Born[2], aberration of a reflecting mirror can easily be expressed. Let us assume that the optical axis of a reflecting mirror is on X-axis of a rectangular co-ordinate system. In discussing a reflecting mirror, it is convenient to picture an inverted reflecting surface and reflected rays right behind the apex of the mirror as shown in Fig. 2.

The equation expressing the j-th reflecting surface is given by

$$X_j=a_j-\frac{Y_j^2+Z_j^2}{2r_j}-\frac{(Y_j^2+Z_j^2)^2(1+b_j)}{8r_j^3} \tag{1}$$

Where a_j is the X co-ordinate of the apex of the mirror, r_j is the radius of curvature of osculating sphere at the apex, b_j is the coefficient of deformation and its value is given as follows

$$\begin{array}{ll}\text{spherical mirror} & b_j=0\\ \text{paraboloidal mirror} & b_j+1=0\,.\end{array} \tag{2}$$

The distances along X-axis are measured from the apex and are given positive signs when measured in the direction against the light. The radius of curvature is positive when the reflecting surface facing incident rays is concave. If a ray starts from an object $0_1(s_1, y_1, z_1)$ and intersects the entrance pupil π_1 at the point $P_1(t_1, \eta_1, \zeta_1)$, the exit pupil π_j' at point $P_j'(-t_j', \eta_j', \zeta_j')$ and the image plane w_j' at $0_j'(-s_j', y_j', z_j')$, the aberrations produced by the mirror system are given as follows.

$$\begin{aligned}(y_j'-\beta y_1)/s_1\beta=&\eta_1(\eta_1^2+\zeta_1^2)B+2y_1(y_1\eta_1+z_1\zeta_1)C+\eta_1(y_1^2+z_1^2)D\\&-y_1(y_1^2+z_1^2)E-\{y_1(\eta_1^2+\zeta_1^2)+2\eta_1(y_1\eta_1+z_1\zeta_1)\}F\\(z_j'-\beta z_1)/s_1\beta=&\zeta_1(\eta_1^2+\zeta_1^2)+2z_1(y_1\eta_1+z_1\zeta_1)C+\zeta_1(y_1^2+z_1^2)D\\&-z_1(y_1^2+z_1^2)E-\{z_1(\eta_1^2+\zeta_1^2)+2\zeta_1(y_1\eta_1+z_1\zeta_1)\}F\end{aligned} \tag{3}$$

Where β is a lateral magnification, and given by

$$\beta=(-1)^j s_1's_2'\cdots s_j'/s_1s_2\cdots s_j \tag{4}$$

B, C, D, E, F are coefficients of aberration and given respectively as

$$B=\frac{s_1^3}{(s_1-t_1)^3}\sum_{j=1}^{j}\left(\frac{h_j}{h_1}\right)^4\left(\frac{b_j}{r_j^3}+\frac{K_j^2}{r_j}\right)$$

1) Karl Schwarzchild: "Untersuchungen zur Geometrischen Optik. Abhandlungen der Königlichen Gesellshaft der Wissenschaften zu Göttingen." **4** (1905).

2) M. Born, "Optik." (Julius Springer, Berlin. 1933) p 73–86.

$$
\begin{aligned}
C&=\frac{s_1t_1^2}{(s_1-t_1)^3}\sum_{j=1}^{j}\left(\frac{h_j}{h_1}\right)^3\left(\frac{H_j}{H_1}\right)^2\left(\frac{b_j}{r_j^3}+\frac{L_j^2}{r_j}\right)\\
D&=\frac{s_1t_1^2}{(s_1-t_1)^3}\sum_{j=1}^{j}\left(\frac{h_j}{h_1}\right)^2\left(\frac{H_j}{H_1}\right)^2\left(\frac{b_j}{r_j^3}+\frac{K_j(2L_j-K_j)}{r_j}\right)\\
E&=\frac{t_1^3}{(s_1-t_1)^3}\sum_{j=1}^{j}\left(\frac{h_j}{h_1}\right)\left(\frac{H_j}{H_1}\right)^3\left(\frac{b_j}{r_j^3}+\frac{L_j(2L_j-K_j)}{r_j}\right)\\
F&=\frac{s_1^2t_1}{(s_1-t_1)^3}\sum_{j=1}^{j}\left(\frac{h_j}{h_1}\right)^3\left(\frac{H_j}{H_1}\right)\left(\frac{b_j}{r_j^3}+\frac{K_jL_j}{r_j}\right)
\end{aligned}
\qquad (5)
$$

The notations involved in these equations are

$$
\begin{aligned}
K_j&=\frac{1}{s_j}-\frac{1}{r_j}=\frac{1}{s_j'}+\frac{1}{r_j},\\
L_j&=\frac{1}{t_j}-\frac{1}{r_j}=\frac{1}{t_j'}+\frac{1}{r_j},\\
h_1&=\frac{s_1}{s_1-t_1},\quad H_1=t_1,\\
\frac{h_{j+1}}{h_j}&=\frac{s_{j+1}}{s_j'},\quad \frac{H_{j+1}}{H_j}=\frac{t_{j+1}}{t_j'}
\end{aligned}
\qquad (6)
$$

If the distance between consecutive mirrors is d_j, this is always positive and the following equation exists:

$$d_j=a_{j+1}-a_j=s_{j+1}-s_j'=t_{j+1}-t_j' \qquad (7)$$

3. Application to the Infrared Spectrometer

In Fig. 1 a rectangular co-ordinate system is taken with the axis of collimator as X-axis and the principal section of the prism as XZ plane. The entrance slit is placed at the focus of the reflecting mirror and perpendicular to the XZ plane, therefore, $z_1=0$. Since its width is usually very small, it is neglected in the following discussion. The light dispersed by the prism is sent to the exit slit by the collimator, but since the exit slit is not in the same place as the entrance slit, the image of the entrance slit is not formed on the axis of the reflecting mirror. As shown in Fig. 1, however, if the separation of slits is small enough when compared with the focal length of the mirror, it may be assumed without much error that both slits are at the focus of the mirror. This means that the Littrow mirror is adjusted so that the image of the entrance slit appears on the entrance slit. The Littrow mirror will then reflect perpendicularly the light that is emitted from the center of the entrance slit. Parallel rays pass through a prism without aberration, but if they are not parallel, some aberration will be caused. To avoid complication arising from the aberration, let

us ignore the refraction of the prism. Since the Littrow mirror is plane and reflects only the dispersed light, it does not affect the aberration so long as the plane is perfect. Therefore, leaving this mirror alone, the rest of the reflecting mirror system which is shown in Fig. 1 can be treated as the centered system as shown in Fig. 3, and so the optical system consists of two mirrors ($j=2$).

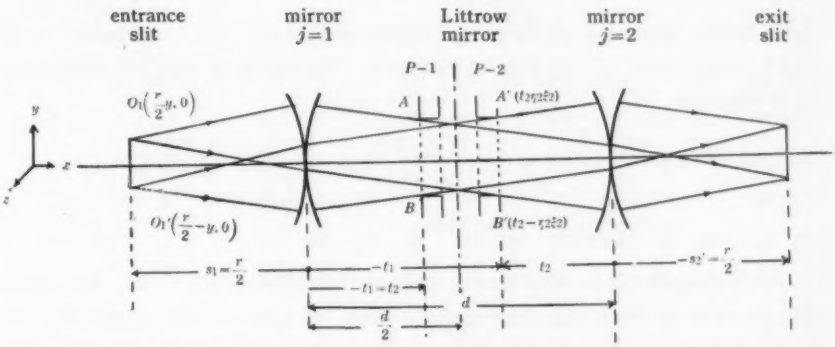

Fig. 3. Modified arrangement of optical system of infrared spectrometer.

If the effective area of the prism is smaller than the effective collimator aperture, the prism acts as the aperture stop of the optical system. Otherwise, the collimator acts as the aperture stop, usually the former is the case. The distance d between the two reflecting mirrors is twice of that between the reflecting mirror and the Littrow mirror, and the prism is placed symmetrically to the Littrow mirror.

As for the definition of the part of the prism acting as the stop, the periphery of the effective plane of the prism corresponding to $A'B'$ in Fig. 3 is taken as the stop.

Thus, the various equations of (3), (4) and (5) can be written in the following way:

$$
\begin{aligned}
&s_1=\frac{r}{2} \qquad && L_1=\frac{1}{t_2-d}+\frac{1}{r} && \frac{H_2}{H_1}=\frac{t_2}{t_2-d} \\
&\beta=1 && L_2=\frac{1}{t_2}-\frac{1}{r} && (8) \\
&K_1=\frac{1}{r} && && \\
&K_2=-\frac{1}{r} && t_2=\frac{(r/2)(t_2-d)}{(r/2)+t_2-d} && \\
&\frac{h_2}{h_1}=1 && t_1'=t_2-d &&
\end{aligned}
$$

As the abscissa of the stop in Equation (3) is that of the co-ordinate of the

stop in the object space, it is necessary to convert η_2 and ζ_2 into η_1 and ζ_1 As lateral magnification is

$$\beta' = \frac{t_1}{-t_1'} = \frac{-(r/2)}{(r/2)+t_2-d} \tag{9}$$

so $\eta_1=\beta'\eta_2$, $\zeta_1=\beta'\zeta_2$.

Since lateral aberration of the image affects resolution of the spectrometer, only $\Delta Z=Z_2'-\beta Z_1$ (where $Z_1=0$) will be discussed. The following equation concerning ΔZ is obtained.

$$-\Delta Z=\frac{b+1}{r^2}\zeta_2(\eta_2^2+\zeta_2^2)+\left[\frac{2(b+1)}{r^4}\{(t_2-d)^2+t_2^2\}-\frac{4d}{r^3}\right]y_1^2\zeta_2 - \frac{2(b+1)}{r^3}(d-2t_2)\zeta_2\eta_2 y_1 \tag{10}$$

In this equation, the first term expresses the spherical aberration, the second the curvature of the image plane and the third the coma. Aberrations $(\Delta Z)_s$ of the spherical mirror $(b=0)$ and $(\Delta Z)_p$ of the paraboloidal mirror $(b+1=0)$ can respectively be expressed by the following equations.

$$(\Delta Z)_s=-\frac{\zeta_2}{r^4}[r^2(\eta_2^2+\zeta_2^2)+2\{t_2^2+(t_2-d)^2-2dr\}y_1^2-2r(d-2t_2)y_1\eta_2] \tag{11}$$

$$(\Delta Z)_p=\frac{4d}{r^3}y_1^2\zeta_2 \tag{12}$$

In which, t_2 should necessarily satisfy the following condition.

$$t_2 \lesssim d/2 \tag{13}$$

From above equations, it is known that only the aberration of spherical mirror is influenced by the position of the stop (prism).

In Equation (11), if $t_2=d/2$, the coma becomes zero, and if $t_2=2r$ and $d=4r$, the curvature of the image plane becomes also zero, and then only spherical aberration remains. In other cases, $(\Delta Z)_s$ increases or decreases by the values of y_1, d and t_2 as can be seen by numerical calculations. As an example, if the effective area of the prism is 6×4 cm, and its base plane is placed at 4 cm from X-axis, abscissas of the stop can be taken as $y_2=3, \zeta_2=4$, and $\eta_2=3, \zeta_2=8$.

Calculated values of ΔZ for various values of y_1, d or t_2 are listed in tables 1 and 2. From these tables, it is noted that,

(a). Equation (11) contains ζ_2^3 and Equation (12) contains ζ_2. Accordingly, when the mirror is used off-axially $(\Delta Z)_s$ becomes rapidly large as the light gets away from the axis, but $(\Delta Z)_p$ does not.

Table 1. Aberration with spherical mirror.

$-(\Delta Z)_s \times r^2$

		$\eta_2=3$ $\zeta_2=4$							$\eta_2=3$ $\zeta_2=8$						
d (cm) \ y_1(cm)	t_2 (cm)	1.5	1.0	0.5	0	−0.5	−1.0	−1.5	1.5	1.0	0.5	0	−0.5	−1.0	−1.5
4r	2r	100	100	100	100	100	100	100	576	576	576	576	576	576	576
2r	r	64	84	96	100	96	84	64	564	544	568	576	568	544	504
	0.8r	51	75	91	100	101	94	80	478	534	559	576	578	565	536
	0.6r	41	67	91	100	106	106	99	458	511	558	576	588	587	573
1.5r	0.7r	63	83	95	100	98	92	70	502	541	566	576	571	559	516
	0.6r	57	78	93	100	100	93	78	489	532	562	576	576	561	532
	0.5r	51	74	91	100	103	98	87	477	524	557	576	581	572	549
r	0.5	73	88	97	100	97	88	93	522	552	570	576	570	552	522
	0.4r	66	83	95	100	99	93	81	508	543	565	576	575	562	537
	0.3r	60	79	93	100	102	98	86	496	534	560	576	580	573	554
0.6r	0.3r	80	92	98	100	98	92	80	536	570	572	576	572	570	536
	0.2r	75	92	96	100	104	97	89	526	558	567	576	584	570	554

Table 2. Aberration with paraboloidal mirror.

$(\Delta Z)_p \times r^2$

	$\eta_2=3$ $\zeta_2=4$							$\eta_2=3$ $\zeta_2=8$						
d(cm) \ y_1 (cm)	1.5	1.0	0.5	0	−0.5	−1.0	−1.5	1.5	1.0	0.5	0	−0.5	−1.0	−1.5
r	36	16	4	0	4	16	36	72	32	8	0	8	32	72
0.8r	29	13	3	0	3	13	29	58	26	6	0	6	26	58
0.6r	22	10	3	0	3	10	22	43	19	5	0	5	19	43
0.5r	18	8	2	0	2	8	18	36	16	4	0	4	16	36

(b) $(\Delta Z)_s$ has a minimum value at $d=2r$ and increases as d becomes small, but $(\Delta Z)_p$ decreases as d becomes small.

(c) $(\Delta Z)_s$ increases slightly as t_2 becomes small, but $(\Delta Z)_p$ is independent of t_2.

(*d*) $(\Delta Z)_s$ is considerably large in both images of central and marginal portions of the slit. $(\Delta Z)_p$ is negligibly small in the image of central portion of the

slit, but rapidly increases as the slit becomes longer.

4. Conclusion

The above shows that, when the off-axiality is considerable, use of a paraboloidal mirror is much preferred. If, however, a spherical mirror is in use, optical arrangement should be carefully planned and set. Since the aberration depends on ζ_2 in both mirrors, the base plane of the prism should be placed as near the axis of the reflecting mirror as the arrangement permits. Hence, in order to lessen ζ_2, it is advisable to set the prism near the axis of the reflecting mirror rather than shortening d, even for a paraboloidal mirror.

As for the position of the prism, with the spherical mirror, the aberration becomes smaller as t_2 approaches $d/2$. Therefore, the prism should be set close to the Littrow mirror. But, with the paraboloidal mirror, since the aberration is independent of the lateral position of the stop, it is not necessary to go over the distance between the prism and the Littrow mirror.

One of the main factors deciding the resolving power of infrared spectrometer is the width of the slit. The greater the available energy and the higher the sensitivity of the detecting system, the narrower the slit can be made. Yet, with a very narrow slit, aberration comes to the fore.

The way the problem of aberration is treated above, can not be said as very accurate, in spite of that, some knowledge on the optical arrangement of infrared spectrometer can be gained.

In conclusion, the author offers hearty thanks to Prof. Yoshio Fujioka, Director of the Institute, and Asst. Prof. Kazuo Miyake for their kind guidance during this piece of work.

On the Contrast and Width of Reflected Multiple-Beam Interference Fringes

Kazuo MIYAKE

Institute for Optical Research, Tokyo University of Education

(Received May 12, 1955)

Discussions are given on (1) under what condition the reflected multiple-beam interference fringes attain high contrast, and (2) if the condition is not fulfilled, how the contrast is weakened.

As for the definition of the width, instead of the customary width for one half of the maximum intensity, the width where the intensity becomes $1/2(I_{max}+I_{min})$ is proposed as it is not only more reasonable but also that the formula for the width becomes much simpler.

1. Introduction

In studying the surface of opaque substances such as metals or in measuring the thickness of thin films by using reflected multiple-beam interference fringes[1], the contrast of the fringes is liable to become too low to be successfully photographed. It happens when either the reflectivity of the silver films used is high or the two reflecting surfaces have very different reflectivities. This trouble can be overcome by preparing a number of silver films of different reflectivities and using one that suits the reflectivity of the surface under examination.

A theory on the reflected multiple-beam interference fringes was advanced by Holden[2]. Experimentally he studied also the anomaly of intensity distribution of fringes[3]. After deriving a general formula, he discussed the half-value width and the contrast of fringes by two surfaces of equal reflectivities referring only briefly to the case of different reflectivities. As silver films have always some degree of light absorption, two highly reflecting surfaces of equal reflectivities do not give a high contrast.

In the first part of the present paper, study is made on the condition under which the contrast of the fringes becomes high and discussion is given how the contrast is impared when the said condition is not fulfilled.

The half-value width is the customary definition of the width of multiple-beam interference fringes. According to this definition, however, the width is

1) S. Tolansky: *Multiple-Beam Interferometry of Surfaces and Films.* (1948).
2) J. Holden: Proc. Phys. Soc. [London] **B62** (1949) 405.
3) J. Holden: J. Opt. Soc. Amer. **41** (1951) 504.

not given when the contrast is very low.

In the last part, $I=(1/2)(I_{max}+I_{min})$ is suggested for the definition of the width, for, this gives a far simpler form of its formula.

2. The Intensity of Reflected Multiple-Beam Interference Fringes

Consider a plane parallel air film bounded by two silvered optical flats and the intensity of monochromatic parallel light reflected normally back and forth between these surfaces.

Let

R_1, R_2 be the reflectivities of front and back planes at their air-silver interfaces,

β_1, β_2 the accompanying phase changes in these reflections,

R_a, α the corresponding quantities for the reflection at the glass-silver interface of the front reflecting plane,

T_1, τ_1 the transmissivity of and the phase change in transmission at the front surface.

According to Holden[4], the intensity of reflected light is given by

$$I_{RX}=R_a+\frac{T_1^2R_2+2T_1\sqrt{R_aR_2}\cos(\Delta-F)-2T_1\sqrt{R_aR_1}\,R_2\cos F}{1+R_1R_2-2\sqrt{R_1R_2}\cos\Delta} \qquad (1)$$

where $\Delta=\delta+\beta_1+\beta_2$ is the phase angle corresponding to the optical separation of the two surfaces and $F=2\tau_1-\beta_1-\alpha$ is the quantity depending only upon the phase changes at the first surface. It was determined experimentally by Holden[5] and Faust[6] that F could be put equal to $(2n+1)\pi$ for such highly reflecting silver films as might be used in multiple-beam interferometry. Hence, putting $F=(2n+1)\pi$ in (1),

$$I_{RX}=R_a+\frac{T_1^2R_2-2T_1\sqrt{R_aR_2}\cos\Delta+2T_1R_2\sqrt{R_aR_1}}{1+R_1R_2-2\sqrt{R_1R_2}\cos\Delta}. \qquad (2)$$

The intensity maxima and minima of the reflected light occur at $\Delta=2n\pi$ and $\Delta=(2n+1)\pi$, and their maximum and minimum values are

$$(I_{RX})_{max}=\left\{\sqrt{R_a}+\frac{T_1\sqrt{R_2}}{1+\sqrt{R_1R_2}}\right\}^2 \qquad (3)$$

$$(I_{RX})_{min}=\left\{\sqrt{R_a}-\frac{T_1\sqrt{R_2}}{1-\sqrt{R_1R_2}}\right\}^2 \qquad (4)$$

4) J. Holden: Proc. Phys. Soc. [London] **B62** (1949) 407.
5) J. Holden: Proc. Phys. Soc. [London] **B62** (1949) 413.
6) R. C. Faust: Phil. Mag. **41** (1950) 1250.

3. Discussion on the Contrast

As the contrast can be defined by $1-(I_{RX})_{min}/(I_{RX})_{max}$, if $(I_{RX})_{min}=0$, the contrast will be the highest. This condition can be expressed by

$$\sqrt{R_a}=(T_1+\sqrt{R_1R_a})\sqrt{R_2} \qquad (5)$$

Formula (5) contains R_a and R_1, and it is a tedious work to calculate their mutual relation for an absorbing film. For simplicity, let us assume $R_a=R_1$ which is, however, not rigorously true except for films held between two mediums of the same reflective index, nevertheless, it lightens the calculation. In fact, Faust[7] showed experimentally that R_a is nearly equal to R_1 for silver films deposited on glass plate. Formula (5) then becomes

$$\sqrt{R_1}=(1-A_1)\sqrt{R_2} \qquad (6)$$

where $A_1=1-(R_1+T_1)$, the absorption factor of the front silver film.

If the reflectivity of the surface under examination is given, the reflectivity R_1, which makes $(I_{RX})_{min}=0$, is obtained by (6), and is plotted in Fig. 1 for different values of A_1.

With any R_1 which does not make $(I_{RX})_{min}$ equal to zero, the contrast becomes lower. Let us examine now how the contrast is weakened.

Putting

$$\sqrt{R_1}=k(1-A_1)\sqrt{R_2} \qquad (7)$$

$(I_{RX})_{min}/(I_{RX})_{max}$ becomes

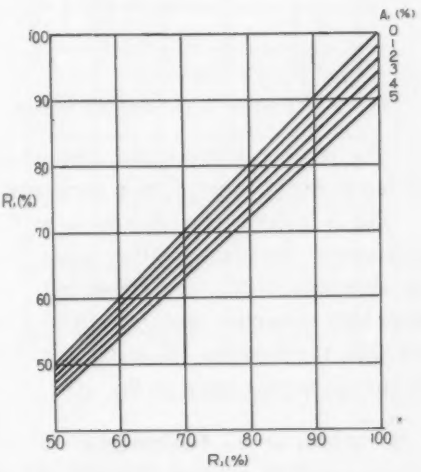

Fig. 1. Combination of reflectivities which makes $(I_{RX})_{min}=0$.

$$\frac{(I_{RX})_{min}}{(I_{RX})_{max}}=\left(\frac{k-1}{k+1}\right)^2\left\{\frac{1+k(1-A_1)R_2}{1-k(1-A_1)R_2}\right\}^2 \qquad (8)$$

which shows how the contrast is affected by k. The relation between k and the contrast for various percentages of $(1-A_1)R_2$ is plotted in Fig. 2. Because of $1>R_1$, we have

7) R. C. Faust: Phil. Mag. **41** (1950) 1240.

$$\frac{1}{(1-A_1)R_2} > k^2 \qquad (9)$$

which means that k has a limiting value for each given value of $(1-A_1)R_2$.

In Fig. 2, we see that the contrast changes very rapidly when the reflectivities of the surfaces are high. Therefore, due consideration should be given to R_1, for, when $k>1$, that is, when the value of R_1 is larger than that given by (7), the deterioration of the contrast becomes conspicuous.

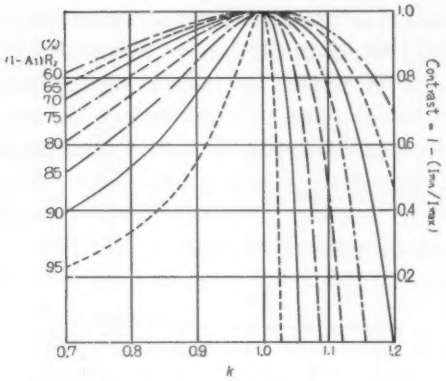

Fig. 2. Variation of the contrast with k.

Next, consider the case $R_1=R_2$ $(=R)$, i.e. $k=1/(1-A_1)$ which is easily realizable. Formula (8) then becomes

$$\frac{(I_{RX})_{\min}}{(I_{RX})_{\max}} = \left(\frac{A_1}{2-A_1}\right)^2\left(\frac{1+R}{1-R}\right)^2 \qquad (10)$$

The relation between the contrast and the reflectivity R given by (10) is plotted in Fig. 3 using A_1 as a parameter.

Fig. 3 tells us that $R_1=R_2$ is a satisfactory working condition when the absorption of the films is low, but when both absorption and reflectivity are high, the condition (6) should not be ignored for the value of R_1.

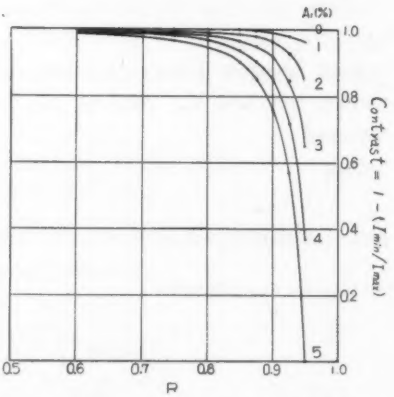

Fig. 3. Variation of the contrast with the reflectivity when $R_1=R_2$.

4. Width of the Interference Fringes

Multiple-beam interference fringes are formed by the interference of multiply reflected light, and they are so sharply defined that the accuracy of measurements with them is very high.

As the definition of the width of the fringes, the half-value width, that is, the width at one half of the miximum intensity $(1/2)(I_{RX})_{\max}$ to wit, is generally used. By this definition, the phase

angle Δ in (2) satisfying the condition (6) is obtained as

$$\cos\Delta=\frac{2\sqrt{R_1R_2}}{1+R_1R_2}, \qquad \sin\Delta=\frac{1-R_1R_2}{1+R_1R_2} \tag{11}$$

and by (6)

$$\sin\Delta=\frac{1-(1-A_1)^2R_2^2}{1+(1-A_1)^2R_2^2} \tag{12}$$

By (12), the values of Δ were calculated as a function of R_2 using A_1 as a parameter and are plotted in Fig. 4 in which the ordinate is the sharpness π/Δ.

We see that the sharpness increases as the reflectivity R_2 becomes high, but the rate of its increase drops with increasing value of the absorption factor A_1. When the condition (6) is not satisfied, calculations of Δ and the sharpness become rather involved and are here left out.

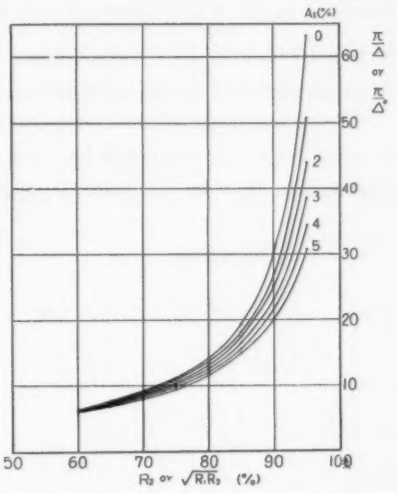

Fig. 4. Sharpness of the fringes.

The half value width for transmitted multiple-beam interference fringes was obtained in a simple form of

$$\sin\frac{\Delta}{2}=\frac{1-\sqrt{R_1R_2}}{2^4\sqrt{R_1R_2}}\cdot \tag{13}$$

If we put $R_1=R_2=R$, it agrees with the formula $\Delta\fallingdotseq(1-R)/\sqrt{R}$ given by Burger and Van Cittert[8] for Fabry-Perot interferometer.

Soejima[9] used the width at which the intensity becomes $(1/2)(I_{max}+I_{min})$ when he treated the theory of Fabry-Perot interferometer. As the definition, this is more reasonable than the customary one, because the latter, $I=(1/2)I_{max}$, does not give any definite width when the contrast is very low. He treated the case in which the reflectivities of the two surfaces were equal and no effect of absorption was taken up.

Adopting Soejima's definition, a simple formula for the width was derived in the case in which the condition (5) fails.

8) H. C. Burger und P. H. van Cittert: ZS. f. Physik **44** (1927) 58.

9) Y. Soejima: *Applied Optics*, Vol. 1, (Edited by the Society of Applied Physics, Japan) Chap. 4, Interferometry. p. 191 (1954) (In Japanese).

Let Δ^* be the phase angle for this width. Calculations for the general case of $R_1 \neq R_2$ were a little complicated but the results are in simple forms which are the same for both transmitted and reflected fringes. They are

$$\cos \Delta^* = \frac{2\sqrt{R_1 R_2}}{1+R_1 R_2}, \qquad \sin \Delta^* = \frac{1-R_1 R_2}{1+R_1 R_2} \tag{14}$$

and are in the same forms as (11). This is obvious because, when the condition (5) is satisfied, $(I_{RX})_{\min}$ is zero, and the two definitions are but one and the same.

With the new definition, the sharpness is determined only by the value of $\sqrt{R_1 R_2}$, and is independent of the way how R_1 and R_2 are combined. It is therefore, not of much importance to discuss the sharpness when the condition (5) is not fulfilled. If $\sqrt{R_1 R_2}$ is taken in place of R_2 as the abscissa in Fig. 4, the curve $A_1=0$ gives the sharpness.

The choice of the definition may depend on the observing condition. As mentioned before, when the contrast is low, that is when $\sqrt{R_1 R_2}$ is small for fringes by transmission or when the case is very much out of the condition (5) for the

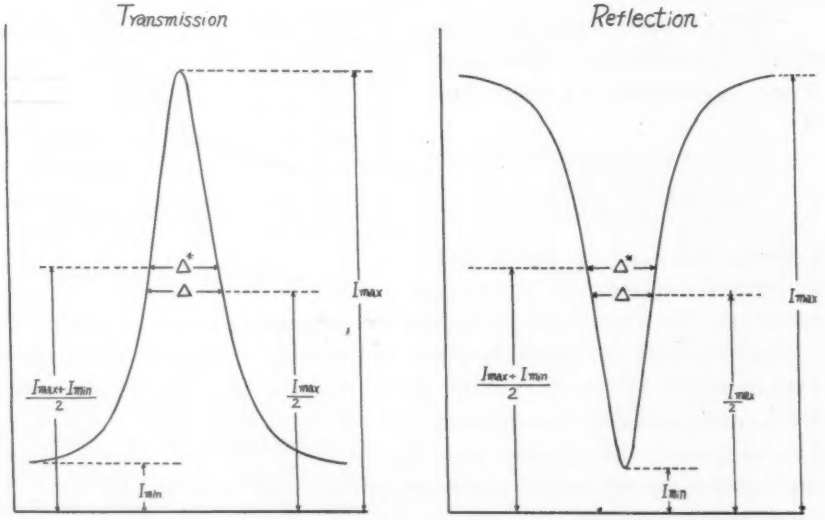

Fig. 5. Definitions of the width of interference fringes.

fringes by reflection, the use of Δ by $I=(1/2)I_{\max}$ may not provide a width. If the film has absorption, the formula for Δ by $I=(1/2)I_{\max}$ is complicated, whereas that for Δ^* by $I=(1/2)(I_{\max}+I_{\min})$ is simple. From these two reasons, it seems reasonable to adopt Δ^* as the width of multiple-beam interference fringes.

Holden[10] calculated the sharpness of reflected and transmitted multiple-beam interference fringes for the case of $R_1=R_2=R$ when there is absorption, and stated that the reflected fringes are sharper than the transmitted ones in the case of equal reflectivities. But this conclusion comes from the definition $I=(1/2)I_{max}$. As seen clearly in Fig. 5, it can not be said that the reflected fringes are essentially sharper than transmitted ones.

5. Conclusion

When reflected multiple-beam interference fringes are used, care should be taken to use a proper silver film as the front reflecting surface to suit the reflectivity of the back surface to avoid blurring of the fringes.

As for the definition of the width of multiple-beam interference fringes, the width at $I=(1/2)(I_{max}+I_{min})$ is convenient at least for theoretical treatments.

The discussion given above can also be applied to interference filters.

The author wishes to express his thanks to Professor Y. Fujioka, at whose institute this work was performed.

10) J. Holden: Proc. Phys. Soc. [London] **B62** (1949) 417.

Infrared Absorption Studies on the Hydrogen Bonds between Various Phenol Derivatives and Some Proton Acceptors

Yoshiki SATO
Institute for Optical Research, Tokyo University of Education
and
Saburo NAGAKURA
Institute of Science and Technology, University of Tokyo

(Received May 3, 1955)

Hydrogen bonding between various phenol derivatives and some proton acceptors has been investigated in detail by measuring the first overtone absorption of O-H stretching vibration of proton donor with grating spectrometer of great resolving power, two new bands are found in the longer wave-length side of O-H stretching vibration of free proton donor when it takes part in hydrogen bonding. Furthermore, it is concluded from the experiment on their dependences on temperature and concentration of proton acceptor that the bands should be due to the formation of hydrogen bonding. Such an occurrence of two absorption bands can approximately be explained by assuming a double minimum potential energy for hydrogen taking part in the hydrogen bond. It is found that the accepting powers of nitromethane and acetnitrile are smaller than those of dioxane and acetone, and is shown that for the interpretation of the hydrogen bond, delocalization energy of non-bonding electrons, which belong to the proton acceptor atom taking part directly in the formation of the hydrogen bond, is more responsible mere electrostatic interaction.

1. Introduction

Up to date, a great number of investigations concerning the hydrogen bond have been made by the use of various physicochemical methods[1]. Especially, infrared absorption may be regarded as one of the most useful and popular methods for this purpose. Accordingly, with a near infrared spectrometer of great resolving power constructed by one of the authors[2], investigation of hydrogen bondings between various phenol derivatives and some proton acceptors was undertaken by measuring the first overtone absorption band of O-H stretch-

1) a) See, for example S. Seki: Chem. and Chem. Industry **6** (1953) 219; b) M, Tsuboi: Domain of Chemistry **7** (1953) 611.
2) Y. Sakayanagi and Y. Sato: Science of Light **3** (1953) 84.

ing vibration of proton donor. As a result, it was found for each set of proton donor and acceptor that two new absorption bands appear in the longer wave length side of O-H stretching vibration of free proton donor. Furthermore, it has been shown by experiment on the dependence of these two bands upon temperature and concentration of proton acceptor that they should all be due to the hydrogen bonding.

In this paper, details of the above-mentioned experimental results are described and some theoretical considerations are given.

2. Experimental and Results

All the measurements were made in a ternary system consisting of donor, acceptor, and solvent, and the wave number difference in the first overtone band of O-H stretching vibration between free and hydrogen bonded proton donor molecules was obtained. Phenol, *m*-, *p*-chlorophenol, o-, *m*-, *p*-cresol and α-, β-naphthol were used as proton donor, and dioxane, methylacetate, acetone, nitromethane and acetnitrile as proton acceptor. Most of these proton donors and acceptors were the same as those used by one of the authors in the near ultraviolet absorption study on hydrogen bonding[3]. Carbon tetrachloride used as a solvent was of a special grade produced by Wako pure Chemical Industries, LTD.

The near infrared spectrometer used has a plane grating of the Littrow mounting as the dispersion system and a PbS photoconductive cell as the detector. The scattered light that comes into question in a spectrometer is more in the Littrow type than in the Ebert type and this was removed by using a filter. The resolving power in the wave-length region of 1.5 μ is about 8000. Calibration of wave-length was made by the use of vibrational-rotational lines of moisture in air and the 2nd order spectrum of Neon.

Some examples* of the absorption curves obtained are given in Fig. 1. As can clearly be seen from the figure, for each set of proton donor and acceptor, there appear two new absorption bands in the wave-length region between OH and CH absorption bands of free donor molecule. Generally speaking, the intensity of the band on the longer wave-length side is greater than that of the other with a few exceptions such as in the case of hydrogen bonding between phenol and methylacetate. These two bands are broad and it seems difficult to determine exact wave numbers of their absorption maxima. By estimating

3) S. Nagakura: J. Chem. Soc. Japan **74** (1953) 153; **75** (1954) 734.

* The effect of the association of proton donor itself seems negligibly small in the concentration region used in the present experiment.

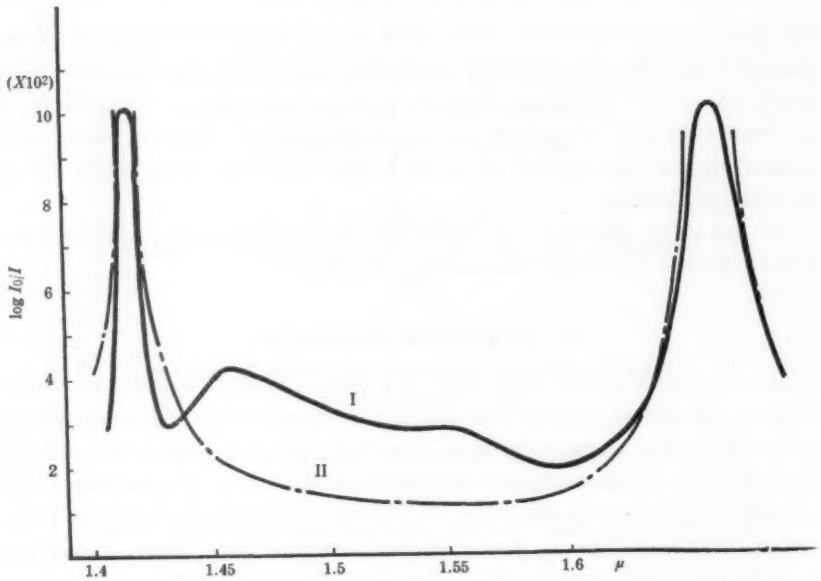

Fig. 1 (a). I Phenol 0.055 mol/l, methylacetate 0.52 mol/l. II phenol 0.095 mol/l.

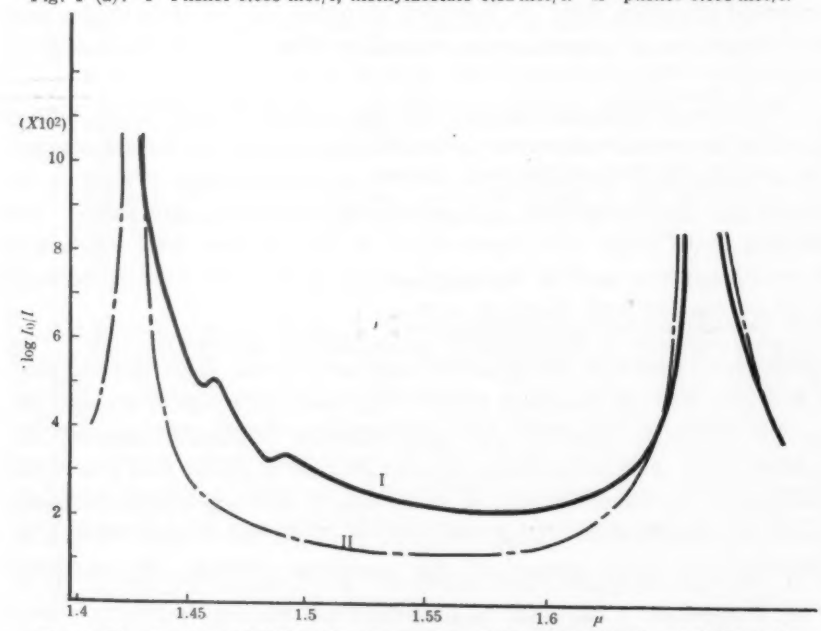

Fig. 1 (b). I Phenol 0.066 mol/l, nitromethane 0.79 mol/l. II phenol 0.095 mol/l.

Fig. 1 (a) (b). Infrared absorption spectra of ternary systems consisting of proton donor, proton acceptor and solvent.

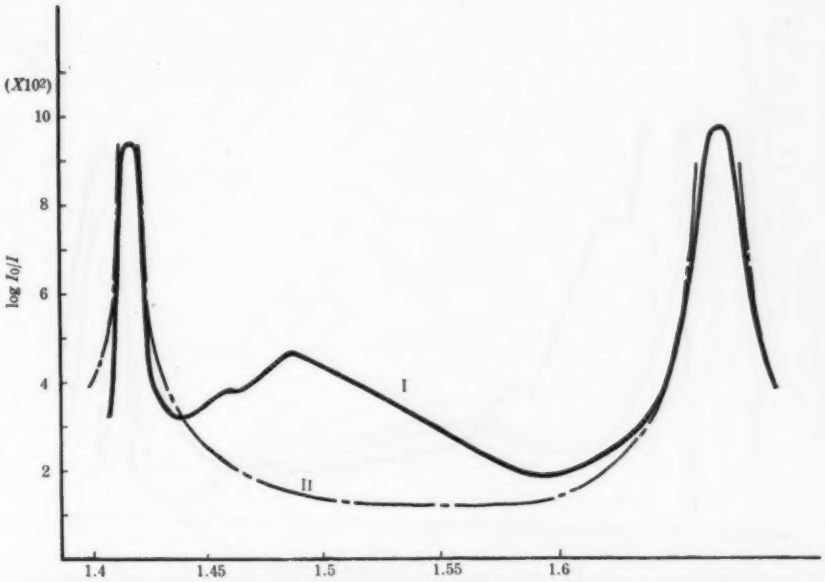

Fig. 1 (c). I phenol 0.053 mol/l, acetnitrile 0.78 mol/l. II phenol 0.095 mol/l.

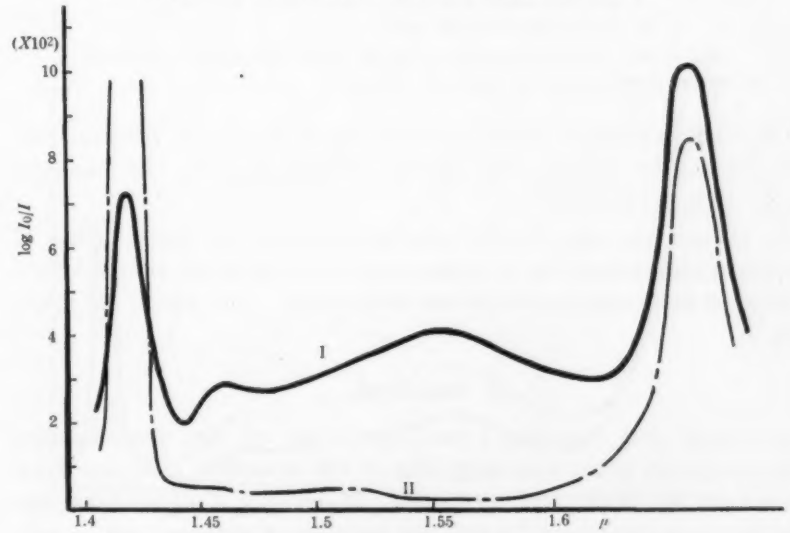

Fig. 1 (d). I *p*-chlorophenol 0.054 mol/l, acetone 0.44 mol/l.
II *p*-chlorophenol 0.045 mol/l.

Fig. 1 (c) (d). Infrared absorption spectra of ternary systems consisting of proton donor, proton acceptor and solvent.

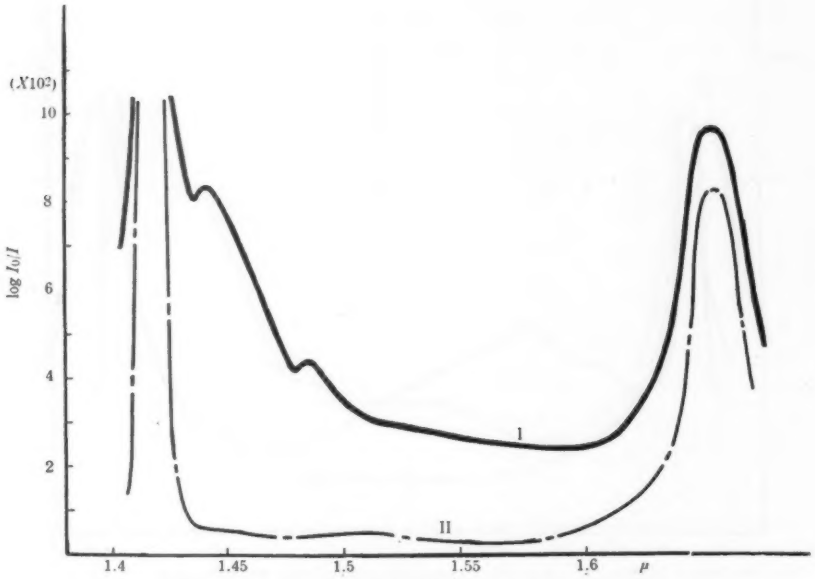

I *p*-Chlorophenol 0.053 mol/l, nitromethane 0.84 mol/l.
II *p*-Chlorophenol 0.045 mol/l.

Fig. 1 (e). Infrared absorption spectra of ternary system consisting of proton donor, proton acceptor and solvent.

their approximate numbers, which is possible, the wave number differences $\Delta\nu_1$ (cm^{-1}) and $\Delta\nu_2$(cm^{-1}) between them and the corresponding free OH absorption band are tabulated in Table 1.

To examine the cause for the occurrence of these two bands, effects of temperature and concentration of proton acceptor were measured with the system consisting of phenol, dioxane and carbon tetrachloride. The results are shown in Fig. 2.

3. Discussions

It is clearly seen from Fig. 1 and Table 1 that the two new absorption bands occur in the longer wave-length side of OH absorption of a free donor when it takes part in the hydrogen bonding. Moreover, it is evident from Fig. 2 that they have close connection with the formation of hydrogen bond as seen by the fact that the intensities of these two bands increase with the increase of concentration of proton acceptor and decrease with the rise of temperature. A phenomenon seemingly analogous to the above is the appearance of more than

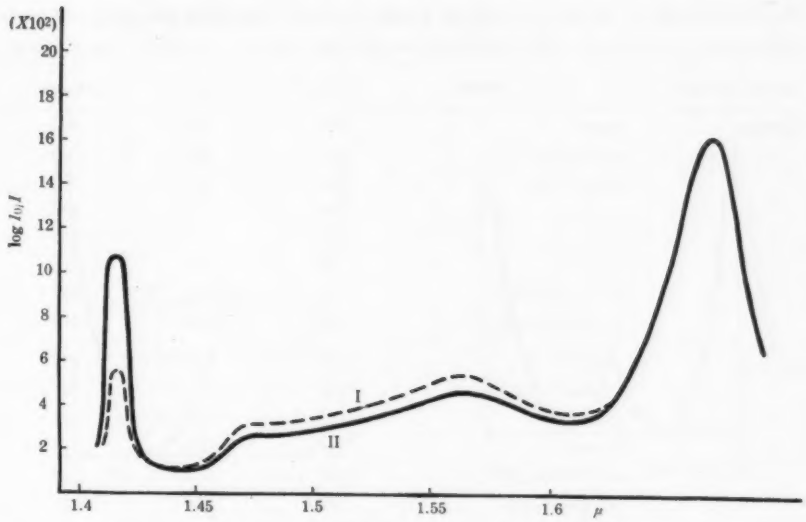

Fig. 2 (a) I phenol 0.086 mol/l, dioxane 0.82 mol/l.
II phenol 0.086 mol/l, dioxane 0.45 mol/l.

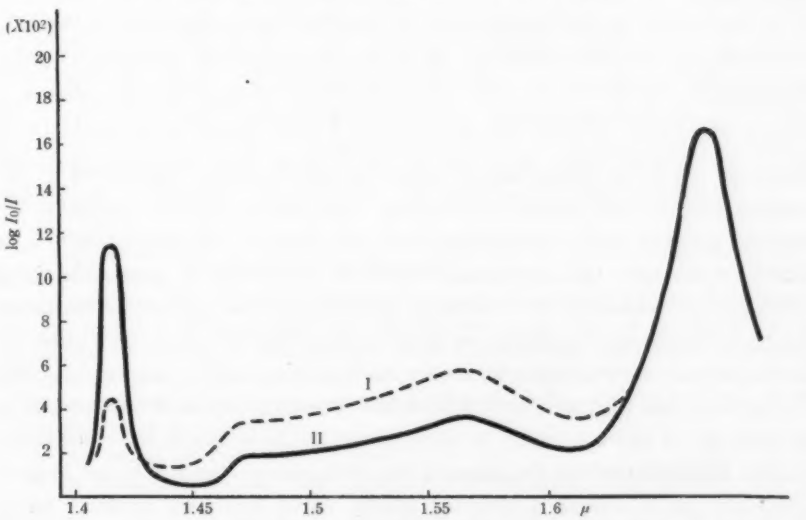

Fig. 2 (b). phenol 0.086 mol/l, dioxane 0.42 mol/l. I 16°C; II 64°C

Fig. 2 (a) (b). Infrared absortion spectra of the ternary system consisting of phenol, dioxane and carbon tetrachloride; (a) the effect of concentration of dioxane, and (b) the effect of temperature.

Table 1. Values of $\Delta\nu_1(cm^{-1})$ and $\Delta\nu_2(cm^{-1})$ and their average values $\Delta\nu_{12}$ (cm^{-1}).

proton acceptor	proton donor	$\Delta\nu_1$ cm^{-1}	$\Delta\nu_2$ cm^{-1}	$\Delta\nu_{12}cm^{-1}$
dioxane	phenol	228	640	434
	α-naphthol	134	645	389
	β-naphthol	191	591	391
	o-cresol	244	637	440
	m-cresol	110	556	333
	p-cresol	223	610	416
	m-chlorophenol	155	491	323
	p-chlorophenol	198	634	416
acetone	phenol	280	634	457
	o-cresol	254	611	432
	m-cresol	124	549	336
	p-cresol	246	590	418
	m-chlorophenol	172	472	322
	p-chlorophenol	209	594	401
methyl acetate	phenol	205	603	404
nitromethane	phenol	193	333	263
	m-chlorophenol	74	251	162
	p-chlorophenol	95	301	188
acetnitrile	phenol	177	313	245
	m.chlorophenol	61	246	153

two bands due to hydrogen bonding which has been found by association of *N*-methylacetamide[4] and phenol[5] in solution. This seems, however, somewhat essentially different from what observed by the authors. In phenol, there is a possibility of chain polymers being formed by association of more than three molecules. Consequently, it is naturally expected that the vibrational frequency of molecule at the end of polymer and at the intermediate portion of it are different and more than two absorption bands due to hydrogen bonding can appear. But in the present case, hydrogen bonding is formed between proton donor and acceptor in the ratio of 1:1 and association of more than three molecules is not conceivable.

One interpretation for the cause of the phenomenon observed in the present experiment is to assume a potential energy curve with two minima[6] for a

4) S. Mizushima, T. Simanouchi, S. Nagakura, K. Kuratani, M. Tsuboi, H. Baba and O. Fujioka: J. Amer. Chem. Soc. **72** (1950) 3490; M. Tsuboi: Bull. Chem. Soc. Japan **22** (1949) 215.

5) R. Mecke: Disc. Faraday. Soc. No. **9** (1950) 161.

6) I. Oshida and U. Ôshika: Busseiron Kenkyu **46** (1952) 95.

proton to form the hydrogen bond as shown in Fig. 3. In a system consisting of phenol and acetone, Tsuboi[7] has found two absorption bands due to hydrogen

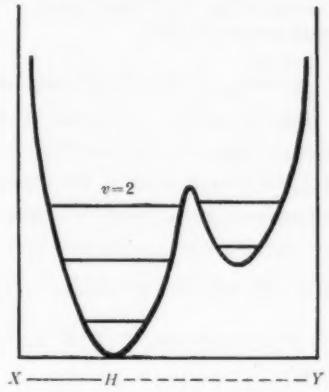

Fig. 3.

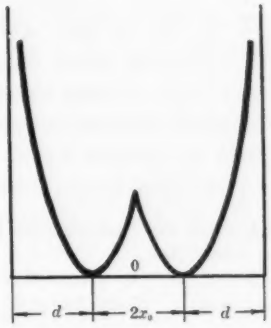

Fig. 4,

$V=\frac{1}{2}k(x+x_0)^2 \quad 0\geq x\geq -\infty$

$+\frac{1}{2}k(x-x_0)^2 \quad 0\leq x\leq +\infty$

bonding for the fundamental tone of O-H stretching vibration. If we assume a symmetrical double minimum potential of the harmonic oscillator type, absorption frequencies of two bands for the fundamental tone and for the first overtone can be calculated as shown in Table 2. The agreement between theoretical and experimental results is fairly good in spite of the rough approximation used in the calculation*. The same treatment may be applied to the other systems.

* Let us calculate the anharmonicity constants $\omega_e\chi_e$ of potential energies for O-H streching vibrations of free and hydrogen bonded phenol molecules. They become 90 cm^{-1}, and 130 cm^{-1}, for free and hydrogen bonded molecule, respectively. From these values it can be seen that the anharmonicity in the potential energy curve is considerably large and becomes still larger by the hydrogen bond. Furthermore, the heights of the two minima[8] may generally be considered different from each other. Therefore, the adoption of the symmetrical double minimum potential of the harmonic oscillator type may be regarded as a rough approximation.

7) M. Tsuboi: Private communication.

8) It seems probable that when a proton and aceton coexist, the structure such as $H-\overset{+}{O}=C\begin{matrix}CH_3\\CH_3\end{matrix}$, in which the proton is combined with the oxygen atom of acetone, is considerably stable. Therefore, it may be inferred that the energy difference between two structures 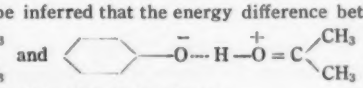 may be comparatively small. (This will be discussed in detail elsewhere.)

Another interpretation may be that the two bands occur by Fermi resonance between O-H stretching band and some other combination or overtone band. But,

Table 2. Calculated and experimental values of two absorption bands observed with a hydrogen bonded phenol molecule.

	$v=0\rightarrow1$		$v=0\rightarrow2$	
	cal.	exp.	cal.	exp.
ν_1	3471	3472	7482	6760
ν_2	3399	3401	6953	6427

height of potential barrier = 38 K cal/mol.

$\omega_e = 3610\,\mathrm{cm}^{-1}$ $k = 6.95$ dynes/cm $d^* = 1.08\,A$

$2x_0 = 0.54\,A$ $0\cdots0^{**} = 2.8\,A$

* This value was obtained from Gordy's experimental formula. W. Gordy: J. Chem. Phys. **14** (1946) 305.

** This distance was presumed from the curve given by Rundle, et al. R. E. Rundle and M. Parasol: J. Chem. Phys. **20** (1952) 1487.

it seems doubtful whether such mechanism can explain the fact that the difference in wave number between the two absorption bands varies with the kind of proton acceptor as shown in Table 1.

Lastly, the relation between the structure and the power of proton acceptor is to be discussed. The power of proton donor or acceptor have often been regarded in terms of the wave number shift $\Delta\nu$ due to the hydrogen bond, but in the present case where two absorption bands are observed, difficulty is encountered in determining which of them should be adopted as the measure of the proton accepting power. Let us assume for the present that the average value of the two shifts given in the last column of Table I predicts the proton accepting power. As seen in the table, proton accepting powers of nitromethane and acetnitrile are very small in comparison with those of dioxane and acetone. This can not be explained on the basis of electrostatic interaction alone, for the dipole moments of the said two substances are very large, namely 3.54 D and 3.94 D[9] respectively.

Recently, the importance of delocalization energy of non-bonding electrons which belong to a proton acceptor atom taking part in the hydrogen bonding directly, in other words, the importance of the contribution of resonance structure such as X^-H-Y^+ to the hydrogen bonded system $X-H\cdots Y$, is emphasized by Nukasawa, Tanaka and Nagakura[10], Tsubomura[11], and Coulson and Daniel-

9) L. G. Wesson: Tables of Electric dipole moment.

10) K. Nukasawa, J. Tanaka and S. Nagakura: J. Phys. Soc. Japan **8** (1953) 792.

11) H. Tsubomura: Bull. Chem. Soc. Japan **27** (1954) 445.

son[12]. The experimental results described above may be considered to give support to their theories which state that the contribution of the delocalization energy to the hydrogen bond, ΔE, is given by[10]

$$\Delta E = 2\delta^2 / M_{HX} - I_Y ,$$

where M_{HX} represents the electron affinity of the vacant orbitals $H-X$, I_Y the ionization potential of the occupied orbital Y, and δ the perturbing exchange energy between the two orbitals. According to this equation, it is expected that the larger the contribution of delocalization energy to hydrogen bond, the smaller the ionization potential of non-bonding electron, which explains the weakness of accepting powers of nitromethane and acetnitrile whose ionization potentials, 11.32 eV[13] and 12.39 eV[14] respectively, are larger than those of acetone and dioxane.

Aknowledgment

The authors wish to express their sincere thanks to Professor Yoshio Fujioka, Director of the Institute for Optical Research, for his deep interest and constant encouragement during the course of the present work, and their gratitude to Dr. M. Tsuboi, University of Tokyo, for his valuable advice and to Assist. Prof. Makoto Hachisu, Institute for Optical Research, for his many valuable facilities offered throughout the present work.

12) C. A. Coulson and U. Danielson: Ark. Fys. **8** (1954) 239, 245.
13) J. D. Morrison: Private communication.
14) J. D. Morrison: J. Chem. Phys. **20** (1952).

On the λ 1600–1350 Absorption System of Nitrogen Dioxide and its Electronic Structure

Kazuo MORI
Scientific Research Institute
(Received August 2, 1955)

Photographs of the absorption bands of NO_2 in the region of λ 1600–1350 have been taken under the medium dispersion (about 2A/mm). The Lyman continuum was employed as the light source for the background. Two separate electronic systems appear to be involved in this region. The relatively long v_1' and v_2' progressions indicate that both the bond length and the apex angle of the molecule change considerably in the transition to the excited electronic state. The complexity of the structure of the bands also suggests that the molecule in its upper state becomes more asymmetrical. From the vibrational analysis it is concluded that the λ 1600–1350 system corresponds to the transition from the double bond orbitals to the antibonding orbital containing the odd electron.

1. Introduction

The absorption spectra of nitrogen dioxide in the region of λ 1600–1350 were first studied by Price and Simpson[1]. They investigated them as an example of the class of triatomic molecules having more than sixteen "molecular electrons". The nitrogen dioxide molecule is interesting as a stable molecule having an odd electron. The determination of the energy levels of NO_2 from its spectrum would be useful for enriching the knowledge about molecular orbitals. However, owing to the odd electron, the spectrum of NO_2 is rather complicated, especially in the visible region[2),3)]. In the near ultraviolet, there is a relatively simple band system[4)], representing one of the few examples of regular band systems belonging to the asymmetric top molecules. In the far ultraviolet, there are two absorption systems. The one is the system between λ 1600 and λ 1350, having relatively sharp bands and showing a wide vibrational structure. The other is the system in the region below λ 1300, which has rather diffuse bands. Concerning the former system, Price et al. concluded from the absorption measurement that all the prominent bands in this region constituted

1) W. C. Price and D. M. Simpson: Trans. Faraday Soc. **37** (1941) 106.
2) T. C. Hall and F. E. Blacet: J. Chem. Phys. **20** (1952) 1745.
3) J. K. Dixon: J. Chem. Phys. **8** (1940) 157.
4) L. Harris, G. W. King, W. S. Benedict and R. W. Pearse: J. Chem. Phys. **8** (1940) 765.

one electronic system, which was represented by a single progression with a frequency interval corresponding to the bending vibration of the excited electronic state. Furthermore, they suggested that the λ 1600–1350 system was probably due to the excitation of "π" bonding electrons originating in the double bond.

The absorption system below λ 1300 shows little vibrational structure, indicating that it is due to the transitions of nonbonding electrons to the excited orbitals. These orbitals are mainly atomic (Rydberg) in character. The Rydberg series corresponding to them was followed to the second member, yielding a value of 12.3±0.2 eV[1] for the ionization potential. Price et al. attributed this ionization potential to a lone pair of electrons located on the oxygen atom and regarded as the first ionization potential of the molecule.

Later, Mori[5] investigated the absorption spectra of NO_2 in the far ultraviolet with a small vacuum spectrograph similar to the one used by Price et al. He proposed that in view of the arrangements of the bands in the λ 1600–1350 region and of the appearance of intensity variation through the bands, there should be another progressions with the symmetrical valence frequency of the upper state besides those with the bending frequency. He attempted a new tentative vibrational analysis using two symmetrical frequencies for the upper level. Moreover, the λ 1600–1350 system was considered to be due to the transition from a double bond orbital to the antibonding ($4a_1$) orbital occupied by an odd electron, independently of the Walsh's article[6], which will be mentioned later.

However, in neither of the above-mentioned measurements for the λ 1600–1350 system, conclusive discussions about the vibrational analysis were possible because of the insufficiency of the resolution.

More recently, the absorption spectra of NO_2 were measured in λ 1600–1350 region with a vacuum spectrograph having a medium dispersion for the purpose of improving the vibrational analysis of the system. At first, the resolution of the fine structure, at least the discrimination between the parallel and the perpendicular types of the bands, was expected to be traced under the dispersion used, but it failed. However, in the previous experiment the bands in this region appeared to be so compactly arranged on account of the small dispersion that even the characters of the band envelopes could not be clearly discriminated, whereas in the present spectrograms the shapes of the bands has become more distinct, rendering the vibrational analysis easier. In view of the foregoing it was thought necessary to reconsider the vibrational structure of the system.

5) K. Mori: Sci. of Light (Tokyo) **3** (1954) 62.
6) A. D. Walsh: J. Chem. Phys. **22** (1953) 66.

As regards the electronic structure of the NO_2 molecule, Mulliken[7] discussed proposing a scheme of electronic levels of angular molecules. He gave a preliminary interpretation of the observed electronic spectra of this molecule in the visible and the near ultraviolet. He used one odd electron in outermost orbital and two electrons each in non-bonding orbitals. Walsh[4] attributed the λ 1600–1350 system to the transitions from the orbitals situated below the nonbonding orbitals. Furthermore, the occurrence of the long v_2' series in the system was considered to be caused by the transition to the $4a_1$ orbital. The $4a_1$ orbital was assumed by Mulliken and Walsh to be very sensitive to the bond direction, that is, descending in energy rapidly with decreasing apex angle. The results of the present work support the above interpretation of the absorption spectra by Walsh and Price, who predicted that the λ 1600–1350 system corresponded to the transition of an electron from the double bond orbital to the antibonding orbital containing the odd electron.

2. Experimental

Photographs were taken with a grazing incidence type vacuum spectrograph with a 3 meter concave grating. The grazing angle was about 8 degrees. The grating has grooves of 15000 lines per inch and a ruled area of 8 cm × 5 cm. The whole apparatus is schematically shown in Fig. 1. A grating, a slit and a plate holder are covered by large cylinder movable on rail, which holds the above optical system and is attached to a heavy plate having openings for evacuation and a slit. Two exposures on the same plate are possible in vacuum by operating a diaphragm in front of the plate holder from outside. The spectrograph had a satisfactory definition and resolving power, and the range between zero and about λ 2000 can be photographed at the first order. The dispersion is about 2 A/mm in the region of λ 1600–1350.

For the absorption background, hydrogen and helium type continuums were first intended to be used as the continuous light source, for they are easy to fit out and have uniform intensity distribution with few impurity lines. They have also an advantage of being free from dust to keep the absorption tube clean to ensure its window transmission. However, the continuum of λ 5000 to λ 1700 of hydrogen and λ 600 to λ 1000 of helium did not cover the region λ 1700–λ 1300 required for the experiment. Lyman continuum, extending from visible to about λ 300, which was the only known continuum* at the time of this

7) R. S. Mulliken: Rev. Mod. Phys. **14** (1942) 204.

*) Most recently, a new source, charged with xenon or krypton and excited by microwave energy, has been reported[8]. The xenon continuum showing strong intensity extends from λ 1500 to λ 2250, and the krypton continuum from λ 1250 to λ 1600. The combination of them is quite suitable for the present purpose.

undertaking, was used in spite of many disadvantages[8]. Tanaka's Lyman tube[9] with a slight modification was employed. The tube is shown in Fig. 1. Among the disadvantages of the Lyman discharge tube, the greatest is the expulsion of dust particles from the capillary, clogging the slit and blurring the window. To decrease the clogging, a small protector, in addition doing a role of an electrode, was added in front of a main protector[9], which not only protects the slit but also prevents the evolution of gasses from the dirty wall and the metal part by the bombardment of high speed electrons or negative ions. Further, three metalic protectors with holes slightly larger than that of the slit were placed before the slit.

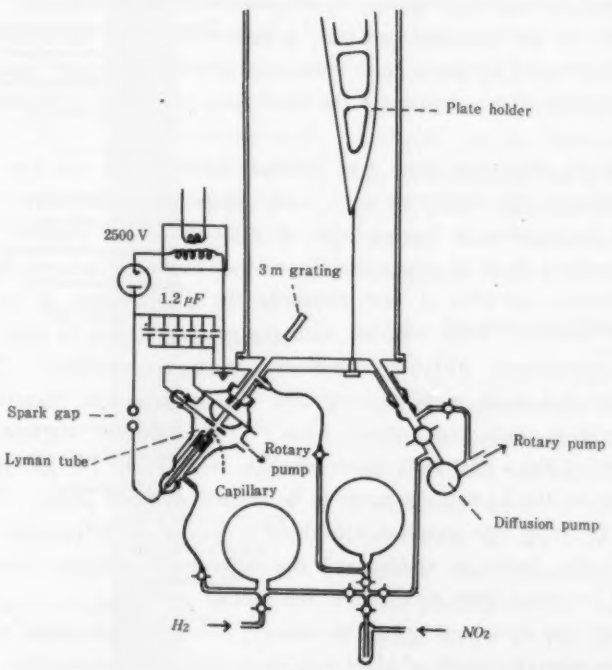

Fig. 1.

In the electrical circuit for the light source, six condensers were put in parallel with the total capacity of 1.2 μF. Large capacity allowed the capillary bore to be larger (about 1 mm in diameter), making the alignment of the discharge tube easier. The difficulty of alignment is another disadvantage of the

8) P. G. Wilkinson and Y. Tanaka: J. Opt. Soc. Amer. **45** (1955) 344.
9) Y. Tanaka: Sci. Pap. Inst. Phys. Chem. Res., Tokyo **42** (1944) 49.

Lyman tube. The voltage applied was 25,000 volts. It was supplied by transformer, 50 KV, 3 KVA, through a Kenotron. The interval of flashes during the discharge was about 1 sec. The time of exposure was on the average one hour.

Schumann plates prepared in the laboratory together with Eastman SWR plates, both 25 cm × 3 cm in size, were used. With the thickness of less than 1 mm, they could safely be bent along the curvature of the focal plane.

The wave-length standard was by a comparison spectrum of a vacuum spark with lines of least ionized Si, O, C and Al.

Nitrogen dioxide, generated by heating lead nitrate and dried with P_2O_5, was purified at −78°C to rid oxygen and other impurities. White crystalline solid obtained in this way was then stored over P_2O_5 in a reservoir. To avoid the reaction of mercury and stopcock grease with NO_2, a calibrated gauge of glass membrane and a silicone fluid manometer for the pressure measurement, and high vacuum silicon grease for the lubrication of ground joint and stopcocks were used.

At first an absorption tube was inserted between the slit and the light source to measure the absorption in a wide range of temperature. However, blurring of the window by fine particles of glass from the capillary wall and also possibly by a film* of evaporated Si or other elements included in the glass were too serious, and after a few discharge the transmission of the window was greatly lowered. This, together with the grating lacking in light intensity, made the experiment with the absorption tube unsuccessful. Thus, the absorbing gas had to be made flowing into the spectrograph chamber, whose mean absorption path was about 1.5 m. The pressure suitable for the measurement of the λ 1600–1350 region of NO_2 was below 10^{-1} mm Hg, which was too low for the Lyman discharge to be started and kept stable. Therefore, the discharge tube was supplied with dried hydrogen at the pressure sufficient to maintain the discharge stable, and the differential pumping was used to prevent the hydrogen from mixing into the sample gas.

Since nitrogen dioxide is apt to be strongly decomposed by light even below λ 4000[10], the reservoir made of glass was blackened to shield the light. Furthermore, it was necessary, to let the gas flow as fast as possible through the chamber to provide a continuous supply of fresh sample gas for the optical path. Owing to the strong intensity of the light source, NO and O_2 produced

10) R. G. W. Norrish: J. Chem. Phys. **11** (1929) 58.

*) Because the temperature of the capillary during the discharge is very high (more than 5000°C) due to the high current density. The window was examined after the exposure, and a closely coated film was found, whose absorption was injurious to the required irradiation.

by photodissociation showed their absorption spectra, but they were weak enough not to hinder the observation. Continuous absorption of N_2O_4, which is in equilibrium with NO_2 at a room temperature, overlapped the NO_2 absorption in the range below λ 4000[2] (especially below λ 2500). Observations on the λ 1600–1350 band system were made at the pressures of a few hundredths of a mm Hg, and at such pressures the superimposed continuous absorption of N_2O_4, was weak. But, at higher pressures this continuum became so strong that the measurement was very difficult. As will be described later, the lack of high pressure data made the vibrational anaysis difficult. As the elevation of temperature hastens the dissociation of N_2O_4, the temperature variation method was necessary for the absorption study of NO_2.

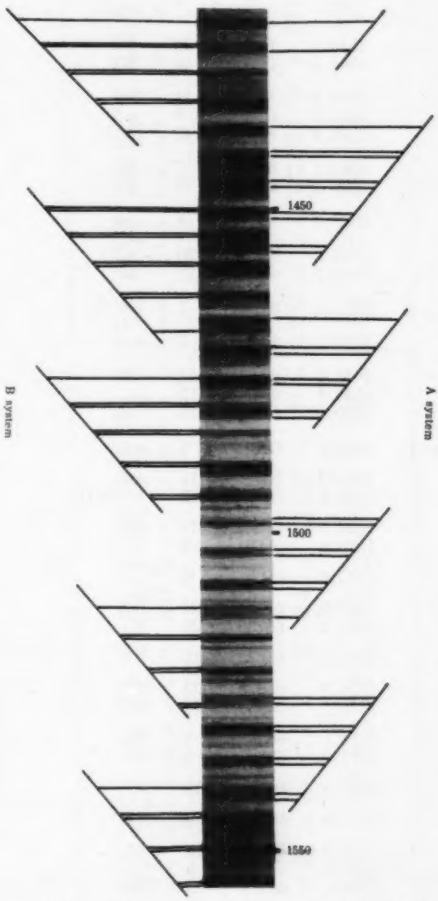

Fig. 2. Absorption spectrum of NO_2 in the region λ 1600–1350, taken with the 3 m vacuum spectrograph of grazing incidence type. The vibrational analysis is indicated on the sides of the spectrum.

3. Results and Discussion

Fig. 2 is an enlarged reproduction of a spectrogram of the λ 1600–1350 absorption system, marked with a schematic representation of the vibrational analysis, which will be mentioned in the later paragraph. Bands, the appearance of which was possible by the excited vibrational levels of the ground state, are not labeled. Table 1 gives the wave-numbers of the band heads as well as their relative intensities which were estimated by eye and checked with microphotometer record.

A characteristic periodicity of about 200 cm^{-1} is clearly shown throughout the region. Therefore, it seems certain that progressions with the 200 cm^{-1}

Table 1. Absorption bands of nitrogen dioxide in the region of λ1600-λ1350. A1, B2 etc indicate the heads of the main bands. A and B bands correspond to speparate electronic systems. α indicates band not included in the main system. α1, α2 etc form 200 cm^{-1} progression, respectively, like the main system.

λ	ν	I		λ	ν	I	
1615.0	61920	1	B2	1544.9	64792	11	B2
1614.5	61939	1	B2	1544.0	64767	10	B1
1609.5	62131	2	B2	1542.0	64851	11	A2
1609.1	62147	1	B1	1541.2	64885	7	α 3
1603.0	62383	4	B2	1540.9	64897	13	A1
1602.7	62395	4	B1	1540.1	64931	7	B2
1600.2	62492	5	A2	1539.9	64939	7	B1
1599.3	62527	6	A1	1538.2	95011	8	α 4
1594.4	62720	4	A2	1536.2	65096	20	A2
1593.6	62751	3	A1	1535.1	65142	21	A1
1592.3	62802	3	α 1	1533.6	65208	7	(Si II)
1589.9	62897	2	A2	1533.1	65227	7	α 4
1588.9	62937	3	A1	1531.2	65308	13	A2
1586.3	63040	5	α 1	1530.3	65347	13	
1584.8	63099	12	B2	1530.1	65355	12	A1
1584.1	63127	8	B1	1529.0	65402	6	α 4
1579.6	63307	7	α 2	1527.2	65479	10	B2
1579.1	63327	8	B2	1526.4	65514	12	B1(Si II)
1578.9	63335	7	B1	1526.0	65531	12	A2
1575.3	63480	5	α 1	1525.3	65561	9	A1
1574.0	63532	8	B2	1523.2	65651	9	α 5
1573.7	63545	8	B1	1522.0	65703	21	B1
1573.0	63573	6	α 2	1521.2	65738	20	B1
1572.8	63581	6	α 2	1518.1	65872	10	α 5
1570.5	63674	9	A2	1516.8	65928	23	B2
1569.5	63715	11	A1	1516.1	65959	19	B1
1567.1	63812	5	α 2	1514.1	66033	3	A2
1565.0	63898	12	A2	1513.2	66085	9	A1
1564.1	63935	15	A1	1512.0	66138	14	α
1561.4	64045	3	α 2	1511.0	66181	8	α 6
1559.9	64107	9	A2	1508.9	66273	19	A2
1558.9	64148	7	A1	1508.3	66300	9	
1557.1	64222	8	α 3	1508.0	66313	25	A1
1555.6	64284	13	B2	1505.9	66405	7	α 6
1555.0	64309	11	B1	1503.5	66498	18	A2
1554.0	64350	6	A1	1503.0	66534	18	
1551.5	64466	15	α 3	1502.8	66542	18	A1
1550.0	64516	19	B2	1499.2	66702	17	A2
1549.4	64541	16	B1	1498.0	66756	7	A1
1546.3	64671	4	α 3	1496.3	66832	9	α 7

λ	ν	I	
1495.0	66890	21	B2
1494.4	66916	21	B1
1493.6	66952	7	A1
1491.1	67065	15	α 7
1489.8	67123	21	B2
1489.0	67159	15	B1
1486.9	67254	4	A
1486.1	67290	6	α 7
1485.0	67340	15	B2
1484.2	67376	13	B1
1482.3	67463	13	A2
1481.4	67504	18	A1
1480.8	67531	9	B2
1480.0	67568	8	B1
1479.0	67613	5	α 8
1477.3	67691	19	B2
1476.7	67719	21	B1
1476.1	67746	21	A1
1474.2	67833	5	α 8
1472.5	67912	15	A2
1471.5	67958	13	A1
1470.6	67999	5	α 9
1469.0	68074	12	B1
1468.1	68115	12	A2
1467.1	68162	14	A1
1465.2	68250	8	α 9
1463.9	68311	19	B2
1463.2	68343	20	B1
1460.0	68499	15	α 9
1458.9	68545	17	B2
1458.4	68568	13	B1
1456.9	68639	10	A2
1455.9	68686	12	A1
1454.6	68747	16	B2
1454.1	68771	16	B1
1451.9	68875	11	A2
1450.6	68937	18	B2, A1
1450.0	68966	11	B1
1447.0	69109	18	A2
1446.0	69156	19	A1
1444.0	69252	11	α
1442.2	69339	15	A2
1441.7	69363	13	
1441.3	69382	13	A1
1440.1	69440	4	α
1438.8	69502	12	B2
1438.1	69536	14	B1
1437.6	69560	15	A2
1434.0	69735	19	B2
1433.3	69769	15	B1
1432.2	69823	4	α
1430.9	69886	4	α
1429.4	69959	17	B2
1429.2	69969	17	B1
1426.1	70121	13	A1
1325.9	70131	13	α
1425.3	70161	13	B2
1425.0	70175	13	B1
1432.8	70235	3	α 10
1422.6	70294	18	A2
1422.0	70323	17	B2
1421.3	70358	17	B1, A1
1419.8	70432	5	α 10
1419.0	70472	5	α 10
1418.2	70512	7	A2
1416.9	70572	5	A1
1414.8	70681	6	α 10
1413.9	70726	13	B1
1413.0	70771	4	A1
1409.5	70947	15	B, A
1406.1	71119	13	α
1405.6	71144	12	B2
1405.0	71174	13	B1
1401.8	71337	10	B2
1401.0	71378	10	B1
1397.2	71572	10	A1, B1
1394.6	71705	5	B
1390.1	71937	5	α
1389.5	71968	6	A1, B
1368.2	72140	9	A, B
1386.0	72150	10	A, B
1382.3	72343	6	B
1380.0	72464	7	B
1378.6	72537	12	α
1377.0	72622	6	α
1374.4	72759	6	α
1371.2	72729	5	α

Table 2. A-system

62492 (5)		62720 (4)		62897 (2)																
62527 (6)	*224*	62751 (3)	*186*	62937 (3)																
1188		*1184*		*1211*																
63674 (9)		63898 (12)		63107 (9)																
63715 (11)	*220*	63935 (15)	*187*	64148 (7)	*202*	64350 (6)														
1182		*1207*		*1208*		*1211*														
64851 (11)		65096 (20)		65308 (13)		65531 (12)														
64897 (13)	*245*	65142 (21)	*213*	65355 (12)	*206*	65561 (9)														
1188		*1171*		*1187*		*1214*														
66033 (3)		66273 (19)		66498 (18)		66702 (17)														
66085 (9)	*228*	66313 (25)	*229*	66542 (18)	*214*	66756 (7)	*194*	66952 (7)												
		1191		*1204*		*1202*		*1210*												
		67463 (13)		67912 (15)		68115 (12)														
		67504 (18)	*242*	67946 (21)	*212*	67958 (13)	*204*	68162 (14)												
		1182		*1191*		*1198*		*1220*												
		68639 (10)		68875 (11)		69109 (18)		69339 (15)												
		68686 (12)	*256*	68937 (18)	*219*	69156 (19)	*226*	69382 (13)	*178*	69560 (15)										
				1184		*1202*		*1195*		*1211*										
						70294 (18)		70512 (7)												
				70121 (13)	*237*	70358 (17)	*219*	70577 (5)	*195*	70771 (4)										
										1197										
										71968 (6)	*193*	72150 (10)								

frequency, which is plausibly assigned to the bending frequency in the excited state, are present. Price et al[1] considered that all the prominent bands in the region form a single progression with only the 200 cm^{-1} frequency, which, however, can not be accepted, because the intervals between neighbouring bands are too irregular for the adoption of such a simple scheme. From the present spectrograms it is clearly seen that this region contains two groups of bands having different shapes. In any case, the large extention of the vibrational

Table 3. B-system

63099 (12)		63327 (8)		63532 (8)														
63127 (8)	*208*	63335 (7)	*210*	63545 (8)														
1210		*1214*		*1222*														
64284 (13)		64516 (19)		64729 (11)		64931 (7)												
64309 (11)	*232*	64541 (16)	*226*	64767 (10)	*172*	64939 (7)												
1205		*1217*		*1192*														
65479 (10)		65703 (21)		65928 (23)														
65514 (12)	*224*	65738 (20)	*221*	65959 (19)														
		1178		*1200*														
		66890 (21)		67123 (21)		67340 (15)		67531 (9)										
		66916 (21)	*243*	67159 (15)	*217*	67376 (13)	*194*	67568 (8)										
		1178		*1184*		*1192*		*1203*										
				68311 (19)		68545 (17)		68747 (16)		68937 (18)								
		68094 (12)	*249*	68343 (20)	*225*	68568 (13)	*218*	68771 (16)	*193*	68966 (11)								
				1193		*1201*		*1198*		*1209*								
				69502 (12)		69735 (19)		69959 (17)		70161 (13)		70320 (17)						
				69536 (14)	*219*	69765 (15)	*226*	69969 (17)	*178*	70175 (13)	*183*	70358 (17)						
				1190		*1180*		*1205*		*1203*		*1214*						
										71337 (10)								
				70726 (13)	*221*	70947 (15)	*227*	71174 (13)	*204*	71378 (10)	*194*	71572 (10)						

structure and the character of the intensity distribution suggest a considerable change of the molecular dimension in the transition.

By picking up succesively one band after another from the red side of the absorption region, pursuing the series of the evenly spaced bands toward higher frequencies at intervals of 200 cm^{-1}, we see that the intensity of some bands becomes weaker. Near a position where a 200 cm^{-1} series ends, another new series begins. Such affairs are repeated throughout the region. Among the

200 cm^{-1} series, neighbouring bands show different shapes, whereas alternate ones have similar band shapes, suggesting they have the same fine structure. For instance, all bands in both groups have the appearance of double heads, whose mean separation is different in the two classes; namely, about 45 cm^{-1} and about 35 cm^{-1}, respectively. After all, the whole 200 cm^{-1} series are divided into two classes having different shapes.

From the foregoing facts, it is plausibly expected that the λ 1600–1350 region contains at least two electronic transitions of comparable intensities. Furthermore, it is natural to consider that in each of the two classes the distances between the corresponding members of two neighbouring 200 cm^{-1} series can be correlated to the symmetrical valence frequency of the upper level. Because, from the symmetry law, the antisymmetrical frequency can not be excited in transitions from the ground state except very weakly as an even overtone according to the Herzberg-Teller rule[11]. Thus all the strong bands were interpreted with only the two symmetrical frequencies in the upper state. From the relative positions of the 200 cm^{-1} series it is seen that the second characteristic frequency ν_1' is some multiple of the deformation frequency of about 200 cm^{-1}. Detailed investigation on the arrangement of the bands and the intensity distribution resulted two schemes, A system and B system, as shown in Tables 2 and 3, using 1200 cm^{-1} as the breathing frequency. In the schemes, progression in each row and column has a single intensity maximum, around which the bands show regular intensity distribution. From considerations based on the Franck-Condon principle, the vibrationless transition should be weak. As mentioned before, the spectra at higher pressures could not be photographed on account of the underlying continuum of N_2O_4. Therefore, the system origins as well as the weak bands corresponding to the lower or higher v' members could not be observed. It is desirable to make measurements at higher temperatures, at which N_2O_4 will be much more dissociated and the underlying continuum much more weakened.

Irregularities of the band separations are observed at some places in the systems. They result probably from perturbation by the other vibrational levels. These pertubations seem also to cause the irregularities of the doublet separations of the bands. It can be considered, too, that superpositions of bands arising from the low-lying excited vibrational levels of the ground state may distort the intensity distributions within some of the bands.

The present photographs taken under relatively high dispersion exhibited the double head structures of the bands, but resolutions of rotational structures

11) G. Herzbeg and E. Teller: Z. Phys. Chem. B**21** (1938) 410.

was not discernable. With the present accuracy, it can not be said whether this failure is due to the still insufficient resolution of the spectrograph or to the diffuseness of the bands. As mentioned earlier, the bands in this region appear to be divided into two groups by the difference in the doublet spacings. Besides, another possible difference may be seen; that is, in the B system, having smaller separations, the head in the shorter wave-length side appear to be more intense, while in the A system, having larger separations, the intensities of two heads seem to be equal, or perhaps the one in the shorter wave-length is stronger. Such large doublet separations, however, cannot be attributed to any doublet separation in the ground state[1]. Because, the ground state of NO_2 is known to be of $^2\Sigma$ character from the measurement of magnetic susceptibility[12] and from the thermodynamic data[13]. Moreover, the separations are too large to be ascribed to the spin doublets. Even though they might be attributed to the excited state, there is the same difficulty in the interpretation of the separation which is too large, if the molecule is considered to be nonlinear[14] in the excited state. However, if the present transition gives a $^2\Pi$ linear state, splitting into two states might occur, and the separation could be rather large. In this case the structure of the bands would resemble the NO γ or ε bands ($^2\Pi \rightarrow {}^2\Sigma$). The above interpretation, however, is in conflict with the result of the present analysis. Of course, there is also a room for consideration that the apparent doublets might be really the separate bands lying close together. On the other hand, systematic examination reveals that head separations are not so regular as might be supposed from the appearance of the spectrogram. This suggests also another possibility that the appearance of the differences of the band shapes as well as the unresolved fine structure might be due to the predissociation[6]. Further, from a strictly numerical point of view, it might be possible to consider both systems as belonging to a single electronic transition, because each 200 cm^{-1} series of the A and B systems is locating just at the middle between the corresponding two neighboring 200 cm^{-1} series of the another system.

In spite of the above-mentioned uncertainty, the fact that the appearance of the band shape is clearly and systematically different between the A and B systems is at the present stage in favour of the adoption of the schemes as shown in Tables 2 and 3.

In any case, the rotational structures of the bands appear to be considerably

12) G. G. Havens: Phys. Rev. **41** (1932) 337.
13) W. F. Giauque and J. D. Kemp: J. Chem. Phys. **6** (1935) 40.
14) H. A. Jahn and E. Teller: Proc. Roy. Soc. **A161**, (1937) 220.

complex, suggesting that in the upper level the molecule becomes more asymmetric than in the ground level; that is, the apex angle of the molecule may decrease with the transition. This supports that the intervals of about 200 cm^{-1} extending over the present region are attributed to the bending frequency of the excited level. Further, the relatively large decrease of the bending frequency with the transition (750 cm^{-1}→200 cm^{-1}) indicates the considerable reduction of the angular restoring force. The type of bands which would have been expected if the angle had remained unchanged or increased in the transition can be seen in the λ 2500 absorption system of the same molecule, and not only the K-structures but also the J-structures were partially resolved[15].

Although nearly all strong bands observed in the λ 1600–1350 region are involved in the schems of Table 2 and 3, there remain a few other weak bands. The interval 200 cm^{-1} occurs again in them. This indicates that they belong also to the A or B system. Whether they are excited by the antisymmetrical vibration in the upper state or originated from the excited levels in the ground state should be made clear by the temperature variation method, but they seem rather to correspond to the transitions from the lower excited levels in the normal state. For, according to the Boltzman distribution law, at a room temperature there will be appreciable numbers of the gas in the lower excited level. In fact, it is seen that they may be correlated to some of the main bands by seperations of about 700 cm^{-1}, which is near the value known for the bending frequency of the ground state.

In order to obtain the more conclusive results about the vibrational analysis the following experiments are essential; to examine the spectrum under higher dispersion to resolve even partially the fine structure; to measure the temperature variation of the absorption intensity in a wide range of temperatures; or to observe the isotope effect of the vibrational structure. In the present wavelengths, however, these measurements are rather difficult in techniques.

A Rydberg series corresponding to the first ionization potential known from the electron impact experiment[16], if present, should be found around the λ 1600–1350 region. But its identification is quite difficult as a consequence of the serious superposition with λ 1600–1350 absorption systems.

Concerning the electronic configuration of the NO_2 molecule, Mulliken[7] and later Walsh[6] discussed in detail, based on the correlation diagrams of molecular orbitals of the XY_2 type molecules. Price and Simson[1] also treated it qualitatively in the report on the absorption measurement.

15) L. Harris and G. W. King: J. Chem. Phys. **8** (1940) 775.
16) E. C. G. Stueckelberg and H. P. Smith: Phys. Rev. **36** (1930) 478.

According to Mulliken, the valence shell molecular orbitals of NO_2 are arranged in the order of energy, as shown in Fig. 3a. The outermost occupied orbital, $4a_1$, containing the odd electron, is considered to correspond to the excited orbital, $3\sigma_g$ of the linear CO_2 molecule. The $3\sigma_g$ orbital, occupying a considerably high energy position in the case of linear molecule, is assumed to descend sharply with the decrease of the apex angle of the triatomic molecule. While CO_2 shows the absorption spectra only in the far ultraviolet, a large variety of absorption bands are known for NO_2 from the near infrared to the ultraviolet. This suggests that in NO_2 not only the above-mentioned $4a_1$ orbital but also some upper unoccupied orbitals would descend with decreasing apex angle. The occupied orbitals, $3b_2$ and $1a_2$ situating just below $4a_1$, correspond to the outermost occupied $1\pi_g$ orbital of the CO_2 molecule, which is almost localized in the O atom and is nonbonding. A Rydberg series corresponding to the ionization potential of $3b_2$ or $1a_2$ has been observed[1),5)] in the far ultraviolet absorption spectra of NO_2 as mentioned before. Four orbitals just below $1a_2$ are considered to contribute strongly to the N–O bond. Of them, $3a_1$ and $1b_1$ form the π bonds, while $2b_2$ and $2a_1$ form the σ bonds. They constitute together the double bonds. In the ground state three upper vacant orbitals have antibonding

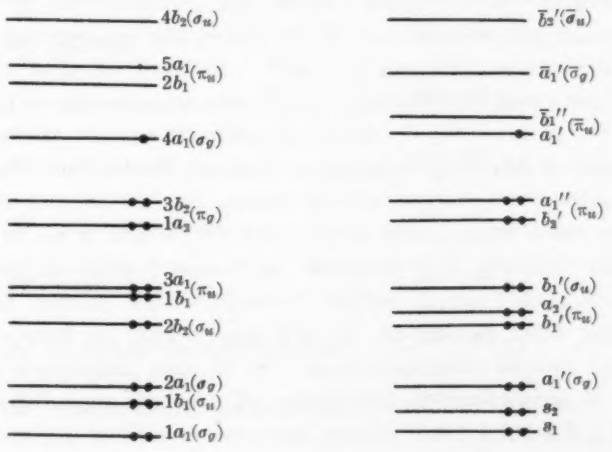

Fig. 3.

nature. Further, Mulliken assumed that among the excited $5a_1$ and $2b_1$ orbitals corresponding to π_u of CO_2 descended with decreasing apex angle, while $4b_2$ corresponding to σ_u rose a little with decreasing angle.

Walsh, in a similar report to that of Mulliken, modified the orbital energy diagram (Fig. 3b). In his diagram, the a_1 orbital occupied by an odd electron corresponds not to the σ_g orbital of the linear molecule, but to the π_u orbital. It is also assumed that a_1 and b_1 corresponding to π_u go rapidly downwards with decreasing apex angle, and that a_2 and b_2 rise sharply. As to the other orbitals occupied by two electrons, there are few discrepancies between Walsh's and Mulliken's interpretations.

After all, the electron configuration of NO_2 in the ground state is assumed as follows:

$\underbrace{(1a_1)^2\ (1b_2)^2}$	$(2a_1)^2$	$(2b_2)^2$	$\underbrace{(1b_1)^2\ (3a_1)^2}$	$\underbrace{(1a_2)^2\ (3b_2)^2}$	$(4a_1)$	$^2A_1$
s	σ_g	σ_u	π_u	π_g	π_u or σ_g	
O	σ-bonds		π-bonds	O	N←→O	

Excited orbitals $(2b_1)$ $(5a_1)$ $(4b_2)$

π_u π_u or σ_g σ_u

According to the above assumptions, allowed transitions with relatively small excitation energies are predicted in order of increasing excitation as follows:

Ground state

$$^2A_1 \xrightarrow[//y]{3b_2\to 4a_1} \cdots (3b_2)(4a_1)^2\ ^2B_2 \quad (1)$$

$$^2A_1 \xrightarrow[\perp z]{4a_1\to 2b_1} \cdots (3b_2)^2(2b_1)\ ^2B_1 \quad (2)$$

$$^2A_1 \xrightarrow[\perp z]{4a_1\to 5a_1} \cdots (3b_2)^2(5a_1)\ ^2A_1 \quad (3)$$

$$^2A_1 \xrightarrow[//y]{3b_2\to 5a_1} \cdots (3b_2)(4a_1)(5a_1)\ ^2B_2 \quad (4)$$

$$^2A_1 \xrightarrow[//y]{1a_2\to 2b_1} \cdots (1a_2)(3b_2)^2(4a_1)(2b_1)\ ^2B_2 \quad (5)$$

$$^2A_1 \xrightarrow[//y]{4a_1\to 4b_2} \cdots (3b_2)^2(4b_2)\ ^2B_2 \quad (6)$$

$$^2A_1 \xrightarrow[\perp z]{3a_1\to 4a_1} \cdots (2b_2)^2(1b_1)^2(3a_1)(1a_2)^2(3b_2)^2(4a_1)^2\ ^2A_1 \quad (7)$$

$$^2A_1 \xrightarrow[\perp z]{1b_1\to 4a_1} \cdots (2b_2)^2(1b_1)^2(3a_1)^2(1a_2)^2(3b_2)^2(4a_1)^2\ ^2B_1 \quad (8)$$

$$^2A_1 \xrightarrow[//y]{2b_2\to 4a_1} \cdots (2b_2)(1b_1)^2(3a_1)^2(1a_2)^2(3b_2)^2(4a_1)^2\ ^2B_2 \quad (9)$$

Forbidden transitions present in the same region are predicted as follows:

$$^2A_1 \xrightarrow{1a_2\to 4a_1} \cdots (1a_2)(3b_2)^2(4a_1)^2\ ^2A_2 \quad (10)$$

$$^2A_1 \xrightarrow{3b_2\to 2b_1} \cdots (1a_2)^2(3b_2)(4a_1)(2b_1)\ ^2A_2 \quad (11)$$

A_1, A_2, B_1, B_2 represents the symmetry classes for nonlinear triatomic molecules, in which the first is the totally symmetric representation. The absorption systems between λ 9000 and λ 3000 in the near infrared and the visible are considered as resulting from transitions (1), (2) and (3). Transitions (4), (5) and (6) give rise to the near ultraviolet absorption systems. The apsorption bands around λ 2500, which was measured in detail by Harris et al[4], were shown to have fine structures of the parallel type. Therefore, the system corresponds with some of the (4)–(6) transitions. Analyzing the rotational structure of the λ 2491 band semi-quantitatively, Harris et al. concluded that in the transition only the bond lengths increased considerably, the apex angle changing little. Thus, they suggested that this transition was correlated with the $4a_1$ orbital, which was considered to be bonding and not to have directional effects. However, as pointed out by Mulliken, the empirical data can better be explained by considering the λ 2500 system to be attributed to the transition of an electron not from $4a_1$ but from the nonbonding $3b_2$ or $1a_1$ orbital to one of the excited orbitals above $4a_1$.

The λ 1600–1350 absorption systems in question correspond to the transitions (7), (8) and (9). The reason is as follows. Taking into account the character of the intensity distributions in the 1200 cm^{-1} and the 200 cm^{-1} progressions, it is plausible that both the bond length and the apex angle of the molecule change appreciably with the transition. This supports partly the proposition that the λ 1600–1350 absorption system is attributed to the transition from some of the lower bonding orbitals to the antibonding $4a_1$ orbital.

On the other hand, all the bands belonging to the A and B systems appear to degrade towards the red. Almost all of them have sharp heads, indicating that both of the K- and J- structures of the bands might shade towards the red. Using the method deviced by Metropolis[17], a schematic diagram was constructed showing the directions of shading of the J and K structures for changes in angle and bond distance (Fig. 4). As the apex angle and the bond length of the ground state of NO_2, those proposed by Moore[7], i.e., $2\alpha=134°$ and $r=1.188$ A, were adopted. The whole field of the diagram is divided by two intersecting full curves into four regions J_+K_+, J_-K_-, J_+K_-, J_-K_+. The subscripts + or − is used to denote whether the J or K rotational structure degrades towards the violet or the red. The field is also divided in another way into four regions by two intersecting dashed curves. On these curved lines, $(v_1')_{max}=(v_2')_{max}$, where $(v_1')_{max}$ denotes the quantum numbers of the strongest band in the pure v_1' vibrational progression and $(v_2')_{max}$ denoted that of the v_2'

17) N. Metropolis: Phys. Rev. **60** (1941) 283.

progression. If some simple assumptions are made, the above relation is approximated by the relation, $\Delta\alpha=\pm 2^{\frac{1}{2}}(\Delta r/r')$, which has been used in this diagram. In the dotted regions of Fig. 4, the deformation is more prominent than the symmetrical valence vibration, whereas in the undotted region the opposite is true. In the case of the λ 1600–1350 system of NO_2 the facts known are as follows: 1) The bands are degraded towards the red, and have relatively sharp heads. 2) Both v_1' and v_2' progressions are appreciably excited in about the

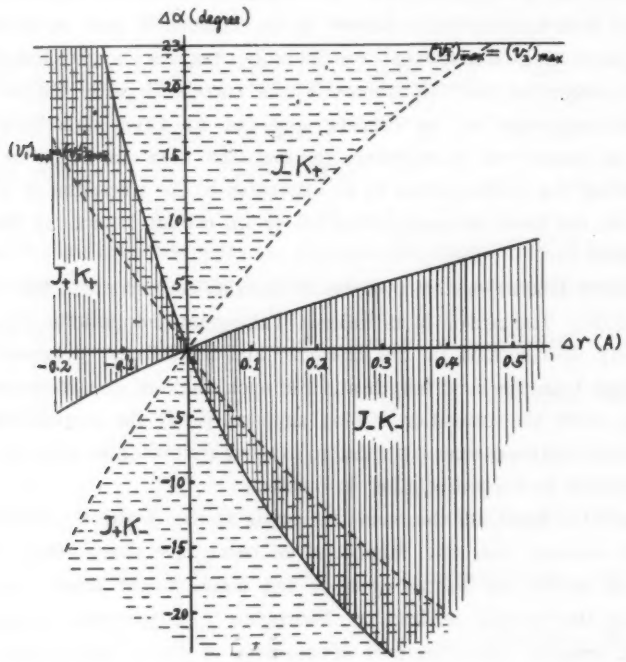

Fig. 4.

same degree, although the v_1' progression is slightly more developed. Referring to Fig. 4, the above facts suggest that the A and B absorption system correspond to the change represented by the region around the right lower dashed line. In this region, it is seen that the bond is lengthened and the apex angle decreased. It is difficult to conclude from the results by Price and Simpson that the λ 1600–1350 system is attributed to the bonding → antibonding transition, because they did not find the v_1' progressions in this system. Whereas, from the present results, the system is reasonably attributed to the strong bonding → antibonding ($4a_1$) transition. Further, the decease of the apex angle is considered to be not so

large as in the case of Price and Simpson's measurement. The above considerations, together with the fact that there seem to be two similar systems in the same region, suggests that one of the transition may be from the π bonding to $4a_1$ antibonding. If the rotational K-structures could be resolved, discriminating between the parallel and the perpendicular types of the bands, it would be made clear whether the present system corresponds to the transition of the π type (7), (8) or the σ type (9).

The absorption in the region of λ 1600–1350 appears to have the intensity[5] comparable with that of the first member of a Rydberg series situating at the shorter wave-length side. This plausibly suggests that the transition is N→V type. The N→V transition[18] according to the molecular orbital theory, means a transition from a bonding to a corresponding antibonding orbital. The $2b_2 \rightarrow 4a_1$ ($\sigma_u \rightarrow \sigma_g$) transition in the Mulliken's diagram is immediately regarded as the N→V type in the strict definition. Therefore, it might be probable that this N→V transition is involved in the A and B systems found in the present experiment. But, in the Walsh's diagram, the $2b_2 \rightarrow 5a_1$ is the $\sigma_u \rightarrow \sigma_g$ type. In this case, the energy of $5a_1$ is assumed to increase with the decrease of the apex angle of the molecule. So, the apex angle becomes slightly larger with the transition $2b_2 \rightarrow 5a_1$ and the molecule approaches to the linear form in the upper state. Further, according to the Walsh's assumption, the transition to $4a_1$ is of the $\sigma_u \rightarrow \pi_u$ or the $\pi_u \rightarrow \pi_u$ type. It is not clear that they are able to have such great intensity as measured in the present experiment. In the Mulliken's assumptions, too, it is not at the stage of full discussion about how much intensity the (7) or (8) transition corresponding to $\pi_u \rightarrow \sigma_g$ ($\perp$ type) has.

Acknowledgment

The author wishes to express his sincere gratitude to Professor Y. Fujioka for his deep interest and encouragement during the course of this work.

Acknowledgment is due to Professor R. S. Mulliken, in particular, for kindly reading the manuscript sent to him privately and making a number of valuable suggestions, to which the author is greatly indebted.

Thanks are also due to Dr. M. Kinoshita for reading the manuscript and giving many helpful suggestions, Dr. Y. Tanaka for his kind suggestions and advice, to Dr. M. Seya for his permission of using the spectrograph and the Eastman SWR plates, and to Mr. K. Goto for his unusual help in the measurement.

18) R. S. Mulliken: J. Chem. Phys. **7** (1939) 20.

Spectrophotometric Studies on the Nature of Erythrocytes

Mitsuo HOMMA and Mitsuto HASEGAWA

(Department of Internal Medicine, School of Medicine, Keio University. Prof. I. Mikata)

(Received October 13, 1955)

Studies have been made on the ultraviolet spectral absorption, particularly, on the Soret absorption band of hemoglobin inside red cell comparing with that of hemoglobin solution outside the cell, using Beckman Spectrophotometer Medel DU, slit width 0.1 m.m., of normal individuals and in cases of various kinds of anemia.

Red blood cell and hemoglobin solution are treated in or with agar-agar gel, CO-gas, 4% $K_3Fe(CN)_6$ solution and 8-Oxyquinoline in-Michaelis' solution respectively, and furthermore the absorption curve of free erythrocyte protoporphyrin dissolved in HCl-solution is studied.

The characteristic erythrocyte is found in aplastic anemia. The Soret absorption band of this erythrocyte is observed at 409 mμ, which is quite different from that of other anemias and normal persons. The chemical activity of hemoglobin in aplastic anemia is reduced as compared with normal hemoglobin and hemoglobin in other anemias, though it is still more active than methemoglobin.

1. Introduction

A number of abnormal hemoglobins[1] were already reported, e.g. Hemoglobin *F* by Leeks & Wolman, Hemoglobin *S* by Paubling et al, Hemoglobin *C* by Itano & Neel, Hemoglobin *D* by Cooke & Itano and Hemoglobin *E* by Itano. These hemoglobins are analyzed and characterized chiefly by electrophoresis.

Spectroscopic studies on the nature of hemoglobin, for the most part, have been carried out in the condition of hemoglobin solution[2][3], and there are a few spectroscopic studies of intact red cell[4][5][6][7].

Among these Metcalf and Kobayashi studied the absorption curve of a single red cell.

Kobayashi proved a spectroscopic specificity of a single red cell found in

1) J. C. White, G. H. Beaven: J. Clin. Path. **7** (1954) 176.
2) D. L. Drabkein, J. H. Austin: J. Biol. Chem. **98** (1932) 719.
3) D. L. Drabkein and J. H. Austin: J. Biol. Chem. **112** (1935) 67.
4) E. J. Robinson: Amer. J. Physiol. **133** (1941) 428.
5) E. M. Jope: in "Hemoglobin" Barcroft Symposium 1949, London Butterworth.
6) W. K. Metcalf: Blood, **6** (1952) 1114.
7) T. Kobayashi: Lecture held at the Keio Medical Society in Tokyo. (1953).

aplastic anemia[8][9].

The above observations may be of help in the differential diagnosis of aplastic anemia from other anemias, especially from aleukemic-leukemia.

Jope was the first investigator who succeeded in demonstrating the absorption spectra in aggregative conditions of erythrocytes.

It is thought that the aggregated red cells may be easier to investigate than a single erythrocyte[10][11].

2. Experimental

Studies were made on the ultraviolet spectral absorption of hemoglobin inside the red cell which was fixed with 0.3% agar gel in Michaelis' solution (ph 7.4) to prevent hemolysis and precipitation, using the Beckman spectrophotometer Model DU, slit width 0.1 m.m., contrasting with that of hemoglobin solutions outside the cell which had been made by hemolysis of the same red cells with distilled water

Soret band, which seems due to the haem molecule and an essential one after the 16 membered porphyrin ring of conjugated double bonds, was observed chiefly on the shift of absorption maxima.

3. Results

The peak of the Soret absorption band of hemoglobin solution always was found at 414 to 415 mμ regardless of the different kinds of anemias. (Fig. 1.)

The maximum absorption of the Soret band of red cell, which was fixed with above mentioned agar gel, appears mostly at 415 mμ in normal adult and in anemias other than aplastic anemia.

In case of aplastic anemia, the peak was observed in the range of shorter wave-length, particulary in 3 patients, who have not been transfused, it was observed at 409 mμ.

These Soret absorption band data are summarized in Table 1.

On the other hand, in cases of aplastic anemia, treated with daily blood transfusion, maximum was found at 415 mμ, but as compared with 415 mμ in case of normal adult, the absorption curve of the former has an inflation towards the shorter side of wave-length, and that of the latter towards the longer side. (Fig. 2.)

---

8) H. Watanabe: Acta haematologica japonica **18** (1955) 1.
9) H. Watanabe: Acta haematologica japonica **18** (1955) 182.
10) M. Homma and M. Hasegawa,: Acta haematologica japonica **17** (1954) 248.
11) M. Hasegawa,: "Saishin Igaku," (Medical Magazine in Japanese) **9** (1954) 546.

Absorption maximum at 409 mμ is rarely found even in normal red cells which were under the influence of uncertain cause. In comparison with that of aplastic anemia, the absorption curve of the former, however, has a moderate inflation towards the longer side of wave-length. (Fig. 3.)

There is a tendency for the maximum to return to longer wave-length from 409 mμ in a relatively short time. But, contrary to it, when the wave-length of maximum absorption lies temporarily at 415 mμ in aplastic anemia by some remedies or unknown reasons, the peak comes back to 409 mμ after some longer time. (Fig. 4.)

Table 1. Apparent wavelength values (in mμ) of the Soret band of erythrocyte in various anemias.

Wave length (in mμ)	aplastic anemia	leukemia	Plumbism	normal adult
415	7	5	2	14
414				
413	1			2
412	3	1		1
411	5	1		
410				
409	11			1

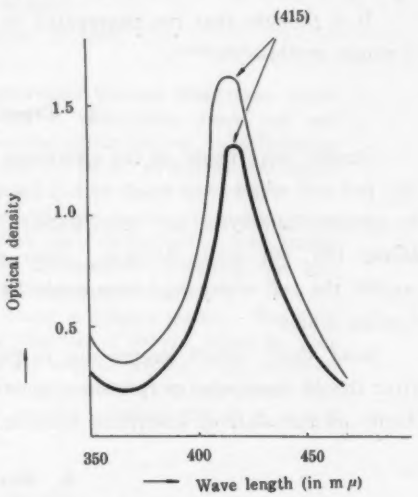

—— normal. —— aplastic anemia.

Fig. 1. Absorption curves in the neighbourhood of Soret band of hemoglobin solution.

An absorption curve shows the sum of absorptions of several substances coexisting in an examined material.

It is supposed that one substance shows the maximum absorption at 409 mμ and the other at 415 mμ, and the two remain in chemical equilibrium.

When the equilibrium between the two substances is lost due to the changes in body metabolism, giving rise to increase or decrease of either substance, the observed absorption curve should be changed by the resulted proportion of the constituents.

By investigation of the absorption curves of erythrocytes in detail, no sharp peak was found. As a sharp peak is characteristic to only chemically pure substance, and the curve is not only relatively flat at the peak, but also inflates towards the longer or shorter wave-length range at the foot, these curves are considered to be synthetic from at least two fundamental substances.

The peak of absorption curves in aplastic anemia erythrocytes does not change so easily as that of normal erythrocytes.

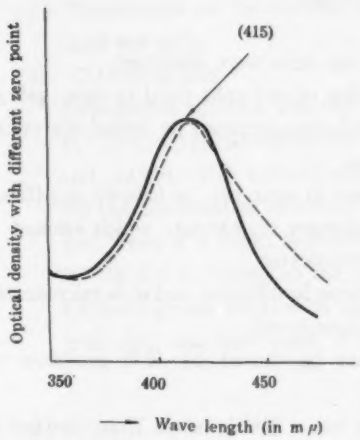

—— aplastic anemia.
- - - normal adult.

Fig. 2. Absorption curves at the Soret band region of erythrocyte fixed in 0.3% agar gel added with Michaelis' solution.

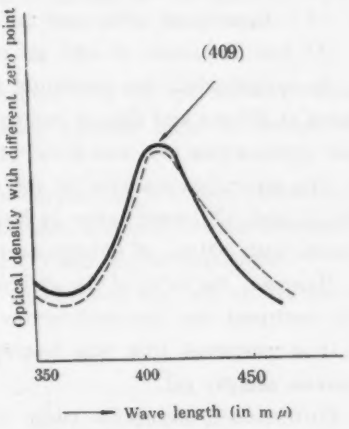

—— aplastic anemia.
- - - normal adult.

Fig. 3. Comparison of absorption curves at the Soret band region of erythrocytes between normal adult and aplastic anemia, in which both absorption maxima lie at 409 mμ.

It is considered that the chemical activity in the aplastic anemia erythrocyte is inferior to that of normal, namely, as the wave-length of 409 mμ shows, the equilibrium is inclined toward one side which is a more stabilized state.

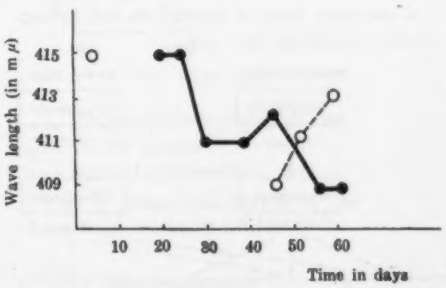

•——• aplastic anemia. ○——○ normal adult.

Fig. 4. Changes in wavelength (in mμ) of the Soret band of erythrocytes in normal and aplastic anemia with lapse of time.

Among the absorption curves of red cells, the peak at 409 mμ seems to be a limit of blue shift.

Viewing blue shift limit, it is suggested that there may be the following two causes.

1. Change of some contents in red cell perharps mainly hemog-

lobins inside red cell.

2. Change of red cell membrane. There may happen some adsorption or chemical binding between hemoglobin and membrane.

Then the following experiments were made.

(1) Experiment using agar gel.

At first, influences of agar gel on the red cells were observed.

In normal adult, the maximum absorption of red cells fixed in agar gel appeared at 415 mμ and that of hemoglobin solution prepared by hemolysis of the same erythrocytes also was found at 415 mμ.

The absorption maxima of red cell fixed in agar gel, is located at 415 mμ after 2 and 12 hours; after 24 hours it changes to 409 mμ, which seemed to coincide with 409 mμ of aplastic anemia erythrocytes.

However, the form of the absorption curve is different and it is microscopically confirmed that the erythrocytes were hemolysed.

It is considered that this hemolysis may be caused by H_2O produced by syneresis of agar gel.

Furthermore, absorption curve of agar has a gentle slope from 350 mμ to shorter wave-length range, and has no influence upon the Soret band.

After these facts it is considered that agar gel itself has no effect on erythrocyte content through the membrane.

Whereas the absorption curve of aplastic anemia erythrocyte shows the peak at 409 mμ, hemoglobin solution made by hemolyzing the same erythrocyte shows the peak at 415 mμ in 0.3% and also 0.85% NaCl solutions, but 407 mμ in agar gel.

Hemoglobin of normal adult, whose erythrocyte shows the peak at 415 mμ, has its peak also at 415 mμ in solutions of 0.3% and 0.85% NaCl but in agar gel, it has at 409 mμ. (Table 2.)

Table 2. Effects on the wavelength (in mμ) of the Soret band of erythrocyte and hemoglobin solution in agar gel.

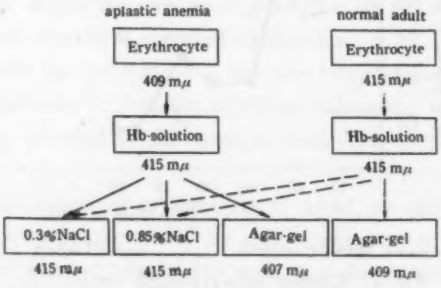

This fact is considered that hemoglobin outside erythrocyte is either adsorbed to or chemically bonnd with high molecular agar.

Condition of hemoglobin inside red cell in aplastic anemia seems similar to the condition, in which hemoglobin is combined with agar.

These facts suggest that the hemoglobin of aplastic anemia is slightly different from the normal hemoglobin and that it might have been denaturated

to some extent, although the denaturation might be of some reversible character, and that hemoglobin inside aplastic anemia erythrocytes is in a condition of low chemical activity.

(2) Experiment on the various chemical influences on hemoglobin solution and red cells.

(a) CO-hemoglobin

Hemoglobin solution and red cells treated with CO gas showed maxima at 419 mμ, and no difference was found between those of normal adult and patients with aplastic anemia.

As the combination between CO and hemoglobin is a very characteristic one, even if a slight denaturation happend in aplastic anemia hemoglobin, it was not so strong as the bond of CO with Fe in hemoglobin.

CO-hemoglobin solution in agar gel also showed the peak at 419 mμ and blue shift was not found. (Fig. 5.)

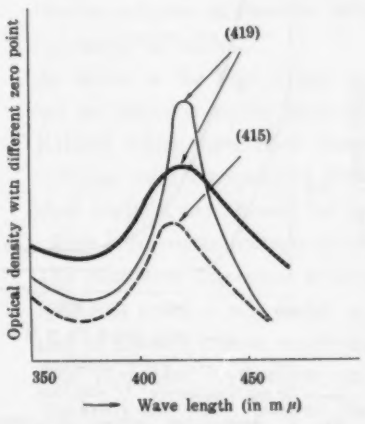

— Erythrocyte containing CO-Hb.
—— CO-Hb solution.
- - - Normal erythrocyte.

Fig. 5. Absorption curves at the Soret band region of CO-Hb.

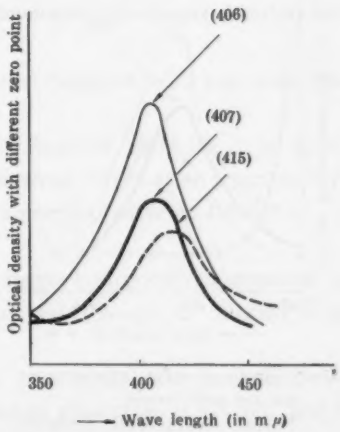

— Erythrocyte containing Met-Hb.
—— Met-Hb solution.
- - - Normal erythrocyte.

Fig. 6. Absorption curves at the Soret band region of methemoglobin.

(b) Methemoglobin

Methemoglobin was prepared by treating hemoglobin solution with 4% $K_3Fe(CN)_6$, and red cell is also treated with 4% $K_3Fe(CN)_6$ in Michaelis' solution to prevent hemolysis.

Maximum absorption of methemoglobin solution lies at 406 mμ, that of

methemoglobin inside erythrocytes lies at 407 mμ and no difference was detected between normal adult and patient with aplastic anemia. (Fig. 6.) As methemoglobin has a decided stable state, hemoglobin of 409 mμ in aplastic anemia shows still higher activity than methemoglobin, and perhaps some activity as hemoglobin is retained.

(c) 8-Oxyquinoline (oxine)

Considering that maximum absorption lies at 409 mμ owing to the decrease of chemical activity of hemoglobin, it is supposed that either hemoglobin has a certain combination with red cell membrane, or it can suppress the chemical activity of hemoglobins, even if membrane is intact, when a certain toxic substance exists in red cell. Oxine is tried in order to reproduce the above condition as oxine combines very strongly with iron.

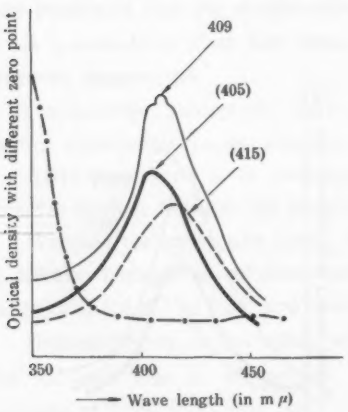

— Aplastic anemia erythrocyte treated with oxine.
—— Normal erythrocyte treated with oxine.
- - - Normal erythrocyte.
-·-·- Saturated oxine in Michaelis' solution.

Fig. 7. Absorption curves at the Soret band region of red cell treated with oxine at 37°C for 12 hours, showing the difference between normal adult and Patient with aplastic anemia.

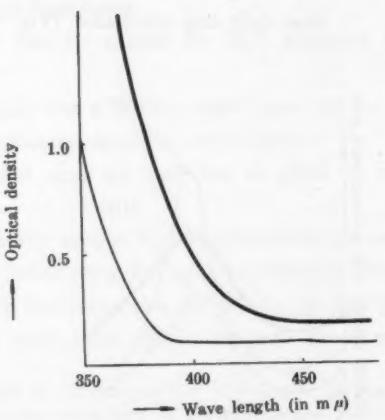

—— 200 γ% oxine-Fe^{+++}solution.
— 20 mg% oxine-Fe^{+++} solution.

Fig. 8. Absorption curves of oxine-Fe^{+++} solution. There are merely end-absorptions and no characteristic maxima lie at the Soret band region.

Saturated solution of oxine in Michaelis' solution was prepared, ph of which was made 7.4 by Veronal buffer, and hemoglobin solution and intact red cell were treated with this saturated solution in vitro. Effects

on the erythrocytes of rabbits, injected intravenously daily 10 c.c. of oxine solution, were also observed.

When erythrocyte is incubated in oxine solution at 37°C for 12 hours in test tube, the peak of absorption curves in aplastic anemia erythrocyte lay always at 405 mμ, whereas that of the same erythrocyte, which is not incubated in oxine solution, in agar gel was observed in the range of 409 mμ to 415 mμ.

Maximum absorption of normal adult erythrocyte treated with oxine solution, however, appeared at 409 mμ. In this case, examining in detail, the absorption curve tends to have another little peak at 405 mμ besides the peak at 409 mμ. When incubated in oxine for a longer time, the peak at 409 mμ shifts eventually to 405 mμ. (Fig. 8.)

Within some shorter time than 12 hours, for example 2 hours, no change of absorption curves is found.

This proves that oxine can not easily pass through the cell membrane. Similar evidence is observed when methemoglobin is prepared inside red cell using $K_3Fe(CN)_6$.

As shown in the Figs. 8 and 9, absorption curves of oxine and oxine-iron has no influence on the Soret band.

Rabbits which have been intravenously injected with 10 c.c. of oxine solution, were accompanied with anemia three weeks after injection, but their erythrocytes showed the peak of absorption curve at 415 mμ.

(d) Free erythrocyte protoporphyrin

The maximum absorption of free erythrocyte protoporphyrin dissolved in 15% HCl solution was found at 409 mμ and it seems to coincide with that of aplastic anemia erythrocyte.

The plumbism erythrocyte, in which free erythrocyte protoporphyrin markedly increases, showed the maximum absorption at 415 mμ, and a variation in the wave-length of the maximum of protoporphyrin is associated with changes in concentration of solvent HCl.

It is assumed that 409 mμ of the absorption curve of red cell does not show the peak 409 mμ peculier to the free erythrocyte protoporphyrin.

4. Summary

1. The Soret absorption band of hemoglobins in and outside red rell was studied using Beckman Spectrophotometer Model DU.

2. In case of erythrocyte, 0.3% agar gel in Michaelis' solution was used in order to prevent hymolysis and precipitation.

3. The Soret band of hemoglobin solution was always observed at 414 to 415 mμ regardless of the kind of anemia.

4. In aplastic anemia, characteristic erythrocyte was found, in which hemoglobin retained a little of its chemical activity.

The maximum absorption of this erythrocyte was found at 409 mμ and clearly different from that of normal adult erythrocyte.

5. This was presumed to be due to slightly denaturated hemoglobin and abnormally combined states of hemoglobin with the red cell membrane or some unknown toxic substance in the cell.

Acknowledgement

The authors wish to express their sincere thanks to Professors I. Mikata and T. Kobayashi for their suggestions and reading the manuscript, and to Assistant Professor Yoshihiko Ohyagi, Tokyo University of Education, for his deep interest, instruction and valuable discussions, and also to Mr. H. Watanabe, Instructor of pathology, and Miss. M. Suzuki, Investigator of individual spectrophotometrical observations.

Polarisation of Raman Lines of Iodic Acid and the Structure of the acid molecule

J. R. SARAF

Physics Department, Lucknow University, Lucknow. (India)

(Received September, 11 1955)

The paper gives the results of depolarisation measurements of a 4.5 N and a 0.2 N Iodic Acid solution. The results show that all the lines are polarised pointing to conclusion that the iodic acid molecule has no element of symmetry and, therefore, is likely to exist mainly in the form of polymer.

The structure of HIO_3 molecule has been shown to be of the type AB_2B', i. e., a pyramid with an isosceles base.

1. Introduction

The number of Raman Lines obtainable depends not only on the number of atoms in the molecule but also on the symmetry possessed by it. The symmetry can be determined from a knowledge of the state of polarisation of the Raman Lines; that is to say, determination of depolarisation factor p for each Raman Line becomes necessary. p indicates the nature of vibration to which the line is due.

Depolarisation measurements for the Raman Lines of Iodic Acid were previously made by Venkateswaran[1] and Shen, Yao and Wu[2],but the results obtained by them do not seem to agree much. In a previous paper the author[3] has reported Raman spectre of Iodic Acid at different concentrations and shown that most of the lines obtained with a concentrated solution of the Acid are due to polymers.

With a view to obtain further information on the subject it was felt desirable to make a re-investigation of the state of polarisation of the Raman Lines of a (1) 4–5 N and (2) 0.2 N solution of the Acid. With the help of the results so obtained classification is made between polymers and monomers, and the previous assignment of frequencies is confirmed.

1) C. S. Venkateswaran, Proc. Indian Acad. Sci. **4A** (1936) 177.
2) Shen, Yao, & Wu.: Phys. Rev. **51** (1937) 235.
3) Saraf: Curr. Sci. **11** (1942) 101.

2. Experimental

The usual experimental technique was used for finding the values of the depolarisation factors of the Raman Lines.

3. Results

The following table gives the values of the depolarisation factors of the the various Raman Lines and their intensities. The results of investigation by other two workers are also added for comparison:

1. Iodic Acid 4.5 N

Raman frequency $\Delta\nu$	Depolarisation Factor		
	Venkateswaran 6 N	Shen, Yao & Wu 6 N	Author 4.5 N
317 (6)	—	—	0.31
332 (6)	0.60	0.81	0.30
354 (4.5)	—	—	0.35
449 (2)	P	—	0.67
642 (4)	0.30	—	0.48
653 (3)	—	—	0.49
789 (10)	0.25	0.43	0.37
806 (8.0)	—	—	0.46
826 (6)	0.25	0.67	0.53

2. Iodic Acid 0.2 N

804 (5)	—	—	0.47
824 (2)	—	—	0.52

4. Structure of the Iodic Acid Molecule

The following considerations will show that there is not much in common between the structures of Iodates and Iodic Acid and hence the two cases may be treated differently. The structure of Iodate ion has been discussed in detail by Zacharisen[4], Huggins[5], Venkateswaran[6], Shen, Yao and Wu[7], Kujumzelis[8] and others, all agreeing with the view that the IO_3^- ion has a symmetrical pyramidal structure with the symmetry C_{3v}, the three Oxygen atoms occupying

4) Zachariasen: Phys. Rev. **37** (1931) 105, 775.
5) Huggins: Phys. Rev. **37** (1931) 447, 1177.
6) Venkateswaran: Proc. Indian Acad. Sci. **4A** (1936) 177.
7) Shen, Yao, Wu: Phys. Rev. **51** (1937) 235.
8) Kujumzelis: Z. Phys. **110** (1938) 760.

the corners of an equilaterel triangle, the Iodine atom being at the apex. On the other hand, the study of the structure of the Iodic Acid Molecule has, however, received comparatively little attention.

The structure of Iodic Acid, however, can now be written as

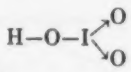

corresponding to the electronic structure

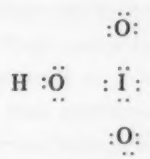

The essential difference between this structure and that of the IO_3^- ion is that in the former case, out of the three Oxygen atoms, two are similar and unattached, while the third is attached to a Hydrogen atom, whereas in the latter case all the three Oxygen atoms are similar and unattached. Thus the Iodic Acid Molecule can be regarded as an Iodate group, with one Oxygen atom different from the other two, i. e., it is of the type AB_2B'.

5. X'ray Evidence

Recently Rogers and Helmholz[9] (1941) have studied, by the method of X'ray analysis, the crystal structure of Iodic Acid. They observe:—

" The X'ray examination shows the presence of discrete pyramidal IO_3 groups in the crystal. Three Oxygen atoms in positions approximately opposed to the three-bonded IO_3 Oxygens and at distances 2.45, 2.70 and 2.95 A complete a distorted IO_6 octahedron, with the three strong bonds and three weaker ones. The Hydroxyl Oxygen atom of each Iodate group has two nearest Oxygens at 2.78 A. There are thus two Hydrogen bonds for each Iodate group forming a moderately strong bifurcated bond. The Oxygen atoms are in a somewhat distorted closest packed arrangement. Crystalline Iodic Acid is an aggregate of HIO_3 Molecules held together by Hydrogen bonds and secondary I-O bonds."

9) Rogers & Helmholz: J. Amer. Chem. Soc. **63** (1941) 278.

The picture formed can be represented as given below:—

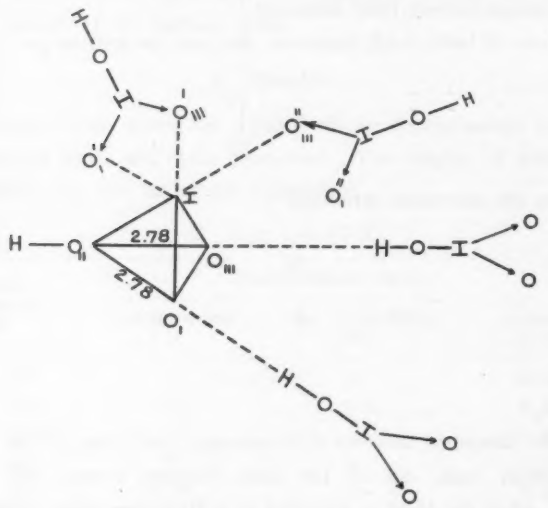

From the diagram it appears that Iodic Acid, in the crystalline state, is penta-coordinated having Hydrogen as well as Halogen bonds both. It seems quite probable that in an Iodic Acid solution the three secondary I-O bonds may become so weak as not to exert their influence at all. Then we are left with a three-coordinated structure only in agreement with Nayar's[10] results that in a concentrated solution only trimers $(HIO_3)_3$ exist.

The other point to be noticed is that the base of the Pyramidal Iodate group is an isosceles triangle. This supports the conclusion that the structure of the Iodic Acid Molecule is a pyramid with an isosceles base (with the symmetry C_s) and is of the type AB_2B'.

6. AB_2B' Molecule

Wilson[11] has calculated the number and state of polarisation of the fundamental vibrations of the AB_2B' type Molecule. He has shown that such a Molecule can be either (a) a plane isosceles triangle with the A atom lying in the plane of the B atoms (C_{2v}), or (b) a pyramid with an isosceles base with the A atom at the apex of the pyramid (C_s).

10) Nayar and others: Z. Anorg. Chem. **240** (1939) 217.
11) E. S. Wilson, (Jr): J. Chem. Phys. **2** (1934) 432.

In view of the previous considerations the plane structure (a) may be rejected and the structure (b) may be accepted. Wilson has given that for such a pyramidal model there are six Raman Lines of which two should be anti-symmetrical and depolarised and four symmetrical and polarised.

7. Discussions of results

As reported in a previous paper a 4.5 N solution of the acid gives three Raman bands at about $\Delta\nu$ 330, 640 and 800 together with a very weak line at $\Delta\nu$ 449. The wide band at $\Delta\nu$ 800 has been shown to be composed of three frequencies at $\Delta\nu$ 789, 806 and 826 in the order of decreasing intensity. The band at $\Delta\nu$ 330 consists of three components at $\Delta\nu$ 317, 332 and 354, while the band at $\Delta\nu$ 640 of two components at $\Delta\nu$ 642 and 653. The lines $\Delta\nu$ 317, 332, 354, 642, 653 and 789 have been attributed to the polymer $(HIO_3)_3$, the line 806 to $(HIO_3)_2$ and the line with the highest shift $\Delta\nu$ 826 to the monomer HIO_3. It is probable that in a 4.5 N solution the Molecules are already trimers with a very small proportion of dimers and monomers, and hence the Raman Spectrum obtained is characteristic of all the three types of Molecules.

A 0.2 N solution gives only two lines at $\Delta\nu$ 804 and 824.

As it is difficult to have pure and simple HIO_3 Molecules free from polymers in a solution of Iodic Acid, it is not possible to get a Raman Spectrum, characteristic of the Monomeric HIO_3 Molecule alone. For this reason one cannot experimentally verify the theoretically predicted results viz. that HIO_3 Molecule should give six Raman Lines, 2 depolarised and 4 polarised.

A 4.5 N solution of the acid gives a large number of lines of which only one viz. $\Delta\nu$ 826 can be attributed to the HIO_3 Molecule, while the other five lines due to the Molecule are not observable.

8. Interpretation of results

For an IO_3^- ion we should get 2 depolarised and 2 polarised line while for a HIO_3 Molecule we should get 2 depolarised and 4 polarised lines. But from the results it is seen that all the lines are polarised to varying degrees and none in depolarised to the limit. This can only mean that the Molecule has no element of symmetry and hence we conclude that the substance exists mainly in the form of polymer.

The only frequency characteristic of the monomer $\Delta\nu$ 825, is polarised. It is therefore, due to one of the symmetrical vibrations of the pyramidal Molecule of the form

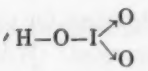

The lines $\Delta\nu$ 824 and 804 obtained with a 0.2 N solution show the same values of p as those in the 4.5 N solution. This shows that the lines $\Delta\nu$ 805 and 824 obtained with the dilute solution have the same mode of vibration as the lines $\Delta\nu$ 806 and 826 obtained in the 4.5 N solution.

The results further show that depolymerisation is incomplete at this dilution also.

The author desires to express his grateful thanks to Dr. P. N. Sharma and to late Mr. M. R. Nayar for their kind interest and guidance in the present work.

On the Infrared-Responsive Behaviors of (Zinc : Cadmium-Sulphide : Selenide)-Type Phosphor Families VI. General Survey and Summary

Sumitada ASANO

Department of Physics, Faculty of Science, Okayama University

(Received September 20, 1955)

Experimental results on the IR-responsive behaviors of some selected members of Zn(S : Se), (Zn : Cd)S and (Zn : Cd)(S : Se) phosphor families are serially reported in several of the previous papers. In the present paper, general features of IR-responsive behaviors of these ZnS-type phoshors are compared with one another and summarized. Further, the type of model, which is most suited for the explanation of these behaviors, is discussed. The quanitative conclusions based on the most suitable model, which contains shallow traps and deep traps, are compared with the experimental results reported in the previous papers. The comparison shows satisfactory agreement between them.

1. Introduction

Hitherto many investigations have been made on the infrared-(abbreviated as IR-) responsive behaviors of ZnS and (Zn:Cd)S phosphors. Recently the optical properties of some Zn(S:Se) and (Zn:Cd)(S:Se) phosphors have been published by several investigators[1], although frangmentally in most cases.

Four ingredients ZnS, ZnSe, CdS and CdSe were prepared through extremely careful procedures from starting reagent-materials with guaranteed purities. With each one of them the amount of copper impurity, which, however small, affects the optical properties of the furnished phosphors strongly, was estimated to be less than 10^{-5}% by spectroscopic or spectrophotometric inspection[2)-6)]. From these ingredients some ZnS-type phosphors* activated with Pb, Mn, Bi. Cu and Ag were synthesized under the same crystallizing conditions. The results of the investigations on their IR-responsive behaviors have been serially reported in several of the previous papers[2)-6)].

1) For example: H. W. Leverentz et al: *Preparation and Characteristics of Luminescent Materials* (John-Wiley & Sons. N.Y. 1948).
2) S. Asano: J. Phys. Soc. Japan **9** (1954) 580.
3) S. Asano: J. Appl. Phys. Japan **23** (1954) 527.
4) S. Asano: Sci. of Light [Tokyo] **4** (1955) 16.
5) S. Asano: Sci. of Light [Tokyo] **4** (1955) 32.
6) S. Asano: Sci. of Light [Tokyo] **4** (1955) 48.

* The term "*ZnS-type phosphors*" is used here in a broad sense that it includes not only ZnS phosphors but also Zn(S:Se), (Zn:Cd)S and (Zn:Cd)(S:Se) phosphors.

Further, by using these ingredients it had beed previously assured that self-activated ZnS-type phosphors (containing no activator) with various host-crystal compositions emit only the host-crystal emission-bands peculiar to their compositions under ultra-violet (abbreviated as UV) excitation and that the phosphors obtained from several different batches with an identical host-crystal composition show the identical optical and crystallographical properties so long as they are synthesized under the same crystallizing conditions. (cf. Figs. 1 a and b)

Since from the above purity and reproducibility tests it may be infered that residual impurities in these ingredients and uncontrollable fluctuations in crystallizing conditions had only neglegible effect upon the optical properties of the furnished phosphors, the individual departure in the optical properties of the composite members* in one family from those of the ZnS member in the same family may be considered as chiefly ascribable to the influence of the added foreign ingredient.

Here in this paper, the general features of the influence of these foreign

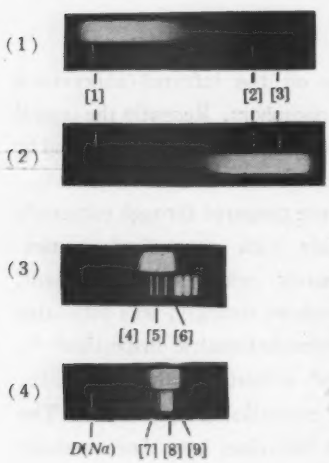

Fig. 1 a. Emission spectra of some self-activated ZnS-type phosphors** at a room temperature. Photographed by Shimadzu GW-30.

No.	Sample	Peak Wave-length	Excitant	Used plate or film.
(1)	ZnS	4650 Å	3650 Å (Hg)	Fuji Panchro.
(2)	8ZnS ·2CdSe	5800 Å	〃	〃
(3)	ZnSe	6500 Å	〃	Sakura 750.
(4)	CdS	>7000 Å	incand. lamp +Mazda V-GIA	〃

wave-length marks:
[1] 4358 Å (Hg) [2] 5461 Å (Hg) [3] 5770~91 Å (Hg)
[4] 6143 Å (Ne) [5] 6506 Å (Ne) [6] 6929 Å (Ne)
[7] 7067 Å (Ar) [8] 7625 Å (Ar) [9] 8115 Å (Ar)
Into all the phosphors were added 2 weight % of KCl as flux and they were crystallized at 850°C for 30 min. in N_2-atmosphere.

* A *composite member* means one of the members in a Zn(S:Se), (Zn:Cd)S or (Zn:Cd)(S:Se) phosphor families, excluding ZnS, and ZnSe, CdS, or CdSe members from them respectively.

** Integrated IR radiescence of the self-activated phosphor CdSe [KCl(2)] 850°C excited by D-line (Mazda Na-lamp+$CuCl_2$ solution-filter) could be evidenced by a PbS-cell (Mazda. Sensitive range: 0.9–2.5 μ. Bias voltage: DC 22.5 V), although its spectral distribution was ignored. The Photo-current from the receptor was amplified by a three-stage AC amplifier which was provided with a R-C T-network tuned at the frequency 500 cps of the incident chopped radiation, and then it was read with a micro-ammeter after rectification. (cf. M. G. Mellon: *Analytical Absorption Spectroscopy* (John-Wiley & Sons Co. N.Y. 1950) pp. 476, 478.)

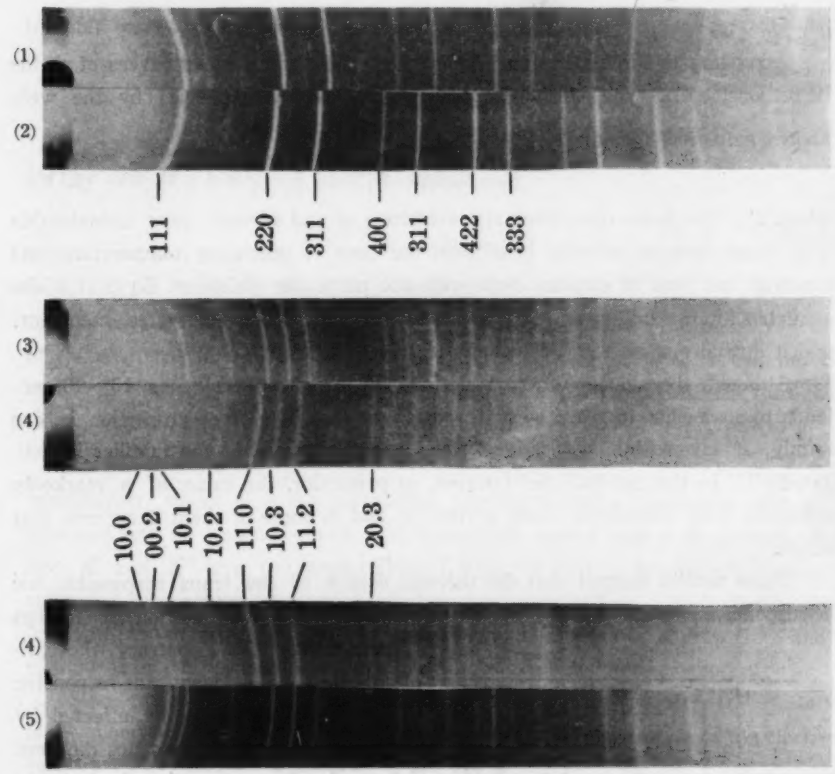

Fig. 1 b. X-ray diffraction patterns of some self-activated ZnS-type phosphors at a room temperature. Cu–K_α radiation, nickel filter.

No.	Sample	Crystal structure	Lattice constants (Å) a	c
(1)	ZnS	cubic	5.40	—
(2)	ZnSe	〃	5.66	—
(3)	CdS	hexagonal	4.14	6.74
(4)	CdSe	〃	4.29	7.01
(5)	8ZnS·2CdSe	〃	3.29	6.43

All the phosphors were crystallized under the same conditions as in Fig. 1 a.

ingredients upon IR-responsive behaviors of ZnS phosphors are summarized by comparing the experimental results reported in the previous papers[2)-6)] with one another, and the IR-responsive mechanism in ZnS-type phosphors are discussed by using a model suited for the explanation of these results obtained.

2. IR-Responsive Natural Decay

According to the experimental results[5),6)], the natural-decay curves of all the IR-responsive ZnS-type phosphors can be approximately expressed by the well-known emperical formula

$$B_n = B_0[b/(b+t)]^{-n}, \tag{2.1}$$

where t is the decay-time after UV excitation. b and n may vary considerably with large changes in initial brightness B_0, time t, operating temperature and the type and kind of excitant even with one particular phosphor. Eq (2.1) is also available for the tail-parts of the decay curves of the Mn-activated members, which intitially show rapidly decaying exponential-parts.

Although the value of the exponent n for a large decay-time $10^2 \sim 10^3$ sec. tends to somewhat increase with increasing foreign ingredient proportion in one family, it lay within the range from 1 to 1.5 for most of the families investigated[5),6)]. In the cub-Zn(S:Se) families, in particular, the value of n markedly increases with increasing ZnSe proportion and in some of them it exceeds that range.

These results suggest that the thermal depths of the traps responsible for IR-responsive natural phosphorescence may vary by the addition of foreign ingredient. On the contrary, the optical depths of the deep trans responsive for IR irradiation are not affected by it[4),5),6)]. Some shallow traps different from the deep traps, therefore, should be expected to be ascribable to IR-responsive natural phosphorescence.

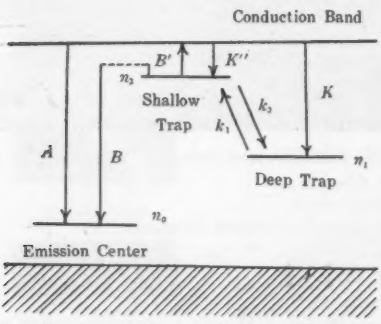

Fig. 2. Assumed model showing allowed electron transitions in IR-responsive natural-decay.

From the experimental results obtained, a model is assumed for IR-responsive natural phosphorescence, as shown in Fig. 2. In this model the natural phosphorescence is predominantly controlled by direct recombinations B between parent emission-centers and electrons in nearby shallow traps and remote bimolecular recombinations A through conduction band. For the sake of simplicity, it is assumed that each state has single multiplicity and that isolated emission-centers and traps do not exist.

Since the life-times of electrons in conduction band and in excited states of centers may be expected to be short (the former is $\simeq 10^{-8}$ sec), the electron

transfer processes in natural decay may be expressed by

$$dn_0/dt=-Bn_3 \tag{2.2 a}$$

$$d(n_1+n_3)dt=-Bn_3 \tag{2.2 b}$$

$$n_0=n_1+n_3 \tag{2.2 c}$$

for the case $B'=K=K''=0$ (case I), and

$$\frac{dn_0}{dt}=-B'n_3\frac{n_0}{n_0+\varepsilon(N-n_1)+\varepsilon''(N-n_3)} \tag{2.3 a}$$

$$n_0=n_1+n_3 \tag{2.3 b}$$

for the case $B=0$ (case II) respectively, where n_1 and n_3 are the numbers (cm^{-3}) of the electrons in deep and shallow traps respectively and n_0 is the number (cm^{-3}) of the holes in emission-centers. k_1, k_2, B and B' represent the time rates (sec^{-1}) of the thermal transitions shown in Fig. 1. ε and ε'' are given by

$$\varepsilon\equiv K/A \quad \text{and} \quad \varepsilon''\equiv K''/A$$

respectively, where A is the probability, (cm^3sec^{-1}) that a conduction electron is captured into an emission-center and recombines with a hole in its ground-state, and K and K'' are the probabilities (cm^3sec^{-1}) that a conduction electron is retrapped into a deep trap and a shallow trap respectively. N is the number (cm^{-3}) of the compound traps, each one of which consists of a deep trap and a shallow trap. N is, therefore, equal to the number of emission-centers.

Since the natural phosphorescence at least several seconds after UV excitation is IR-quenchable according to the results obtained, the exhaustion of the electrons in deep traps under IR irradiation urges the electrons in shallow traps to return quickly into deep traps. Further, the natural phosphorescence is mainly controlled by the transitions B and B'. k_1 and k_3 may be assumed, therefore, to be considerably larger than the other transition probabilites concerning the both types of traps. From the above assumption the relation.

$$k_3n_3=k_1n_1 \tag{2.4}$$

is approximately valid during whole exhaustion run, if an equilibrium state in electron distribution is realized initially during UV excitation.

Substituting Eq (2.4) into Eq (2.2 b), we obtain

$$n_3=n_{30}\exp\{[-B/(1+\kappa)]t\} \tag{2.5}$$

where $\kappa\equiv k_3/k_1$, and n_{30} is the initial value of n_3. The density (W/cm^3) B_n of phosphorescence radiance, therefore, is given by

$$B_n=p_Bh\nu_BBn_{30}\exp\left[-\frac{B}{1+\kappa}t\right] \tag{2.6}$$

where p_B is the quantum efficiency of the transition B. When $\kappa\gg1$, a large

portion of trapped electrons are in deep traps and then the natural phosphonescence is persistent. On the contrary, when $\kappa \ll 1$, deep traps do not play any effective role in natural phosphorescence.

If the retrapping probabilities K and K'' are neglegible in Eq (2.3 a), then a solution similar to Eq (2.5) is obtained, and B_n also is given by an expression similar to Eq (2.6), where B, p_B and $h\nu_B$ are replaced by B', P_A (quantum efficency of the transition A) and $h\nu_A$ respectively.

If $\varepsilon=\varepsilon''=1$ in Eq (2.3 a), B_n is given by the inverse-square decay formula

$$B_n = p_A \frac{B' n_{00}^2}{2N(1+\kappa)} \Big/ \left[1+\frac{B' n_{00}}{2N(1+\kappa)} t\right]^2 \tag{2.7}$$

where n_{00} is the initial value of n_0.

If there are shallow traps of various depths and if their distribution where exponential, that is, trap density were given by

$$N_E = G \exp\left[-\alpha(E-E_0)\right]$$

then

$$n_{30} = \gamma N_E = \gamma G \exp\left[-\alpha(E-E_0)\right],$$

where γ is the degree of repletion in shallow traps, and E_0 and G are the depth of the top-most shallow trap and the trap density at $E=E_0$ respectively. If each shallow trap associates with each one of deep traps from Eq (2.6) we obtain

$$dB_n = p_B h\nu_B B \gamma G \exp\left[-\alpha(E-E_0)\right] \exp\left[-\frac{B}{1+\kappa} t\right] dE .$$

Substituting $B=s\exp(-E/kT)$ into the above equation and integrating it from $E=E_0$ to ∞ under the assumptions that γ and κ are independent of trap depth E and that $\exp(-E/kT) \fallingdotseq 0$ for the lowest of the shallow traps, we obtain

$$B_n = \frac{B_0(1+q)}{(s't)^{1+q}} \int_0^{s't} y^q \exp(-y)dy , \tag{2.8}$$

where

$$B_0 \equiv P_B h\nu_B \gamma G s k T \exp(-E_0/kT)/(1+q) ,$$

$$s' \equiv \frac{s}{1+\kappa} \exp(-E_0/kT) ,$$

$$q \equiv \alpha k T$$

and s: frequency factor ($\sec^{-1}$)

In the case where $\varepsilon=\varepsilon''=0$ in Eq (2.3 a), an equation similar to Eq (2.8) is obtained.

From Eq (2.8) $B_n \propto t^{-(1+q)}$ for large value of t. If traps are distributed uniformly, that is $\alpha=0$, then $B_n \propto t^{-1}$. (hyperbolic decay)

In the case of Eq (2.7), it has been reported that the contribution from a

finite number of discrete traps at various depths shows an exponential-decay for large decay time[7]. Since the values of ε and ε'' are estimated to be 0.5~1 for for ZnS phosphors[8], the assumption that $\varepsilon=\varepsilon''=0$ in Eq (2.3 a) seems somewhat unreasonable.

On the other hand, there is little or no detectable retrapping during natural phosphorescence of many ZnS-type phosphors according to Garlick[9] and Levshin[10]. Moreover, the peak difference between natural and IR-stimulated phosphorescences[11], IR-quenching of natural phosphorescence and quick decay of IR-stimulated phosphorescence after interruption of IR irradiation are not definitely explained in the case II. The case I is, therefore, more reasonable for the explanation of the IR-responsive mechanism of natural phosphorescence.

It is, however, probable that both idealize recombination patterns assumed alternatively will be operative simultaneously to some extent in real phosphor crystals, as shown in many photo-conductivity experiments. But in IR-responsive natural decay the processes in the case I, which are analogous to Lenard's "*Zentren verschiedener Dauer*", will be predominant. In this case the shallow trap is of a metastable quasi-exciton state (whose positive hole is frozen in an emission-center, whereas the electron wanders in its vicinity) can be transfered into the emission-center over a potential barrier by absorbing phonons. (monomolecular recombination) Even if the processes in the case II are oprative, the motions of electrons between ionized centers and nearby traps are infered to be of short-range type, for example, as quasi-direct recombinations[3] or electron transfer via exciton states.

The electron transfer via exciton state is visualized as follows: A great number of electrons, which bad been excited into conduction band from filled band during excitation, are trapped in shallow and deep traps, particularly in the early stage after excitation. The effective number of trapped electrons, therefore, increases. A created positive hole in filled band migrates through the crystal. It may approach to a trapped electron and stay there for a while ($>10^{-13}$ sec.), being attracted by the residual field of the trapped electron. Then the trapped

7) R. T. Ellickson et al: Phys. Rev. **70** (1946) 290.
8) A. Smakula: Z. Phys. **59** (1930) 603.
9) G. F. J. Garlick et al: Proc. Roy. Soc. A **188** (1947) 485; Proc. Phys. Soc. [London] **60** (1948) 574; Proc. Phys. Soc. [London] **62** (1949) 317.
10) V. L. Levshin: Zhur. Eksp. Teor. Fiz. (SSSR) **18** (1948) 149; Izv. Akad. Nauk SSSR Ser. Fiz. **12** (1948) 217.
11) S. Asano: J. Phys. Soc. Japan **10** (1955) 903.

electron may be transfered to an exciton state*, if a widely spreading wave function of the exciton overlaps that of the trapped electron and the latter may be activated by phonons to pass over (or through) a potential barrier. The created exciton may propagate quickly through the crystal[12] and the excited electron may be captured into an emission-center, while the positive hole may diffuse away, leaving the electron in the center[13]. Since in the above process the collapse of the exciton (that is, direct recombination of the excited electron with the hole by multiple-phonon production) may probably occur, in particular, at crystal imperfections, this process will be of short-range type and its quantum efficiency of luminescence will not be so high.

Although the quasi-direct recombination and the transfer via exciton are of bimolecular type, the retrapping may be considered to be neglegible during these processes and little or no photoconductivity will be observed, compared with the case of ordinary long-range bimolecular recombination. Consequently in this case also Eq (2.8) is valid as stated above.

With increasing proportion of foreign ingredient the energy intervals between the excited states and the ground-state in emission-centers decrease gradually[4]. Similarly the distribution of the shallow traps would become somewhat dense with them. This means the increase in α and the reduction in E_0 in Eq (2.8). On the other hand, the quantum efficiency p_B of the transition B will derease owing to the perturbation caused in emission-centers by foreign ingredient. And p_A also will decrease, because conduction electrons recombine with holes by phonon ejection via small distorted domains around foreign ingredient-atoms which are located substitutionally[14].

Further, the reduction in E_0 results in the conspicuous reduction in initial effective number n_{30} (or τ) of the trapped electrons. As the resultant effect of these foregoing inferences, the exponent n in natural decay tends to somewhat increase and the initial phosphorescence-radiance rapidly decreases with increasing foreign ingredient proportion as shown in the experiments[5),6)].

These inferences well coincide also with the results obtained in thermoluminescence experiments, where it has been reported that the shallow traps responsible for natural phosphorescence of ZnS phosphors at room temperature

12) W. R. Heller et al: Phys. Rev. **84** (1951) 809.
13) D. L. Dexter et al: Phys. Rev. **84** (1951) 377.
14) G. F. Garlick et al: J. Opt. Soc. Amer. **39** (1949) 935.

* This transfer causes the change of polarization of surrounding ions and then a stable exciton state may be represented by a concave adiabatic potential curve on a "configurational coordinate" diagram. (cf. I. M. Dykman et al: Dokl. Akad. Nauk SSSR **83** (1952) 825.)

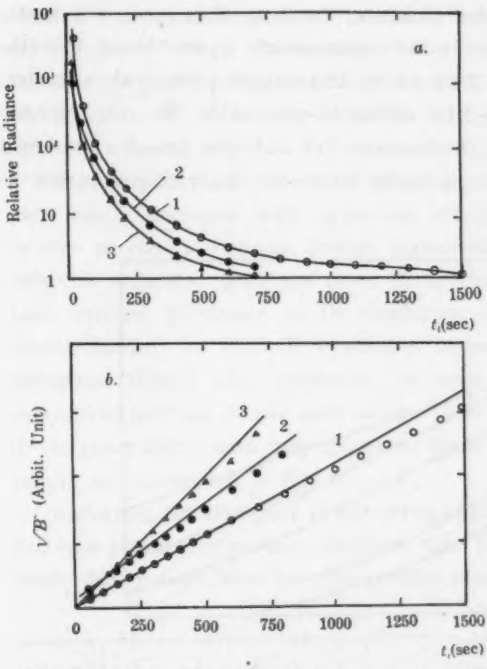

Fig. 3. (a) Semi-log plots of decay-curves of IR-stimulated and -quenched phosphorescences at a room temperature.

(b) Dependence of reciprocal square-root of phosphorescence radiance upon irradiation time.

Curve no. 1. 9.5 ZnS·0.5 CdSe:Pb[Cl_2](1) 850°C
t_n=3 min. (Stimulated phosphorescence)
2. 9 ZnS·ZnSe:Mn[Cl_2](1) 850°C
t_n=30 sec. (Stimulated phosphorescence)
3. 9 ZnS·CdS:Bi[$(NO_3)_3$](0.1) 1100°C
t_n=2 sec. (Quenched phosphorescence)
UV excitation: Mazda HL-300+Mazda UVD-2, distance at 25 cm for 3 min.
IR irradiation: Mazda Heating Lamp (100 V. 100 W. S-type) +Mazda IRD-1.
IR irradiance: 8.5 mW/cm².
t_n: Natural-decay duration before IR irradiation.

gradually disappear with increasing proportion of CdS[15].

When $B'=s\exp(-E/kT)$ finally approaches to the normal light emission probability ($\simeq 10^8\,\mathrm{sec}^{-1}$), the experimental separation between both recombination types, becomes difficult[16].

3. IR-Stimulated or -Quenched Phosphorescence

The decay curve of the IR-stimulated or -quenched phosphorescence on a log-log plot has somewhat different aspect from that of the natural-decay curve. It has comparatively gentle slope in early stage of the irradiation time and approaches finally to a constant slope near −2, bending gradually downwards[5),6)]. Fig. 3a shows some of these decay curves plotted on semi-log plots and Fig. 3b the dependence of the reciprocal square-root of brightness upon irradiation time. Even when the brightness has fallen by a factor larger than 10^3, there is still definite curvature as shown in Fig. 3a. What does happen is that the points plotted in Fig. 3b nearly fall on straight lines except for very large decay

15) H. W. Leverentz: *Introduction to Luminescence of Solids*. (John-wiley & Sons. N.Y. 1950) p. 178.

16) V. A. Arhangelïskaya: Dokl. Akad Nauk SSSR **100** (1955) 233.

time*. Besides, with one particular phosphor, the final slope near −2 hardly varies with applied IR irradiance. In the measurements it was found that the final slope was nearly equal to −2 for all the IR-stimulable (Pb- or Mn-activated) members and lay within −1.8∼−2 for all the IR-quenchable (Bi-, Cu-, or Ag-activated) members, whereas in IR-stimulable SrS and SrSe phosphors the final slope has been reported to deviate markedly brom −2 and rather approach to −1.[7]

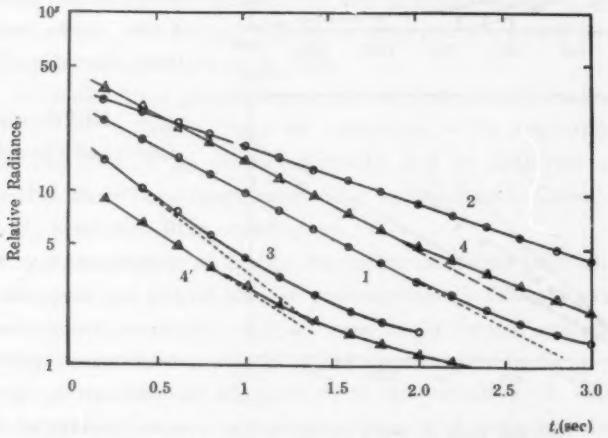

Fig. 4. Semi-log plots of the initial parts of some IR-stimulated phosphorescences at a room temperature.

Curve no. 1.	9.5 ZnS·0.5 ZnSe:Mn[Cl_3](1)	850°C	t_n=1 min.
2.	9.5 ZnS·0.5 CdS:Pb[Cl_2](1)	850°C	t_n=5 min.
3.	8 ZnS·2CdS:Pb[Cl_3](1)	850°C	t_n=5 min.
4.	ZnS:Pb[SO_4](5)Cu(0.005)	1100°C	t_n=5 min.
4'.	〃	After preliminary IR irradiation for 15 sec.	

All the phosphors were excited and irradiated under the same radiation arrangements as in Fig. 3.

According to the foregoing results, the tail-parts (after several seconds from the beginning of IR irradiation) on the decay-curves of the IR-stimulated or -quenched phosphorescence can be expressed approximately by the formula

$$B=B_0[b/(b+t)]^{-2} \tag{3.1}$$

As shown in Fig. 4 the initial part, within a few seconds after the beginning of IR irradiation, on a decay curve of IR-stimulated phosphorescence, which was

* The definite deviation from the straight line could not be observed in Figs. 19 and 20 of reference 2, in which the observed time interval was shorter than in this paper.

obtained from an oscillogram[5),6)], seems to have approximately an exponential-decay form[17),18)] Since the duration of this initial stage is short, it could not be definitely determined whether this part obeys to an exponential-decay formula rigorously or not. At any rate Eq (3.1) is not available for this initial part.

According to the experimental results the duration of the initial exponential-part rapidly decreases with increasing proportion of added foreign ingredient. In the phosphors rich in foreign ingredient the exponential-part cannot be definitely separated from the power-decay tail-part. When the phosphors had been exposed previously to IR irradiation for an appropriate duration, the exponential-part in next IR irradiation becomes shorter than when they are stimulated shortly after excitation. In some doubly activated phosphors the exponential-part has one or more bends. The exponential-part changes gradually to the power-decay part with increasing decay-time. Some of these experimental results are exemplified in Fig. 4.

Surveying the similarity in the decay characteristics of all the IR-responsive ZnS-type phosphors, we can predicate that the addition of foreign ingredient ZnSe, CdS or CdSe does not substantially alter the IR-responsive mechanism of ZnS phosphors and that IR-responsive behaviors observed in ZnS phosphors are invariantly succeeded into the composite members.

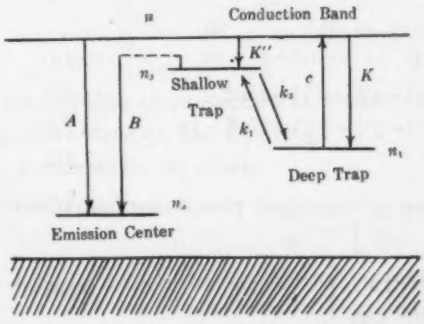

Fig. 5. Assumed model showing allowed electron transitions under IR irradiation.

The allowed transitions corresponding to the case II under IR irradiation are shown in Fig. 5.

If the retrapping probabilities K and K'' and the IR-responsive transition probability c (sec^{-1}) which is proportional to IR irradiance, are considerably large, the transition B also can be regarded as approximately bimolecular as stated in the previous paper[2)]. Then the electron transfer processes under IR irradiation are expressed by

$$dn_0/dt = -An_0n - (B/N)n_3n_0 \qquad (3.2\,a)$$

$$dn/dt = -An_0n + cn_1 - Kn(N-n_1) - K''n(N-n_3) \qquad (3.2\,b)$$

$$d(n_1+n_3)/dt = -(B/N)n_3n_0 + Kn(N-n_1) + K''n(N-n_3) - cn_1 \qquad (3.2\,c)$$

17) G. R. Fonda: J. Opt. Soc. Amer. **36** (1946) 382.
18) C. Bull et al: J. Opt. Soc. Amer. **41** (1951) 718.

and $$n_0=n+n_1+n_3 \tag{3.2 d}$$

where n is the number (cm^{-3}) of conduction electrons. The model used here is substantially identical to that in the previous paper[3], in which the existence of shallow traps, which are not necessarily essential in the decay process of IR-stimulated or -quenched phosphorescence, was ignored and the influence of isolated deep traps was taken into account instead.

When considerable number of isolated emission-centers associated with shallow traps exist, natural phosphorescence is partially non-quenchable for IR irradiation as observed in some Cu-activated ZnS-type phophors. When isolated deep traps are distributed in a stimulable phosphor crystal, remarkable IR stimulation can be observed even long after excitation[4].

The relative magnitude of p_A and p_B determines the type of the phosphor, namely IR-stimulable or -quenchable.

Substituting

$$n_0/N\equiv\eta\,,\quad n/N\equiv\xi\,,\quad n_1/N\equiv\chi\,,\quad A\equiv a\tau\,,$$
$$B/AN\equiv\beta\,,\quad c/AN\equiv\gamma\,,\quad K/A\equiv\varepsilon\,,\quad K''/A\equiv\varepsilon''\,,$$
$$a\equiv AN\,,\quad \tau\equiv at\quad\text{and}\quad n_3\equiv n_1/\kappa$$

into Eqs (3.2), we obtain

$$d\eta/d\tau=-\eta\xi-(\beta/\kappa)\chi\eta \tag{3.3 a}$$
$$d\xi/d\tau=-\eta\xi+\gamma\chi-\varepsilon(1-\chi)\xi-\varepsilon''(1-\chi/\kappa)\xi \tag{3.3 b}$$
$$(1+1/\kappa)d\chi/d\tau=-(\beta/\kappa)\chi\eta+\varepsilon(1-\chi)\xi+\varepsilon''(1-\chi/\kappa)\xi-\gamma\chi \tag{3.3 c}$$
and $$\eta=(1+1/\kappa)\chi+\xi\,. \tag{3.3 d}$$

The density (W/cm^3) of IR-stimulated or -quenched phosphorescenceradiance B_S or B_Q is given by

$$\left.\begin{aligned} B_S&=p_A h\nu_A AN^3\xi\eta \\ \text{or}\quad B_Q&=p_B h\nu_B(BN/\kappa)\chi\eta \end{aligned}\right\} \tag{3.4}$$

respectively. Eqs (3.3) may be treated with the methods similar to those in the previous paper:[3]

(1) Approximate solution for large τ value is given by

$$\eta=\frac{1}{k\tau+c}\,,\quad \xi=\frac{P}{k\tau+c}\quad\text{and}\quad \chi=\frac{Q}{k\tau+c} \tag{3.5}$$

where

$$k\equiv\frac{\gamma\kappa+(\varepsilon+\varepsilon'')\beta}{\gamma\kappa+(\varepsilon+\varepsilon'')(1+\kappa)}\,,\qquad P\equiv\frac{\gamma\kappa}{\gamma\kappa+(\varepsilon+\varepsilon'')(1+\kappa)}$$
$$Q\equiv\frac{\kappa(\varepsilon+\varepsilon'')}{\gamma\kappa+(\varepsilon+\varepsilon'')(1+\kappa)}$$

From Eqs (3.4) we obtain

$$B_S,\ B_Q \propto [c_1\tau+c_2]^{-2}\ . \tag{3.6}$$

(2) $\beta/\kappa \ll \gamma \ll \varepsilon \simeq \varepsilon''$

In this case the situation is more simplified by absence of isolated traps. Then the equations to determine η, ξ and χ as functions of irradiation time τ are given by

$$\left.\begin{aligned} &\chi=\eta\kappa/(1+\kappa) \\ &[\kappa\gamma/(1+\kappa)]\tau=2\varepsilon\left(\frac{1}{\eta}-\frac{1}{\eta_0}\right)-(1-\varepsilon)\ln(\eta/\eta_0) \\ \text{and}\quad &\varphi[2\varepsilon+(1-\varepsilon)\eta]-[\kappa/(1+\kappa)]\eta=0\ , \end{aligned}\right\} \tag{3.7}$$

where $\varphi \equiv \xi/\gamma$, and η_0 is the initial value of η. From Eqs (3.7) $\varphi\eta$ and $\chi\eta$ may be plotted against $[\kappa\gamma/(1+\kappa)]\tau$ in a similar manner as in the previous paper[2].

The experimental results are in good agreement with Eqs (3.6)[2),5),6)]. Even when the contribution from many deep traps with different stimulabilities and retrapping probabilities is taken into account, the resultant form similar to Eqs (3.6) can be obtained[19].

(3) Eliminating ξ from Eqs (3.3 a) and (3.3 b), we obtain

$$\frac{d\eta}{d\tau}=\frac{(d\xi/d\tau-\gamma\chi)\eta}{\eta+\varepsilon(1-\chi)+\varepsilon''(1-\chi/\kappa)}-(\beta/\kappa)\chi\eta$$

If the life-time of an electron in conduction band is short, we can put $\xi \fallingdotseq 0$ in the above equation and Eq (3.3 d).

Consequently we obtain

$$\frac{d\eta}{d\tau}=-\left[\frac{\gamma\kappa+2\beta}{2(\kappa+1)}\right]\eta^2 \tag{3.8}$$

in the case where $\varepsilon=\varepsilon''=1$.

$$\therefore\quad \eta=\left[k'\tau+\frac{1}{\eta_0}\right]^{-1}$$

where

$$k' \equiv \frac{\gamma\kappa+2\beta}{2(\kappa+1)}$$

Further, from Eqs (3.8) and (3.4) we obtain

$$B_S=p_A h\nu_A cN\frac{\kappa}{2(\kappa+1)}\frac{\eta_0^2}{(k'\eta_0\tau+1)^2} \tag{3.9 a}$$

$$B_Q=p_B h\nu_B BM\frac{1}{\kappa+1}\frac{\eta_0^2}{(k'\eta_0\tau+1)^2} \tag{3.9 b}$$

19) S. Asano: J. Appl. Phys. Japan **24** (1955) 57.

Eqs (3.9) are truly valid for all the decay time when $\varepsilon=\varepsilon''=1$. If we take account of absorption effect caused by the thickness of the phosphor layer, stimulalted or quenched phosphorescence-radiance (W/cm^2) B_S or B_Q on the layer surface is given by[7].

$$B_S \text{ or } B_Q=\frac{B_0(1+q)}{(s\tau)^{1+q}}\int_0^{s\tau} y^q(1+y)^{-2}dy \tag{3.10}$$

from Eqs (3.9) under the condition that $2\beta/\kappa\ll\gamma$,

$$\left.\begin{aligned} &\text{where} && s=\gamma\bar{\eta}_0\kappa/2(\kappa+1)\\ &\text{and} && q=(\mu_3+\mu_2)/(\mu_3+\mu_1) \quad \text{or} \quad (\mu_3+\mu_2-\mu_1)/(\mu_3+\mu_1)\\ &&& B_0=p_A h\nu_A cN\bar{\eta}_0{}^2\frac{\kappa}{2(\mu_3+\mu_1)(\kappa+1)(1+q)}\\ &\text{or} && p_B h\nu_B BN\bar{\eta}_0{}^2\frac{1}{(\mu_3+\mu_1)(\kappa+1)(1+q)} \end{aligned}\right\} \tag{3.11}$$

for B_S or B_Q respectively.

μ_1, μ_2 and μ_3 are the absorption coefficients for IR radiation, visible phosphorescent emission and UV excitant respectively, and $\bar{\eta}_0$ is the value of η_0 on the layer surface. When $\log B/B_0$ in Eq (3.10) is plotted against $\log s\tau$, the final slope approaches to -2 when $q\geq 1$ and to $-(q+1)$ when $q\leq 1$[7].

Since the value of q for B_Q is smaller than that for B_S [cf. Eqs (3.11)], the experimental results that the decay curves of all the IR-stimulated phosphorescences on log-log plots have final slopes near -2, whereas some of the IR-quenched phosphorescences have slightly smaller final slopes than -2 (in absolute value), may possibly be explained by the absorption effect.

In the early stage after UV excitation, a large number of electrons, which have been excited in conduction band from filled band, either return to the filled band quickly by phonon ejection (that is, simultaneous or rapid sequential production of phonons) or fall into ionized emission-centers by optical transitions. But some of them are trapped in shallow and deep traps as stated in Section 2. In this stage the latter process is more predominant than the IR-responsive natural-decay process. Since the number of conduction electrons n is considerably large, the equations to determine roughly the electron transfer processes are then given by putting $\beta=\gamma=0$ in Eqs (3.3) If $\varepsilon=\varepsilon''=1$, we obtain

$$\left.\begin{aligned} &\xi=(\xi_0/\eta_0)[\exp(-2\tau)]\eta\\ &\eta^{-1}=\eta_0{}^{-1}+\frac{1}{2}(\xi_0/\eta_0)[1-\exp(-2\tau)]\,, \end{aligned}\right\} \tag{3.12}$$

where ξ_0 is the initial value of ξ.

20) R. C. Herman et al: J. Opt. Soc. Amer. **38** (1948) 999.

As seen from Eqs (3.12) and (3.3 d), the number of trapped electrons increases to reach to a constant value with increasing decay time.

Furthermore, it will be much larger owing to the additional trapping of electrons excited from filled band. When τ becomes considerably large, the number of conduction electrons decreases and then IR-responsive decay process stated in Section 2 becomes to predominate.

The electron transfer processes under IR irradiation in this early stage also are approximately determined by the equations, which are given by putting $\beta=0$ ($\gamma \neq 0$) in Eqs (3.3). The solution in the case where $\varepsilon=\varepsilon''=1$, is given by[20]

$$\left.\begin{aligned} \xi &= [\alpha-(\alpha-\xi_0/\eta_0)\exp(-\sigma\tau)]\eta \\ \eta^{-1} &= \eta_0^{-1}+\alpha\tau-\sigma^{-2}\left[\frac{\kappa\gamma}{1+\kappa}-\sigma\left(\frac{\xi_0}{\eta_0}\right)\right](1-e^{-\sigma\tau}) \end{aligned}\right\} \tag{3.13}$$

where $$\sigma \equiv \frac{\kappa\gamma}{1+\kappa}+2\,, \qquad \alpha \equiv \frac{\kappa\gamma}{(1+\kappa)\sigma}\,.$$

ξ_0 and η_0 are the values of ξ and η at the beginnig of IR irradiation respectively. Eqs (3.12) are the special case when $\gamma=0$ in Eqs (3.13). From Eqs (3.13) the initial value of $d(\xi\eta)/d\tau$ is given by

$$[d(\xi\eta)/d\tau]_{\tau=0}=\eta_0^2\left[\frac{\sigma}{\eta_0}\left(\alpha-\frac{\xi_0}{\eta_0}\right)-2\left(\frac{\xi_0}{\eta_0}\right)^2\right]$$

In order that $[d(\xi\eta)/d\tau]_{\tau=0}>0$, it is necessary that

$$\frac{\kappa\gamma}{1+\kappa}>\frac{2p(p\eta_0+1)}{1-p}$$

where $$p \equiv \xi_0/\eta_0\,.$$

Since p takes a large value (<1) in the early stage of natulal decay as seen in Eqs (3.12), only a retardation of natural decay rather than conspicuous stimulation of phosphorescence is observed by IR irradiation of ordinary intensity in this stage even in the phosphors which are markedly stimulable in the later stage. (cf. Figs. 9 and 11 in reference 2). For example, η_0 and p are of the order of $10^{-5}\sim10^{-7}$ and $10^{-2}\sim-10^{-4}$ during ordinary UV excitation ($\simeq$15$\sim$20 μW/cm^2) respectively[21] and $\gamma\simeq10^{-3}$ for the IR irradiation of 10^{-3} W/cm^2.[2]

With increasing natural-decay duration the number of trapped electrons increases rapidly as stated above and then decreases slowly owing to the transitions B, to which the IR-responsive natural phosphorescence is chiefly ascribable. Fig. 6 shows the relative simulation-peak[5),6)] (that is, the difference of the

21) H. Kallmann et al: Phys. Rev. **87** (1952) 91.

radiances before and after the beginning of IR irradiation) in a (Zn:Cd)(S:Se):Mn phosphor family after various durations of natural decay. These experimental results well coincide with the conclusion stated above.

In the early stage after UV excitation the densities of ionized centers and electrons in deep traps in a phosphor crystal are considerably large. The quick quasi-direct recombinations[3] take place then by IR stimulation, where the retrapping process may be assumed to be neglegible. These quasi-direct recombinations with neglegible retrapping may cause the initial exponential-decay even when deep traps of various depths are operative. [cf. Eq (2·8)]

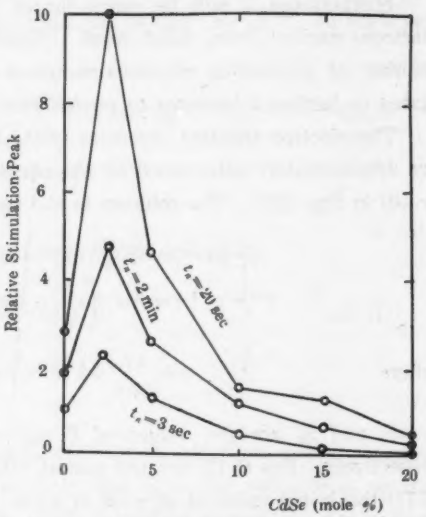

Fig. 6. Dependence of relative stimulation-peak of some selected members in (Zn:Cd)(S:Se):Mn[Cl_2] (1) 850°C phosphor family upon natural-decay duration t_n. All the measurements were made at a room temperature under the same exciting and irradiating conditions as in Fig. 3.

The numbers of ionized emission-centers and electrons in deep traps decrease by preliminary IR irradiation. The numbers of stimulable centers and deep traps contributing to IR stimulation decrease rapidly with increasing proportion of added foreign ingredient as will be stated in the later section. The exponential-part is not, therefore, observed definitely in phosphors exposed to preliminary IR irradiation or in those rich in foreign ingredient.

4. Spectral IR-Responsivity

From the experimental results most important general features on IR spectral-responsivity of ZnS-Type phosphors are itemized as follows:

(1) Starting from a ZnS phosphor and adding increasing proportion of foreign ingredient, the stimulation or quenching bands at about 0.8 μ and 1.3 μ remain distinct showing no displacement of their peak wave-lengths, until the after-glow loses its persistence at about 30, 40 and 20 mole percents of ZnSe, CdS and CdSe respectively.

(2) With any one of the members, the stimulability or quenchability of the

two bands are nearly the same when activated with Pb, Bi, Cu or Ag, whereas with all the Mn-activated members the stimulability and quenchability of the band at 1.3 μ are remarkably smaller than those of the band at 0.8 μ. In some Pb-activated stimulable Zn(S: Se) members also the anomaly similar to that found in the Mn-activated members is observed[3)4)].

(3) The spectral-stimulability and -quenchability curves of a stimulable phosphor (activated with Pb or Mn) well coincide with its own spectral-exhaustibility curve all over the wave-length range including the two bands[5)6)].

(4) The part of phosphor layer which has been stimulated out thoroughly by one of the IR radiations at the wave-lengths 0.8 μ and 1.3 μ shows no detectable stimulation by the IR radiation at the other wave-lengths.

(5) With one stimulable member, the colors of the two phosphorescences stimulated by IR radiations at the wave-lengths 0.8 μ and 1.3 μ are identical.

The results stated in the item (1) are explained by the inference that the number of the deep traps responsible for IR responsivity decreases with increasing foreign ingredient proportion as stated in the previous paper[4)]. Among the emission-centers associated with compound traps, only those which are not much affected by foreign atoms may contribute to stimulation in stimulable phosphors. Isolated emission-centers, which have lost their associated traps, therefore, cannot effectively contribute to either natural phosphorescence or stimulation and quenching. This situation means the reduction of N and p_A in Eqs (3.4) and (3.9) with increasing proportion of foreign ingredient.

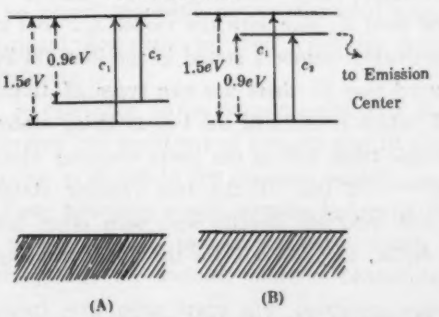

Fig. 7. Two assumed models showing the IR-responsive transitions c_1 and c_2 from deep traps.

From the item (4), we can assume that (I) the two deep traps corresponding to 0.8 μ and 1.3 μ are intimately associated with each other by two transfer processes operative with large time rates in opposing directions as stated in the previous papers[3)4)] or that (II) the two bands correspond to the two transitions from one deep trapping state to conduction band and to an upper metastable trapping state, in which an electron from the deep trap can enter into a shallow trap or directly into an excited state of the parent emission-center. Fig. 7 illustrates the two models based on the two transfer patterns.

On the other hand, from the item (3) it can be infered that the IR-responsive

transfer processes corresponding to the two bands should have nearly equal quantum efficiencies of luminescence. From Eqs (2.2a) and (3.2a)

$$n_0(0)-n_0(t_i)=\int_0^{t_i} Bn_3dt=L_n(t_i)/p_Bh\nu_B \tag{4.1}$$

$$n_0(0)-n_0'(t_i)=\int_0^{t_i} An n_0dt+\int_0^{t_i}(B/N)n_3n_0dt$$
$$=L_s(t_i;\lambda)/p_Ah\nu_A+L_Q(t_i;\lambda)/p_Bh\nu_B \tag{4.2}$$

$$n_0(t_i)=\int_{t_i}^{\infty} Bn_3\alpha t=L'_n(t_i)p_Bh\nu_B \tag{4.3}$$

and

$$n_0'(t_i)=L_{in}(t_i;\lambda)/p_Bh\nu_B\,, \tag{4.4}$$

where $L_n(t_i)$, $L_s(t_i;\lambda)$ and $L_Q(t_i;\lambda)$ are the light-sums of natural, IR-stimulated and -quenched phosphorescences during the time t_i respectively. $L_n'(t_i)$ and $L_{in}(t_i;\lambda)$ are the residual light-sums after the natural-decay duration t_i and the IR irradiation of duration t_i respectively.

$Ls(t_i;\lambda)$, $L_n(t_i;\lambda)-L_Q(t_i;\lambda)$ and $L_n'(t_i)-L_{in}(t_i;\lambda)$ are the spectral-stimulability, -quenchability and -exhaustibility respectively, which had been measured in the experiments. From Eqs (4.1)—(4.4) we obtain

$$\frac{L_n'(t_i)-L_{in}(t_i;\lambda)}{p_Bh\nu_B}-\frac{L_s(t_i;\lambda)}{p_Ah\nu_A}+\frac{L_n(t_i)-L_Q(t_i;\lambda)}{p_Bh\nu_B}=0$$

In order that all terms in the above equation have similar dependences upon λ, the relation $p_A\equiv$const.$\times p_B$ should be valid. Since p_B is obviously independent of λ, p_A also should be so in the wave-length range including the two bands.

The results state above and in the item (5) side with the model (A). But in order to explain the anomaly in Mn-activated members stated in the item (2) by using the model (A), it must be assumed that (I) there are two types of traps, namely the double traps, each one of which consists of the two trapping states associated with each other, and the single traps having the lower trapping state only, as stated in the previous papers[3)4)19)] or that (II) the two trapping states corresponding to 0.8 μ and 1.3 μ do not associate directly with each other but indirectly via a shallow trap and that $k_3\ll k_1$, that is $\kappa\fallingdotseq 0$, for the upper trapping state.

In the model (B) the anomaly obseved in Mn-activated members may be explained by the assumption that an electron stimulated to the upper metastable trapping state cannot easily migrate into a shallow trap or an emission-center and returns to original lower trapping state with larger probability. This situation is analogous to the case that ε in Eqs (3.5) and (3.7) is remarkably large and then stimulation and quenching are inconspicuous as shown in Figs. 16 and

17 in reference 2.

The experimental fact that the stimulation band and 1.3 μ disappears at low temperature[18] may be explained by any one of the models. In general, the model (A) is convenient to explain the parallelism in the phosphorescence characteristics of the two bands, whereas the model (B) to explan their dissimilarity Although it would be difficult to determine by experimental evidence which is the real one among the two models assumed in Fig. 7, the model (A) seems to be somewhat preferable for the explanation of the results obtained.

5. IR Responsivity *versus* Foreign Ingredient Proportion

As stated in the previous paper[8], homogeneous host-crystals are produced at least at a temperature higher than 850°C by thermal diffusion. In a near-ZnS member (that is, a composite member containing a comparatively small proportion of foreign ingredient) the foreign atoms Cd or (and) Se should be located substitutionally with a weak, uniform concentration in phosphor crystals. In this stage the foreign atoms may be regarded as local impurity-atoms in ZnS host-crystals perturbed only slightly. The substitution causes, therefore, small local distorsions distributed uniformly.

With increasing proportion of added foreign ingredient every part in the host-crystal comes to be subjected to the overlapped effect from many surrounding foreign atoms and furthermore the foreign atoms themselves begin to interact with one another. The atomic-spacing of the host-crystal, therefore, is elongated gradually in obedience to Vegard's law[4)5)6)]. In this stage the foreign atoms can be no longer regarded as isolated local singularities in the host-crystal and the structural departure in their vicinities from the regular host-crystal part is ambiguous.

In reference to the experimental fact that in these near-ZnS members the radiances and durations of natural and IR-stimulated phosphorescences markedly increase as stated in the previous paper[8], we can deduce that the local distorsion in these members would promote indirectly the formation of deep traps (probably in the regular ZnS host-crystal part), which are responsive for IR irradiation. Consequently the isolated emission-centers in the ZnS phosphor come to be associated with deep traps and moreover, considerable number of isolated deep traps are formed additionally. Similar examples are found also in well-known stimulable phosphors ZnS: Pb[SO_4]: Cu and ZnS: Mn[SO_4]: Cu, where the optimum proportion of these sulphates is sbout 3~4 mole percents[4)17)].

Since the optical depths of the deep traps are not affected by the quantity and kind of added foreign ingredient, the locally distorted domain itself would

not become a deep trap but the formation of deep traps will be rather hindered in this distorted domain ligated intimately to the foreign atom. If a stable deep trap were formed in such a distorted domain, its optical depth would be strongly affected by the degree of distorsion, consequently by the kind of foreign atom added.

Although the number of locally distorted domains increases with increasing number of foreign ingredient atoms, the localization of distorsion becomes ambiguous beyond a certain foreign ingredient proportion, which depends upon the ionic-radii of the foreign atoms added, and the region non-ligated to foreign atoms decreases rapidly with it. The number of effective deep traps, therefore, reaches to muximum at that proportion, beyond which it decreases again.

This will be also the reason why Bi-, Cu- or Ag-activated composite phosphors containing several mole % of foreign ingredient show a weak, instanstaneous stimulation, although the corresponding ZnS phosphors are completely quenchable[4)5)6)]. It is visualized by considering that B_t may take a detectable value in Eq (3.9 a), if N is considerably large even when p_A is small.

According to current views, an electron in a phosphor crystal is trapped not only in the neighborhood of a crystal imperfection but also it may be trapped or become stagnate in a regular crystal part by creating its own irregularity, for example, as Landau's type self-trapped electron or polaron. The self-trapping field $V(r)$ is given by[22)]

$$V(r)=-\frac{e}{r^2}\left(\frac{1}{\varepsilon}-\frac{1}{\varepsilon_0}\right) \tag{5.1}$$

and the self-energy $E(k)$ and effective mass m^* of a polaron are given by[23)]

$$\left.\begin{aligned} E(k)&=W+\frac{(\hbar k)^2}{2m^*} \\ \text{and} \\ m^*&=m\left(1+\frac{W}{6\hbar\omega}\right) \\ \text{respectively, where} \\ W&=-\frac{1}{2}\left(\frac{1}{\varepsilon}-\frac{1}{\varepsilon_0}\right)e^2\left(\frac{2m\omega}{\hbar}\right)^{1/2} \\ \omega&=\omega_t(\varepsilon_0/\varepsilon)^{1/2} \end{aligned}\right\} \tag{5.2}$$

k: total wave number.

ε: optical dielectric constant ($=n^2$).

ε_0: static dielectric constant.

e: absolute electronic charge.

22) N. F. Mott et al: *Electronic Processes in Ionic Crystals* (Oxford Univ. Press, London 1940) p. 86.

23) H. Fröhlich: Advances in Phys. **3** (1954) 325.

m: effective mass of conduction electron*

ω_t: *Restsrahlenfrequenz* (circular).

On one hand, there is the following relation between ε and ε_0 of a diatomic polar crystal[24].

$$\varepsilon_0=\varepsilon+\left(\frac{\varepsilon+2}{3}\right)^2 s^2\frac{4\pi(Ze)^2N}{\omega_t^2M} \tag{5.3}$$

where Z: valency of the constituent ions (absolute value).

N: number of "basic units"** in unit volume.

M: reduced mass of the constituent ions.

In a ZnS-type crystal, in particular, the parameter s in Eq (5.3), indicating the effective charge of the constituent ions is considerably less that unity (for example, $s=0.48$ in cub-ZnS) and $\varepsilon\gg\varepsilon_0-\varepsilon$[25] owing to the homopolarity in binding energy, compared with typically polar alkali-halide crystals. Therefore, from Eqs (5.1) and (5.2) $|V(r)|$ and $|W|$ (accordingly the coupling constant $\alpha=-W/\hbar\omega$) then are not so large. Since the energy level (below conduction band) of the self-trapped electron is -0.13 eV even in predominantly polar NaCl crystal[26], that in ZnS-type srystals will be much smaller (in absolute value). The values of W and m^*/m in cub-ZnS ($\varepsilon=5.07$, $\varepsilon_0=8.3$, $\lambda_t=2\pi c/\omega_t=33\,\mu$), which are computed from Eqs (5.2) by using for m the electronic mass, are -0.06 eV and 1.22 respectively, while those in NaCl are -0.17 eV and 1.95 respectively.

According to the above estimation, the self-trapping and the production of polaron will not play any essential role in phosphorescence phonomena of ZnS-type phosphors at least excepting a low temperature range. In these phosphors most of trapped electrons may be considered to be captured in the neighborhood of lattice imperfections of various types.

Eqs (5.2) are derived, however, under the restriction that no more than a single phonon belongs to each wave number vector and that the energy $E(k)$ of the system is less than $\hbar\omega$ above the energy W of the ground state ($k=0$)[27]. No doubt, this restriction should be removed for a room temperature range, where a great number of phonons ($=[\exp(\hbar\omega/kT)-1]^{-1}$ in thermal equilibrium) may belong to each wave number vector and the electronic energy may be much

24) B. Szigeti: Trans. Faraday Soc. **45** (1949) 155.

25) J. R. Tessman et al: Phys. Rev. **92** (1953) 890.

26) J. J. Markham et al: Phys. Rev. **74** (1948) 1014.

27) M. Gurari: Phil. Mag. **44** (1952) 392.

* A Bloch type electron, for which the periodic field only is taken into account, disregarding the interaction with lattice vibration.

** A *basic unit* means the smallest unit from which the lattice can be built up by primitive translations.

larger than $\hbar\omega$. For this case a new approach, which has not yet been found, would be required. If the energy depression of the system and the effective mass of polaron were larger in this case, and furthermore such a polaron might be depolarized by being excited thermally into an upper quasi-free Bloch state, where the polarization potential-well cannot accompany the electron and the interaction with lattice vibration is much smaller (that is, coupling constant $\alpha \fallingdotseq 0$), the hyperbolic decay of ZnS-type phosphors would be possibly explained by this process similarly as by the thermal release from Tamm's surface traps[28].

6. Conclusion

Surveying the foregoing discussions on IR-responsive behaviors of ZnS-type phosphors, we can reach to the following conclusions.

(1) Spectral IR-responsivity curve of a ZnS phosphor, in general, is not strongly affected by the addition of ZnSe, CdS or CdSe, except for some stimulable Zn(S: Se) families and their peak wave-lengths at about 0.8 μ and 1.3 μ remain constant. Further, the peak wave-length of the stimulated phosphorescence also hardly varies with addition of these foreign ingredient and is peculiar to the added stimulable activator-atoms[11]. These facts sharply contrast with the characteristics that the atomic-spacing, peak wave-lengths in fluorescence and IR-quenchable natural phosphorescence, absorption edge and other optical properties vary gradually with foreign ingredient proportion.

(2) The deep traps which are concerned in IR responsivity seem to be ascribable to perturbed atom-groups consisting of Zn and S atoms. These atom-groups can remain, to some extent, unaffected in composite host-crystals of a near-ZnS phosphor and associate with nearby perturbed emission-centers in these host-crystals probably via other electron traps or carriers i. e. shallow traps, exciton states or quasi-exciton states etc. or their serial combinations.

Since the optical depth of a deep trap caused by an omission defect or that of an exciton state in composite host-crystals should depend on their atomic-spacing[29)30)], these states themselves will not be the deep traps responsive to IR irradiation.

(3) IR-responsive mechanism in ZnS phosphor is not substantially altered by the addition of foreign ingredient. The electron transfer under IR irradiation is mainly according to the bimolecular recombination at least in the tail-part, although an exponential-part is observed in the earlier stage by quasi-direct re-

28) H. M. James: Phys. Rev. **71** (1947) 137.
29) R. W. Gurney et al: Proc. Phys. Soc. [London] (sup.) **49** (1937) 32.
30) N. F. Mott: Trans. Faraday Soc. **35** (1938) 500.

combination or other processes.

(4) IR-responsive natural-decay about several seconds after excitation is mainly according to direct recombination between ionized centers and electrons in nearby shallow traps associated with deep traps, or to some short-range motions between them through conduction band with neglegible retrapping probability, whereas the remote bimolecular recombination are predominant in the earlier stage of natural-decay as well as during excitation[31]. In this stage IR stimulation of brightness and photo-conductivity is not so conspicuous[2].

(5) By taking the general view of the results on the decay characteristics, it is infered that a phono-stimulated (thermo-stimulated) electron in conduction band would have smaller mobility owing to the stronger interaction with lattice vibration (in particular, with an optical vibrational-mode localized in the neighborhood of the activator-atom) than that of a photo-stimulated conduction electron. The former can move within shorter range only and then the retrapping is neglegible, whereas the latter can move in longer range and then the retrapping is conspicuous. When the densities of trapped electrons and their acceptors are considerably large, the photo-stimulated electron may show also a process analogous to the short-range motion by quasi-direct transition or the like.

The recombination probability A and the retrapping probabilities K and K'' in Eqs (2.2) and (2.3) are given by σv, where σ and v are the capture cross-section for each transition and the velocity of the electron in conduction band respectively. Whether the transition is radiative or non-radiative, σ depends on the both eigenfunctions of the initial and final states of the total system which consists of the electron and the lattice interacting with it[32]. Accordingly the values of A, K and K'' for a phono-stimulated electron may be somewhat different from those for a photo-stimulated one, although the degradation of electron energy may occur in conduction band owing to multiple-phonon production. (*Vielfachstösse*)

(6) The anomalous inccease in radiances and durations of natural and IR-stimulated phosphorescences in near-ZnS members will be infered to be ascribable to the fact that the effective numbers of shallow traps and deep traps increase owing to small local distorsions formed by foreign atoms, although any definite experimental evidence confirming it directly could not be obtained.

In closing, the author thanks to Mr. Y. Tomishima for helpful discussions.

31) N. A. Tolstoĭ: Dokl. Akad. Nauk SSSR **95** (1954) 249.
32) For instance: R. Kubo et al: *Busseiron-Kenkyū* [Japan] **73** (1954) 43.

Errata

On the Infrared-Responsive Behaviors of (Zinc:Cadmium-Sulphide:Selenide)-Type Phosphor Families

IV. Zinc:Cadmium-Sulphide Phosphors

Sumitada ASANO

Science of Light **4** (1955) 32~47

Page	Line		(should be read)
34	17	the among	among
37	foot-note	7) (1955) **4** (1955)	7) **4** (1955)
47	9	(Zn:Gd)S	(Zn:Cd)S
〃	15	(Zn:Cp)S	(Zn:Cd)S

On the Infrared-Responsive Behaviors of (Zinc:Cadmium-Sulphide:Selenide)-Type Phosphor Families

V. Zinc:Cadmium-Sulphide:Selenide Phosphors

Sumitada ASANO

Science of Light **4** (1955) 48~60

Page	Line		(should be read)
48	foot-note	3) **4** (1955) 16	3) **4** (1955) 32
52	〃	11) S. Asance:	11) S. Asano:
54	13	Fig. 1e and 2	Figs. 1e and 2
57	Fig. 5	ander	under
58	12	paralled	parallel
59	Fig. 8	unde	under
60	2	anormalous	anomalous
〃	13	ZnS	ZnSe
〃	14	paper[11], therefore,	paper[11] is, therefore,